Nanocapillaries combined with optical tweezers as a single molecule technique for studying DNA-protein complexes

PAR

Roman BULUSHEV

EPFL

ÉCOLE POLYTECHNIQUE
FÉDÉRALE DE LAUSANNE

Suisse
2017

"Unless you try to do something beyond what you have already mastered, you will never grow."

— *Ronald E. Osborn*

Abstract

Interactions of proteins with DNA are essential for carrying out DNA's biological functions and performing a cellular cycle. Such processes as DNA replication, expression and repair are performed by an organised action of various proteins. To better understand the function of protein machinery many methods have been developed over the years. They can be divided into two categories: single molecule and bulk techniques. In comparison to bulk experiments, where the effect of an ensemble of proteins is measured, single molecule techniques analyse each molecule one by one. This fact allows to detect rare events and avoid averaging over the population. Moreover, some single molecule techniques can be used for measuring dynamics and active processes of biomolecules.

The objective of this thesis was to make a single molecule technique combining nanocapillaries and optical tweezers for characterisation of DNA-protein complexes. There were three main steps in this thesis: 1) building and characterisation of the setup 2) using it for detection and characterisation of DNA-protein complexes and 3) localisation and discrimination of DNA-protein complexes.

On the first step of the project we combined two single molecule techniques: optical tweezers and glass nanocapillaries. We characterised the electrophoretic force acting on DNA in this setup by using nanocapillaries with openings of different sizes, at different applied voltages and with DNA molecules of different lengths. We observed that the position-dependent electrophoretic force acting on the DNA depends on all above mentioned parameters. We modelled the system and found out that this effect is due to a non uniform distribution of the potential inside the nanocapillary, which originates from its elongated shape.

After having built and characterised the setup, we detected proteins bound to DNA during their controlled translocation through the opening. The proteins were visualised by a sudden decrease in the force acting on the bare DNA followed up by its slow restoration when the capillary was moved further away. We made a stochastic model to explain this force profile. From the fits of the model to experimental results we extracted the effective charges of DNA-protein complexes inside the nanocapillary. In the case of all three proteins (RecA, EcoRI and RNAP) the effective charge was of opposite sign than the one in solution. We attributed this fact to the dominant impact of the drag force in comparison to the electrostatic force inside the nanocapillary.

In the last step of the project we showed the ability to localise and discriminate DNA-protein

complexes in our setup using dCas9 and RNAP proteins. During controlled translocation of the DNA-protein complexes we measured multiple parameters, including protein's location on the DNA, work required to translocate the complex, and conductance change. We demonstrated that the measured location of the proteins is shifted from the designed binding site. We made a model that explained this phenomenon and that can account for the shift in our experiments. In addition, protein-specific work and conductance parameters allowed us to discriminate between RNAP and dCas9 proteins.

Key words: *optical tweezers, glass nanocapillary, solid-state nanopore, DNA translocation, single molecule measurements, force measurements, DNA-protein complex, protein binding site.*

Résumé

Les interactions entre les protéines et l'ADN sont nécessaires pour réaliser les fonctions biologiques de l'ADN et pour accomplir un cycle cellulaire. Les processus tels que la réplication, l'expression et la réparation de l'ADN sont faites par les actions organisées de différentes protéines. Au fil des années, beaucoup de méthodes pour découvrir les fonctions des protéines ont été développées. Elles peuvent être classifiées comme des techniques à molécule unique ou d'ensemble. En comparaison les expériences d'ensemble où l'effet d'un groupe de protéines est mesuré, les techniques à molécule unique analysent chaque molécule une par une. Par conséquent, les évènements rares peuvent être détectés. Par ailleurs, quelques techniques à molécule unique peuvent être utilisés pour les manipulations mécaniques de biomolécules, c.-à-d. : la torsion, l'étirement, etc.

Le but de cette thèse est l'introduction de la technique qui combine les nanocapillaires et les pinces optiques pour caractériser les complexes de ADN-protéine. Il y a eu trois étapes dans ma thèse : 1) la construction et la caractérisation de l'installation expérimentale 2) la détection et la caractérisation des complexes d'ADN-protéine et 3) la localisation et la discrimination des complexes d'ADN-protéine.

D'abord, nous avons combiné deux techniques à molécule unique : les pinces optiques et les nanocapillaires de verre. Dans cette installation nous avons caractérisé la force sur l'ADN en utilisant les nanocapillaires avec des pores de tailles différentes, des voltages différents et avec de l'ADN de différente longueur. La force électrostatique dépend de tous les paramètres ci-dessus. Nous avons fait un modèle de notre système et nous avons trouvé que c'est grâce à la distribution non uniforme du potentiel à l'intérieur du nanocapillaire qui vient de sa forme allongée.

Après avoir construit et caractérisé l'installation nous avons détecté des protéines attachées à l'ADN pendant la translocation contrôlée à travers le nanocapillaire. Les protéines ont été détectées par une brusque réduction de la force sur l'ADN accompagnée par sa lente restauration pendant le déplacement continu du nanocapillaire. Nous avons fait un modèle stochastique pour expliquer ces profils et nous avons calculé les charges effectives des protéines dans le nanocapillaire. Pour toutes les protéines (RecA, EcoRI et RNAP) la charge effective observée est de signe opposé à celle en solution. Nous avons expliqué cet effet par la force de traînée (due à l'écoulement hydrodynamique) plus forte que la force électrostatique.

La derniére étape a été de localiser et de discriminer des complexes d'ADN-protéine avec les

protéines dCas9 et RNAP. Pendant la translocation contrôlée nous avons mesuré les paramétres différents, y compris : le site d'attache des protéines, le travail requis pour une translocation de complexe et le changement de la conductivité. Nous avons démontré que le site d'attache des protéines mesuré est déplacé du site de liaison théorique. Nous avons fait un modéle pour expliquer cet effet et corriger le site d'attache mesuré. De plus, les travaux et les conductivités mesurés nous ont permis de discriminer entre les complexes de RNAP et dCas9.

Mots-clés : *pinces optiques, nanocapillaires de verre, solid-state nanopore, translocation d'ADN, expérience à molécule unique, mesure de la force, complexes d'ADN-protéine, sites de liaison des protéines.*

Contents

Contents

List of Figures

List of Tables

1 Introduction

DNA-protein interactions ubiquitously regulate almost all aspects of cellular function, including chromosome maintenance, DNA replication, transcriptional regulation, and DNA repair [1, 2]. Most of these interactions occur after complex protein search and binding to a sequence specific DNA target. Because of the broad spectrum of possible interactions it is crucial to gain a better understanding of DNA-protein association, especially the intricacies of binding.

Over the years, numerous methods have been developed to elucidate the role of DNA-protein interactions in cellular processes and to facilitate the translation of research into biotechnological applications [3]. Such methods can be allocated either to the category of experiments performed in bulk or at the single molecule level. Electrophoretic mobility shift assay (EMSA) [4], nuclease footprinting [5], SELEX-based approaches [6], protein-binding microarray approaches [7, 8], and chromatin immunoprecipitation-based microarray (ChIP) [9, 10, 11] are among the most frequent bulk methods used to reveal sequence-specific protein binding to DNA. While quantitative analysis of thermodynamic and kinetic parameters can be assessed by surface plasmon resonance (SPR) [12], by EMSA, or, more recently, by mechanically induced trapping of molecular interactions (k-MITOMI) [13].

Single molecule techniques have emerged to complement the bulk methods by studying dynamics and active processes happening on molecular level. Such techniques can operate at low concentrations of biological samples and can allow to perform measurements in real time under equilibrium conditions [14]. In addition to that, single molecule methods provide a tool for mechanical manipulation of biomolecules, e.g. their stretching, twisting, etc [15]. To date there is a wide variety of techniques used to study biomolecules on a single molecule level, including AFM [16], FRET [17], TIRF [18], super resolution microscopy [19] and magnetic tweezers [20].

Every technique (bulk and single molecule) has its advantages and disadvantages and is suitable for a specific application. There is no method that can reveal all parameters of DNA-protein interactions. In this thesis we developed a single molecule technique combining optical tweezers and nanocapillaries. It allows to measure the location of DNA-protein com-

plexes and discriminate them, however the unique niche of this technique can be revealed with its further development. One can envision extraction of charges and sizes of DNA-protein complexes and study the effect of the electric field on DNA-protein complexes.

To provide more details of the developed setup, optical tweezers and nanopores/nanocapillaries will be discussed in this chapter as well as the technique obtained by their combination. Firstly, the principle of each method will be introduced and then relevant examples of studying DNA-protein interactions with each technique will be described.

1.1 Optical tweezers

Optical tweezers (optical trap) is arguably one of the most popular single molecule techniques nowadays. It uses a tightly focused laser beam to trap and manipulate nano- and micrometer sized objects in three dimensions. The forces applied by photons are strong enough to have an impact on this scale. The first optical trap based on a single laser beam, reported in 1986, was used for trapping dielectric particles in the size range of 25 nm to 10 μm [21]. Afterwards an optical trap was literally used as tweezers for positioning and manipulation of various artificial [22] and biological objects, i.e. bacteria [23], cells [24], organelles [25], macromolecules [26], etc. Optical tweezers can even go below the limit of single molecule studies and be employed for trapping single atoms in order to study quantum physics phenomena [27]. On top of that, an optically trapped bead can be also used as a force transducer allowing to measure piconewton forces [28]. This fact along with their Ångstrom spatial resolution and microsecond temporal resolution makes them a powerful tool for studying biophysics of nucleic acids [29], proteins [30] and especially DNA-protein interactions [28].

1.1.1 Principle and calibration

There are two main forces on an optically trapped object: gradient and scattering forces that arise from the momentum applied on the particle by photons [31, 32] . The gradient force always directs in the way to bring a dielectric particle to the centre of the trap, where the light intensity is maximal (Fig. 1.1). The scattering force pushes the particle further away form the focal point in the direction of light propagation. Moreover, to correctly locate a trapped particle inside an optical trap one has to take into account the gravitational force.

Even though the theory of optical tweezers is relatively complicated, it can be simplified to two regimes that allow to explain the mechanism of trapping. When the particle is much larger than the laser's wavelength the ray optics regime can be applied [31]. In this case the mechanism of trapping can be explained by the fact that the restoring (gradient) force always acts in the direction of the focus for any lateral and axial displacements of the bead (Fig. 1.1). In the case when a particle is much smaller than the wavelength (Rayleigh regime) it can be considered as a perfect dipole in an inhomogeneous electromagnetic field. The gradient in the light intensity produces a Lorentz force on the particle that directs it towards the focus [31].
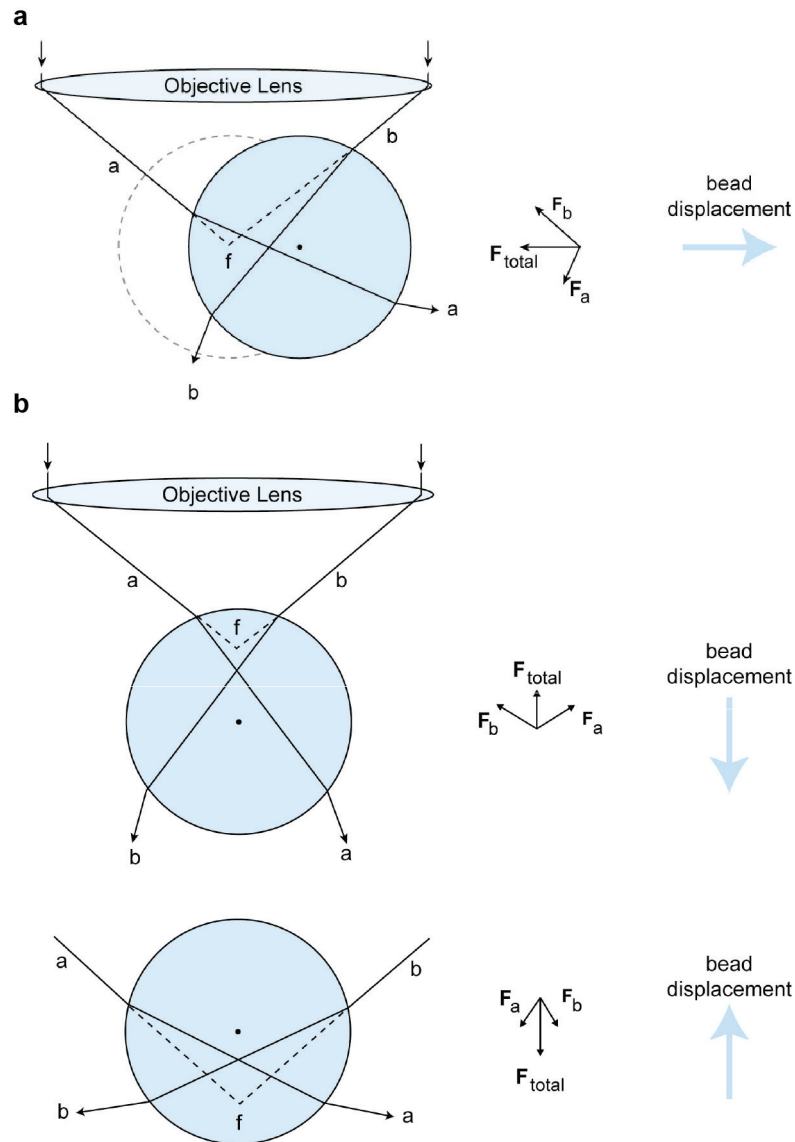
Figure 1.1 – **Principle of optical trapping in the ray optics regime.** When a bead is laterally (a) or axially (b) displaced from the focus, the total force on the bead F_{total} draws it to the centre of the trap, where the intensity is highest, keeping the particle trapped. Two rays a and b are presented with the corresponding forces F_a and F_b they apply on the particle. The figure is adapted from [31].

As it was mentioned above, an optically trapped particle experiences a restoring force that draws it to the centre of the trap. This force can be described with the equation F=-kΔx, where Δx - is the displacement of the particle from the trap centre and k - is the stiffness. Thus to measure a force signal in experiments, both displacement and stiffness have to be known.

Calibration of optical tweezers is a procedure that allows to measure the stiffness (k) of optical tweezers. Two calibration techniques have been used in this work and therefore will be

discussed here in detail. The first one is based on measuring the power spectral density (PSD) of thermal fluctuations of a trapped bead. The stiffness of the trap can be obtained using the equation $k = 2\pi\beta f_0$ [31], where $\beta = 3\pi\eta d$ - is the drag with η - the fluid viscosity, d - the diameter of the bead and f_0 - the cutoff frequency. While the drag is usually known, the cutoff frequency can be extracted from the PSD of a trapped bead that has a Lorenzian profile, described by [31]:

$$S(f) = \frac{\rho^2 k_B T}{\pi^2 \beta (f_0^2 + f^2)} \tag{1.1}$$

where k_B - is Boltzmann's constant, T - is the absolute temperature and ρ - is the sensitivity (will be discussed later). Examples of using the PSD method for calibration are shown in Fig. 2.10 a and b.

Stokes drag method is another way to calibrate optical tweezers used in this work. In this case generated fluid movements create a drag force on the trapped bead that leads to its displacement. In equilibrium the drag force is equal to the force that keeps the bead in the optical trap:

$$k\Delta x = \beta v \tag{1.2}$$

where v - is the fluid velocity. Knowing the drag force and measuring the bead's displacement the trap's stiffness can be estimated. An example of calibration of optical tweezers with the Stoke's method is presented in Fig. 2.10 c.

Another part of the equation F=-kΔx contains displacement (Δx). If a photodiode is used as a detector in optical tweezers (Fig. 2.7), Volts are used as a final unit for measuring the displacement. This signal has to be converted to meters for further force calculations. A conversion factor (sensitivity) for this operation can be extracted by scanning a stuck bead as it is shown in Fig. 2.10 d [32]. Importantly, the lateral and axial positions of the scanned bead should be the same as for the optically trapped one in order to obtain accurate results. It is worth mentioning, the sensitivity can also be extracted from thermal fluctuations of a bead inside a laser beam (eq. 1.1).

1.1.2 Studying DNA-protein interactions

First studies of properties of DNA and proteins with optical tweezers were performed in the 1990s [33, 30]. Nowadays optical tweezers are used in many biophysical applications, including replication, transcription, recombination, repair, reorganization, etc. and they keep

finding new niches [28]. Below three classical examples of using optical tweezers for studying DNA-protein interactions will be provided.

The first example is based on the fact that optical tweezers allow not only to measure the force but also to apply it. This force can be used to probe the stability of DNA-protein interactions and find the force value at which DNA-protein complexes can be disrupted (Fig 1.2) [34] . In addition to that, optical tweezers allow to study the kinetics of disruption of DNA-protein complexes and their reversible assembly [34]. Interestingly, a similar method based on a movement of a coverslip with attached DNA could also be used to locate proteins on a DNA molecule as it was shown in Wang's lab [35]. The location of the complex was estimated based on the additional peak in the force signal, corresponding to disruption of the complex. The resolution of this technique was $\approx$ 25 bp.
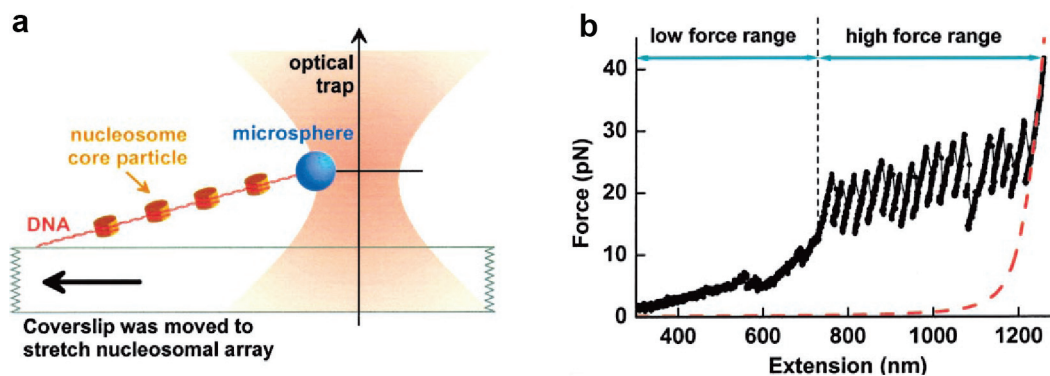
Figure 1.2 – **Disruption of individual nucleosomes with optical tweezers.** (a) Schematic of the experiment. (b) Force versus extension profiles for DNA (red dashed line) and DNA-nucleosome complexes (black line). At forces >15 pN the sawtooth pattern was observed corresponding to disruption of individual nucleosomes. The figure is adapted from [34].

The high spatial and temporal resolution of optical tweezers opens up another niche for them - studying of movement of motor proteins on DNA. A classical example of such a protein is RNA polymerase (RNAP) that is responsible for performing transcription. Numerous single molecule studies of transcription have been performed starting from the 1990s [36, 37, 38, 39, 40] using the continuously improving optical tweezers setup. After introduction of a position clamp, which holds the trapped bead in the same position using a nanopositioning stage, and dual optical tweezers, a single base pair stepping of RNAP was observed with a resolution of 3.4 Å (Fig. 1.3) [39]. Moreover, pausing and backtracking of RNAP was revealed and forces applied by the enzyme during its movement were measured in this work. The possibility to measure and apply torque with optical tweezers allowed to additionally study the effect of supercoiling of DNA on the velocity of RNAP [40]. These results provided further insights into how the coiling of DNA affects the regulation of transcription. It is worth mentioning, studying of motor proteins with optical tweezers is not limited to transcription and also includes DNA replication [41], repair [42], and reorganisation of DNA [43].

Additional capabilities of optical tweezers can be discovered by their combination with other

Figure 1.3 – **Measuring of single steps of RNA polymerase with dual-beam optical tweezers.** (a) Schematic of the setup. RNAP was attached to a weakly trapped bead and DNA to a strongly trapped bead, respectively. This modification reduced the noise associated with the drift in the axial direction. (b) Position of RNAP versus time. Addition of NTPs to the buffer activated transcription and revealed a velocity curve of the enzyme with a single-step resolution. The figure is adapted from [39].
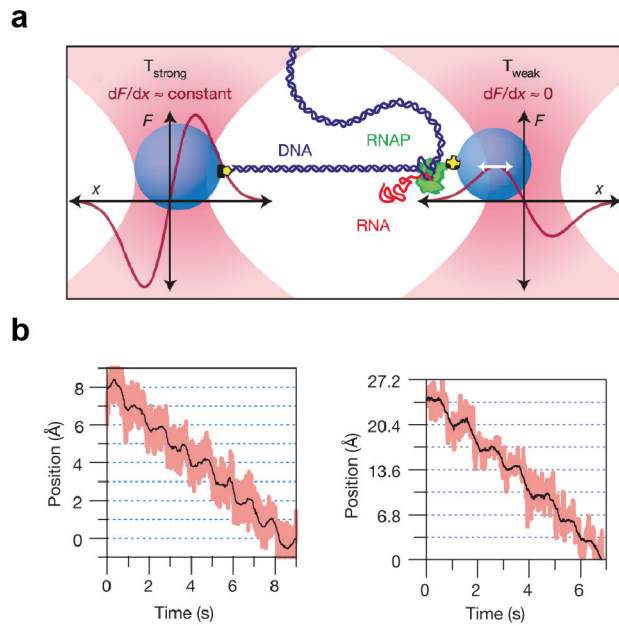
Figure 1.4 – **Triggering RAD51 disassembly from DNA using optical tweezers combined with fluorescent microscopy and microfluidics.** Kymograph shows the decrease in the length and fluorescence after triggering the disassembly by addition of Mg^{2+}. The figure is adapted from [45].
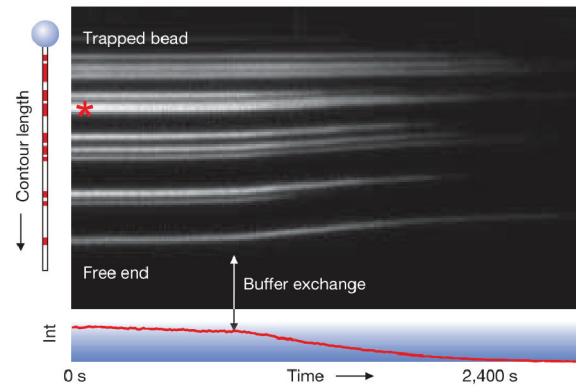
techniques, e.g. super resolution microscopy and microfluidics [44, 45, 46]. Using such a setup, assembly/disassembly of a protein responsible for homological recombination (RecA or its eukaryotic analogue RAD51) was studied using a fluorescently modified protein. The measured signal was based on the extension of DNA after binding of the protein [45, 46]. It was shown that assembly nucleation is a slow process followed up by a fast bidirectional growth phase. In this work a microfluidics cell served as a method for fast exchange of a solution. It also allowed to study different compositions of buffer. Moreover, it was shown that protein disassembly consists of RAD51 bursts and long pauses. In Fig. 1.4 one could see a decrease in the contour length and fluorescent intensity of DNA after disassembly of RAD51 molecules triggered by addition of Mg^{2+}. Moreover, it has been shown that applying an external force using optical tweezers leads to slowing down of disassembly or even its complete stalling.

In conclusion, optical tweezers emerged to be among one of the most powerful single-molecule techniques and allowed to reveal numerous biophysical phenomenon. Its versatility
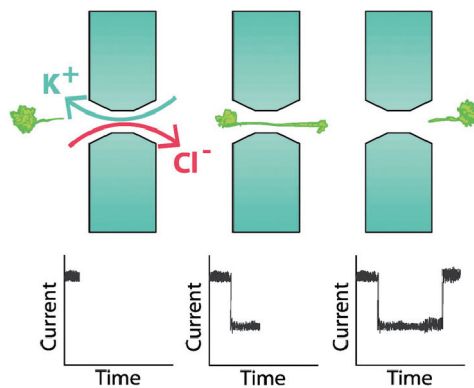
Figure 1.5 – **Principle of nanopore-based sensing.** Application of the electric field induces translocation of K^+ and Cl^- ions through the pore generating a stable current. A translocating molecule partially occupies the pore and decreases its conductance. After the translocation is finished the current level restores to the initial values. The figure is taken from [63].

and commercial availability makes it an attractive tool that will be developing in the future to fulfil the aim of better understanding the influence of DNA-protein interactions on specific cellular functions.

1.2 Nanopores

Nanopore-based sensing is another emerging single molecule technique that will be discussed here in detail. Except for sensing applications, nanopores can be potentially used as power generators [47], nanoreactors [48] and platforms for water desalination [49, 50]. They also help to study fundamental principles in physics and biology, including the mechanism of operation of biological pores [51] , nanoflows [52] and behaviour of biomolecules in confinement [53]. Interestingly, comparing to optical tweezers nanopores allow high throughput measurements and are usually easier to operate.

1.2.1 Types of nanopores and principle of sensing

A nanopore is an opening of a nanometre size that acts as a single connector between two chambers filled with a salt solution. After application of an electric field across the pore the voltage-driven movement of ions starts to take place resulting in a stable baseline current (Fig. 1.5). Objects translocating through the pore occupy some volume and consequently decrease the conductance of the pore (Fig. 1.5). The main parameters measured during a translocation event are amplitude, correlating with the volume of the object, and dwell time, reflecting the length and charge of the object. Various objects have been detected with nanopores starting from biological molecules as single nucleotides [54], DNA [55], RNA [56] , proteins [57] , DNA-protein complexes [58] as well as viruses [59], particles [60] and even nanotubes [61]. To date many different substrates for formation of nanopores have been used (Fig. 1.6) [62], however they can be divided into two categories: solid-state and biological pores.

Biological nanopores are represented by bacterial protein ion channels and are usually reconstituted in a lipid membrane for sensing applications [64]. There are more than 300 biological

channels [65], however the most commonly used ones in biological sensing are α-hemolysin (α-HL), *Mycobacterium smegmatis* porin A (MspA) and outer membrane porin F (OmpF) due to their accessibility, robustness and size of the opening enabling for translocation of ssDNA. In 1996 α-HL, a bacterial toxin membrane pore, was used as the first biological pore for sensing polynucleotides [66]. In this work it was postulated that with further improvement the method could be used for ultrafast and cheap sequencing of DNA. This idea became the main driver of the field. However, more than 15 years were required to optimise the technology to demonstrate the proof of principle of sequencing of DNA with nanopores [67]. The company Oxford Nanopore has been producing sequencers based on this technology for more than 10 years. Still being far from commercial success, these portable devices keep improving their accuracy and have already been applied for sequencing the genome of the Ebola virus *in-situ* in Africa [68].
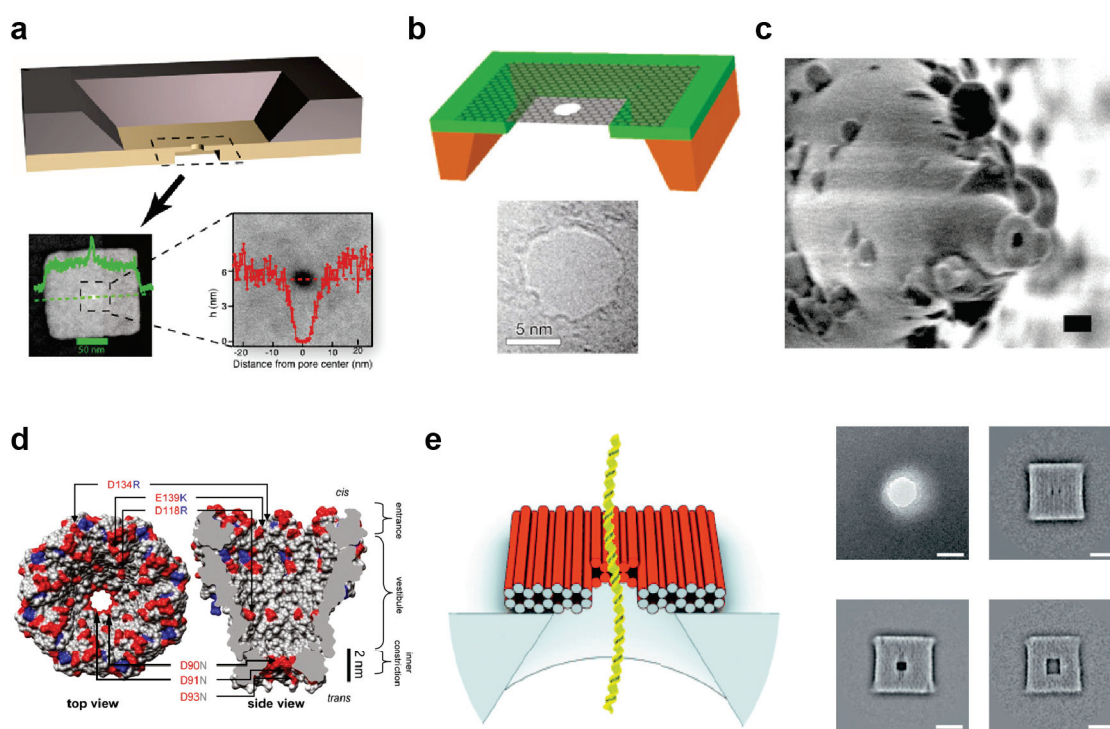
Figure 1.6 – **Different types of nanopores.** (a) A nanopore drilled by TEM in a silicon nitride membrane [69].(b) A pore in a suspended single layer graphene membrane [70]. (c) A pore formed by pulling a glass capillary [71]. (d) A MspA pore from *Mycobacterium smegmatis* [72]. (e) An origami pore inserted in a solid-state pore [73]. The figure is adapted from [62].

In contrast to biological pores, solid-state nanopores are artificially fabricated [64]. On the first step of fabrication a relatively thin (several nanometers) membrane should be produced. For the first nanopores Si_3N_4 or SiO_2 membranes with a thickness of tens of nanometers are normally fabricated using clean room facilities [74, 75, 76]. Quite recently single-layer materials suspended on an opening emerged as a substrate for pore formation [70, 77]. After fabrication of a thin membrane a pore can be drilled in it using a focused ion beam (FIB) or

a transmission electron microscope (TEM) [75, 76]. However, there are other techniques for production of pores that have emerged in the last 15 years. Among them one can include dielectric breakdown [78], electrochemical reaction [79] - formation of a pore due to the applied voltage, tracked etched method [80] or fabrication of glass nanocapillaries using a laser-assisted puller [81].

Pulling of glass nanocapillaries is a method for production of low-cost nanopores without the need of clean room facilities (see section 2.1 for further details). This fact allows the use of nanopore-based sensing in developing countries [82, 83, 84]. Glass capillaries were introduced in the late 1970s [85] for patch clamping applications, however the first single molecule resistive pulse experiments were performed in 2010 using λ-DNA as an analyte [71]. Capillaries can be pulled to diameters of 15 nm [86] and due to low capacitance of the glass they provide good signal-to-noise characteristics [87]. Interestingly, depending on the pulling parameters the capillary tips can be tailored to different shapes, including blunt, bullet and hourglass shapes [88]. In addition, the size of the nanocapillary opening can be reduced even more by means of electric irradiation [89], atomic layer deposition [90] or lipid coating [91].

At the interface between solid-state and biological pores one can place DNA-origami pores. These pores are made out of DNA that is folded in a specific three dimensional shape (Fig 1.6 e). As a substrate for origami nanopores a lipid bilayer [92], solid-state pores [73] or even glass nanocapillaries [93] can serve. One of the main advantages of such pores is the ability to tailor their structure in order to provide the selectivity of cargo transport [94, 95].

1.2.2 Detection of DNA-protein complexes

Studying of DNA-protein complexes is one of the numerous applications of nanopore-based sensing that emerged a few years ago. There are two possible scenarios in this application when the pore is larger or smaller than the complex. In the first case nanopores are used as sensors since a complex can translocate through them. In the second case the pore is larger than dsDNA and smaller than the complex. This system is used for probing the stability of DNA-protein complexes.

Since normally biological pores are too small to allow the passage of a DNA-protein complex, solid-state pores were used for sensing applications. In the first studies, a DNA-RecA complex was translocated through a pore made in silicon nitride [98, 96]. As it was mentioned previously (section 1.1.2), due to positive cooperativity RecA forms filaments on DNA [98, 96]. Nevertheless, using not saturating concentrations of RecA, patches of DNA-protein complexes can be obtained. Being larger in diameter than bare DNA these filaments will correspond to higher conductance drops comparing to the DNA level (Fig. 1.7 a). However, taking into account the nature of RecA interactions with DNA it is impossible to detect a single bound protein. In the follow up studies single complexes of DNA with such proteins as RNA polymerase [58], nucleosomes [99], antibodies [100], zinc fingers [101] and single-stranded binding protein [102] were detected based on the current signatures. While DNA-specific
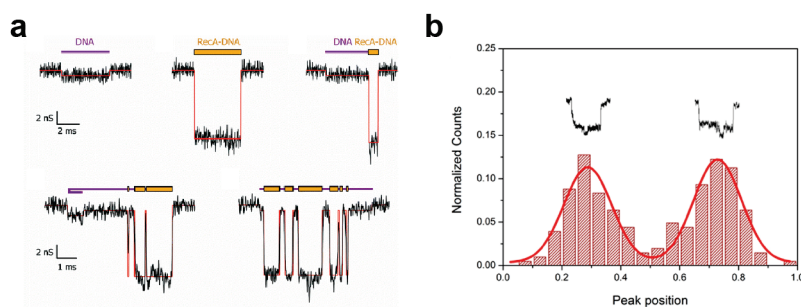
Figure 1.7 – **Detection of DNA-protein complexes with nanopores.** (a) Conductance signals of DNA, fully coated DNA-RecA and DNA partially covered with RecA. The figure is adapted from [96]. (b) Revealing the location of a zinc finger protein on its binding site. Two localisation histograms were observed since there are two possible directions for translocation of DNA. The figure is adapted from [97].

antibodies were uniformly distributed along a DNA molecule [100], zinc fingers [97] were identified at their specific binding sites. In the case of zinc fingers, nanopores allowed for discrimination of different conformations of the DNA-protein complexes (specifically or non-specifically bound) based on the shape of current drops [101]. In another sensing application methylated DNA fragments, markers of cancerogenesis, were detected with nanopores [103]. They were revealed by additional peaks corresponding to methyl-binding proteins [103].

In the case of a protein larger than the pore, a free end of DNA is used to drive the complex to the opening where the protein will stall the whole complex at the entrance (Fig 1.8). This process will result in the decrease of the baseline conductance [104, 105, 106]. Consecutive ramp of the voltage results in the increase in the force pulling the DNA through the pore and leads to the disruption of the complex at a certain force level. This experiment has similarities with the disruption of a DNA-protein complex using optical tweezers (Fig. 1.2) [34], however, providing higher throughput. One biological application tested with this technique is the influence of CpG methylation on nucleosome stability [105]. In these experiments it was shown that forces of similar magnitude had to be applied to disrupt the complexes at methylated and non methylated sites. This result led to the conclusion of negligible effect of methylation on stability of the complexes.

In conclusion, nanopores are an emerging sensing platform enabling single molecule resolution. The fabrication procedure of nanopores has developed drastically during the years aiming to decrease its costs of production and increase the sensing capabilities. The main advantages of nanopores are a high throughput and label-free detection as well as versatility that allows them to be combined with other technologies as it will be shown further.

1.3 Nanopores/nanocapillaries combined with optical tweezers

Combination of two techniques optical tweezers and nanopores was performed for the first time in Dekker's lab in 2006 [107]. Similar setups were also reported in two other groups later
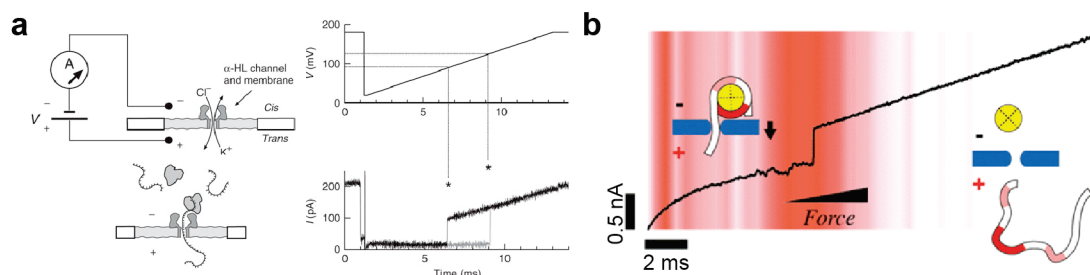
Figure 1.8 – **Measuring the stability of a DNA-protein complex in nanopores.** (a) After insertion of a single α-hemolysin in a lipid bilayer an end of ssDNA free from ExoI was driven inside it. Ramp of the voltage resulted in the disruption of the complex at a certain force level. Two different complexes of ssDNA-ExoI are shown in the figure (black and grey lines). The figure is adapted from [104] (b) A DNA-nucleosome complex unravelled in a solid-state nanopore by continuously increased voltage. The figure is adapted from [105].

on [108, 109]. Currently the technique is used in Anselmetti's lab, whereas in Keyser's and Radenovic's group glass nanocapillaries are in use instead of solid-state nanopores. During 10 years several single molecule biophysical phenomena were studied with this technique, which will be discussed here.

1.3.1 Combination of nanopores with optical tweezers

There were two main reasons for the combination of optical tweezers with nanopores 1. to control high translocation speeds of nucleic acids and 2. to obtain further insights into their translocation dynamics. In comparison to free translocations, addition of optical tweezers to nanopores gives the opportunity to measure the same event multiple times by performing back and forth cycles. In addition to measuring the current, one can record the electrophoretic force on nucleic acids inside nanopores using optical tweezers. Since the electrostatic force (F_{el}) is proportional to the potential (V) $F_{el} = qV$, where q is the charge, in these experiments the effective charge of dsDNA/RNA inside nanopores can be extracted [107, 110].

To perform experiments, first streptavidin-coated beads are modified with biotinylated dsDNA/RNA molecules and afterwards using optical tweezers the beads are positioned close to the nanopore (Fig. 1.9 a). It is worth mentioning, the precise location of the pore can be revealed by the increased baseline current due to induced heating of the solution by a laser beam [111]. Application of a positive voltage to the trans chamber results in a simultaneous displacement of the bead towards the pore and current drop (Fig. 1.9 b). The change in these signals was interpreted as an insertion of DNA inside the pore [107, 112]. The force acting on the DNA and measured with optical tweezers revealed 75 % reduction of its charge inside the nanopore. This effect was explained as a result of the electroosmotic flow (EOF) that takes place due to the negative charge of the pore walls and DNA backbone. The strength of the EOF depends on the size of the pore as it was shown later [113]. In small pores (radius < 5 nm) the Debye layer is compressed by the pore wall and the EOF originating from the DNA molecule is

11
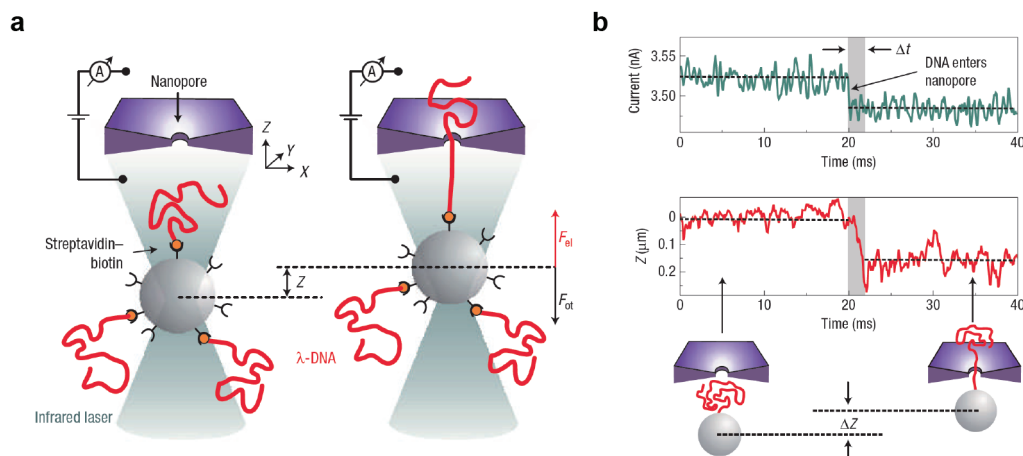
Figure 1.9 – **Combination of nanopores and optical tweezers.** (a) An optically trapped bead coated with DNA is positioned in the proximity of the nanopore. Application of the electric field leads to an insertion of the DNA and consequent displacement of the bead in the direction of the pore. (b) The DNA event was detected by a simultaneous displacement of the bead from equilibrium and a change in the baseline current. The figure is adapted from [107].

reduced. Moreover, the reduction of the negative charge of pore's walls by coating them with lipids also resulted in up to 85 % increase of the total force acting on the DNA [114]. These findings prove relevance of the EOF and consequently the drag force during translation of DNA through nanopores.

Not only were translocations of bare nucleic acids studied in this system, but also DNA-protein complexes. After the formation of a DNA-protein complex experiments were performed as described above. As the first example a DNA-RecA filament was used with the linear charge density ≈ 2 times more negative than that of bare DNA [115]. In agreement with theory the measured force acting on the complex was 2-4 times higher than on dsDNA not coated with RecA [115]. Moreover, a difference in the conductance drop was observed due to the difference in the sizes of DNA and DNA-RecA [115]. However, in this setup the interference of the reflected light from the bead and the membrane severely complicated the force measurements along the length of DNA whilst pulling it out [112]. To avoid this problem, two solutions were proposed using detection of backscattered light combined with spatial filtering [109] or video-based detection [116]. These modifications allowed for detection of single DNA-bound proteins along the DNA length (Fig. 1.10) [117, 118]. DNA-protein complexes were characterised by additional deviations in the force signal with respect to the level of the bare DNA (Fig. 1.10). In the case of DNA-EcoRI the force acting on the complex was lower than on the bare DNA. Mirrored profiles were observed for DNA-RecA patches. A stochastic model was developed that allowed to extract the effective charges of the complexes from the experimental results.
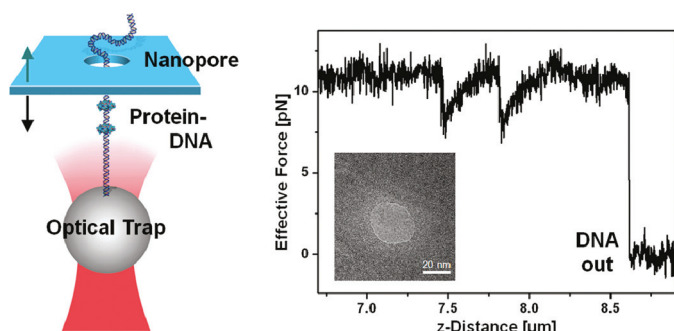
Figure 1.10 – **Detection of single DNA-protein complexes in nanopores combined with optical tweezers.** After formation of a complex between λ-DNA and EcoRI it was inserted in the nanopore and controllably pulled out. Two additional peaks in the force signal of the bare DNA correspond to DNA-EcoRI complexes. The figure is taken from [118].

1.3.2 Combination of nanocapillaries with optical tweezers

Glass nanocapillaries were used in combination with optical tweezers instead of pores for the first time in Keyser's group [119, 120]. There are a couple of advantages of having a nanocapillary instead of a nanopore in this system:

- fast fabrication and high signal-to-noise ratio of nanocapillaries [87];

- simple design of a fluidic cell;

- straightforward way to find a pore;

- stronger stiffness of optical tweezers in a lateral direction;

- absence of the light interference with a membrane;

- ability to integrate nanocapillaries with fluorescent imaging [121].

Detailed description of the setup and detection of biomolecules in it will be provided in the section Methods and Results and discussion, however some of the results obtained using this technique will be discussed below. Addition of optical tweezers allowed to characterise the electroosmotic flow generated by glass nanocapillaries measuring the rotation of an asymmetrical optically trapped bead [52, 122] (Fig. 1.11 a). Velocity and vorticity fields were mapped out in the proximity of a nanocapillary that were in good agreement with the classical Landau-Squire solution of the Navier Stokes equation [52]. Interestingly, reversal of the electroosmotic flow was observed at low salt concentrations (< 1 mM) that was explained by a major impact of the flow arising from the surface outside of the nanocapillary [122]. In addition to studying nanojets, nanocapillaries combined with optical tweezers shed light on the behaviour of DNA molecules in crowded environments [53] and the mechanism of its relaxation [123] (Fig. 1.11 b).

a

b
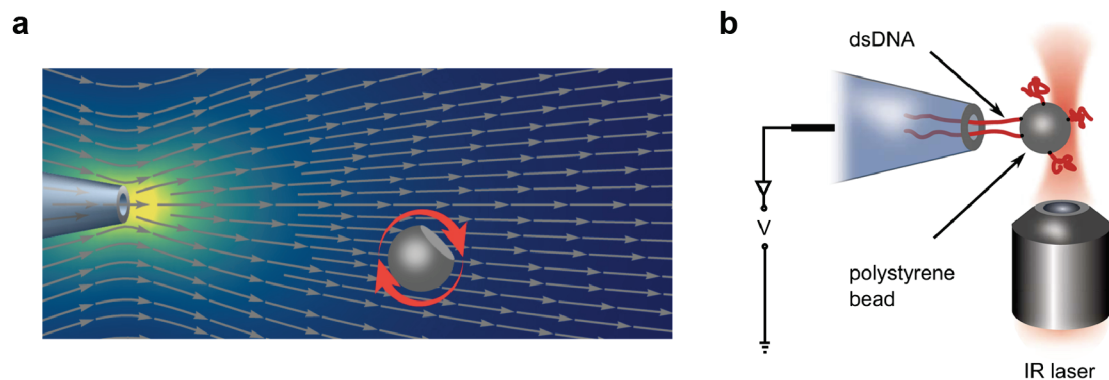
Figure 1.11 – **Combination of nanocapillaries with optical tweezers.** (a) Measurement of the rotational frequency of an optically trapped bead in the proximity to the nanocapillary allows to quantify the electroosmotic nanojets. The figure is adapted from [52]. (b) Application of the voltage across the nanocapillary opening leads to insertion of DNA molecules attached to an optically trapped bead. Several DNA molecules can be inserted for probing the force acting on them in crowded environments. The figure is adapted from [53].

In conclusion, the ability to measure the force and current signals and controllably translocate molecules through the opening makes nanopores/nanocapillaries combined with optical tweezers a powerful and flexible tool to study various applications from physics to biology.

2 Methods

All techniques that were used in the thesis are presented in this chapter. It provides details of how nanocapillaries were fabricated and integrated with optical tweezers, how experiments of insertion, stalling and reverse translocation of DNA were performed, how DNA-protein complexes were formed and finally how the system was modelled.

2.1 Fabrication of nanocapillary-based devices

Nanocapillary-based devices were used in experiments with free translocation of biomolecules and in combination with optical tweezers. In both cases the following procedure was performed: 1. fabrication (pulling) of a nanocapillary 2. tailoring of its size (shrinking) and 3. integration in a fluidic cell. In this section details of each step are described.

2.1.1 Laser-assisted pulling

In order to make nanopores, capillaries were pulled using a P-2000 laser pipette puller (Sutter) (Fig. 2.1 a). As a source of nanopores two types of quartz capillaries (Hilgenberg) with a 0.3 mm inner and 0.4 or 0.5 mm outer diameters were used. The second type was used only for free translocations of biomolecules, whereas the first one for both experiments with optical tweezers and free translocations. Due to the lower thickness of capillaries with an outer diameter of 0.4 mm it was easier to focus on the tip in experiments that involve optical tweezers. Depending on the type of capillary and required diameter of the opening, different pulling programs were used (Table 2.1). We pulled capillaries to diameters >100 nm and adjusted their opening sizes by further shrinking under scanning electron microscope (see next section). We noticed that the program's output (diameter, taper length, opening angle, tip shape, etc.) change between different machines of the same brand and also vary with time and ambient conditions. Thus, during the project the pulling programs had to be adjusted several times.
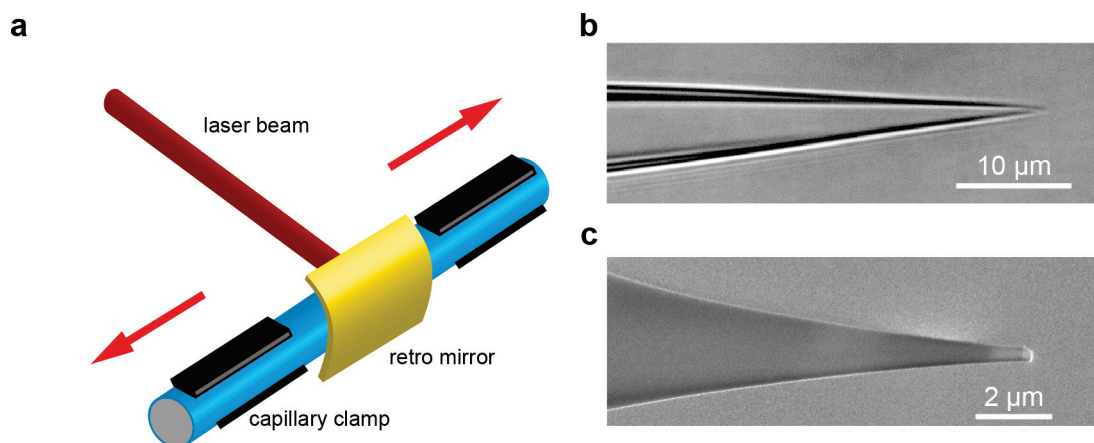
Figure 2.1 – **Fabrication of a nanocapillary with a laser-assisted pipette puller.** (a) A purchased capillary is fixed with two clamps from two ends. Activation of a program leads to simultaneous heating of the capillary in the centre with an IR-laser and moving two clamps apart. At the final point additional force is applied resulting in formation of two almost identical capillaries. (b) and (c) images of pulled capillaries under optical and scanning electron microscope, respectively.

Table 2.1 – **Programs used for pulling of quartz capillaries with an inner diameter of 0.3 mm and outer diameter of 0.4 mm using a P-2000 laser pipet puller.**

program	heat	filament	velocity	delay	pull	diameter, nm
1	620	0	30	140	200	100-150
2	580	0	30	140	120	200-300
3	620	0	30	140	150	150-200
4	600	4	10	145	0	
	600	4	10	145	140	200-300

2.1.2 Shrinking

On the next step the sizes of pulled nanocapillaries were tailored to the openings required in experiments. Pulled nanocapillaries were placed in a custom-made aluminium holder (Fig. 2.2) and imaged under scanning electron microscope (SEM) Merlin (Zeiss). Electron irradiation heats the glass and the surface stress leads to shrinking of the opening [89]. The shrinking rate is ~ 25 nm/sec and it depends on the accelerating voltage and beam current of SEM. Higher currents augment the energy density inside the glass and lead to higher shrinking rates. Higher shrinking rates are also observed at lower voltages due to lower penetration depths of electrons that do not increase the energy density at the surface [89]. In practice shrinking of a nanocapillary took on average a few minutes. The working distance was 2-6 mm, magnification 50-250 X, beam current 400-600 pA and acceleration voltage 2-3 kV. In Fig. 2.3 there is an example of a nanocapillary with a starting diameter of 37 nm that was continuously shrunken to the size of 6 nm. This is the capillary with the smallest size we were able to fabricate. Usually the resolution of SEM Merlin limits the opening size just below 10 nm in diameter. This size is approximately twice smaller than for just pulled capillaries [86]

and in the range with the size of capillaries coated with Al_2O_3 [90].
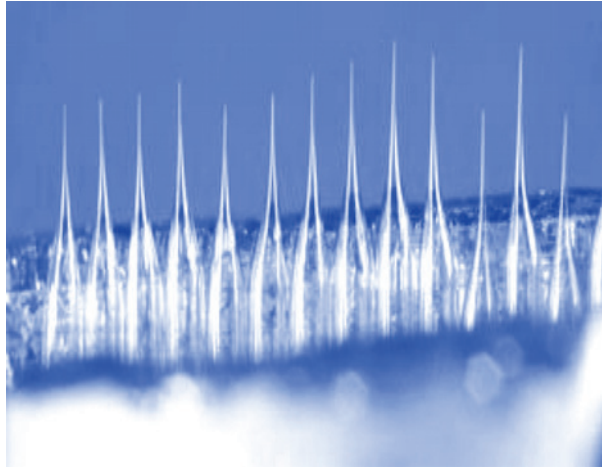
Figure 2.2 – **Photograph of capillaries in a SEM holder.** The photograph was taken by Lorenz Steinbock.

The geometry of a shrunken capillary deviates from a cone (Fig. 2.4 a) and can be approximated by two truncated cones , where T and t - the taper lengths of large and small cones, respectively, β and α - the opening angles of large and small cones, respectively, R_0 - the radii of the opening (Fig. 2.4 b). Longer exposure times of nanocapillaries to electron irradiation normally result in more restructured tips. It is worth mentioning, even though this technique allows to control the size of nanocapillaries in real time, the geometries of nanocapillary tips can vary between different capillaries. This happens due to variation of the position of capillaries in the holder and stochastic nature of shrinking.
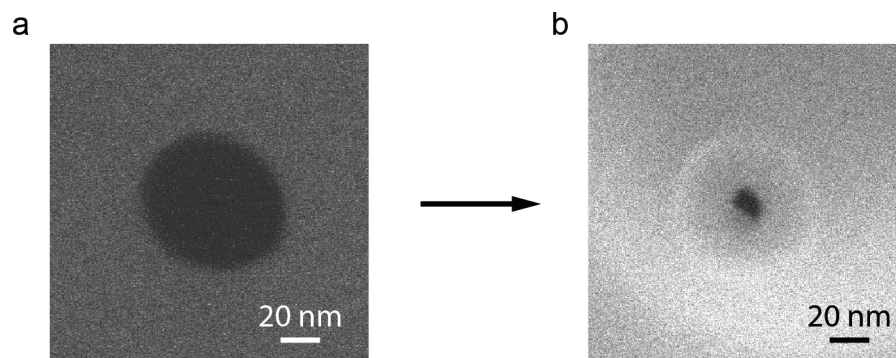
Figure 2.3 – **Shrinking of a nanocapillary under SEM** (a) A capillary of 37 nm in diameter was continuously shrunken to (b) 6 nm under SEM. The images were taken by Lorenz Steinbock.

2.1.3 Integration in a fluidic cell

To perform experiments with shrunken nanocapillaries we transferred them to a fluidic cell that consists of two reservoirs made from PDMS (Fig. 2.5). Cis and trans chambers of the

Figure 2.4 – **SEM micrograph and sketch of a shrunken nanocapillary.** (a) Nanocapillary ≈ 23 nm in diameter shrunken under SEM. (b) We approximated the geometry of a shrunken nanocapillary with two truncated cones, where T and t – the taper lengths of large and small cones, respectively, β and α – the opening angles of large and small cones, respectively, R_0 – the radii of the opening.
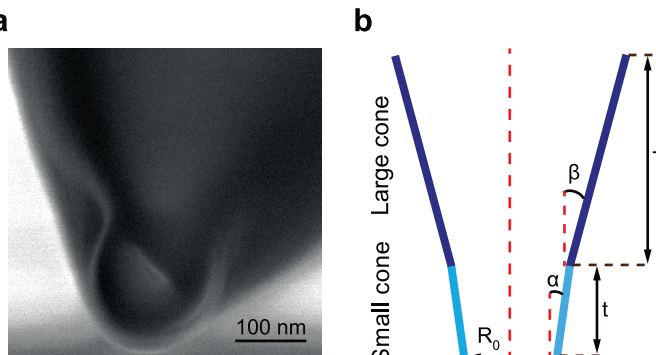
fluidic cell were connected only through a nanocapillary opening. The cell was sealed from the bottom with a 0.15 mm thick coverslip (Menzel-Glasser). To make the surface of PDMS and glass hydrophilic, the sample cells were treated with oxygen plasma at the power of 50 W for 2-5 min. Afterwards the chambers were filled with a buffer filtered through an Anotop 25 filter (Watman) with a pore size of 0.02 μm. The buffer varied depending on the application and its composition is presented in each chapter of Results and discussion. Before an experiment, air bubbles inside the nanocapillaries were removed by evacuating them with a vacuum pump for 1-5 min. It is worth mentioning, omitting of the plasma cleaning step would not allow us to completely fill a nanocapillary with a buffer. We also noticed that it was easier to get rid of bubbles in capillaries with large sizes.
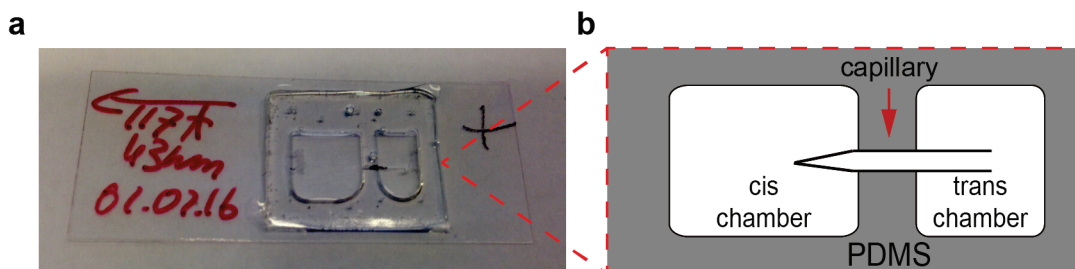
Figure 2.5 – **Nanocapillary fluidic cell.** (a) A photograph of the cell containing a 43 nm nanocapillary with an outer diameter of 0.4 mm. (b) A schematic of the fluidic cell that is shown in (a).

To apply an electrical field in experiments Ag/AgCl electrodes were used. The electrodes were chlorinated right before the experiment by applying a DC voltage of 1-3 V in 1-2 M KCl solution for 30-60 sec. Coating of the electrodes was confirmed by a change in their colour.

Fluidic cells filled with a buffer were not stored for more than one day. They were not reused after experiments due to potential change of the salt concentration inside capillaries during their storage and absorption of biomolecules and other substances during experiments. Thanks to the fast and cheap fabrication process a new fluidic cell could be easily fabricated.

2.1.4 Passivation of capillary walls with lipids

During experiments with optical tweezers and nanocapillaries we noticed that sometimes DNA and DNA-protein complexes get stuck to the capillary. In this case, the signal traces became noisy and sometimes nanocapillaries had to be discarded. To prevent non specific interactions of biomolecules with glass we followed three basic rules:

1. keep the salt concentration in the experimental buffer low (normally <0.1 M KCl for experiments with optical tweezers). The repulsion between two negatively charged surfaces of DNA/protein and glass can be decreased due to the significant effect of screening at high salt concentration [124].

2. avoid using nanocapillaries with low diameters (<20 nm) to increase the distance between a DNA/protein molecule trapped inside and glass walls.

3. add a surfactant TWEEN 20 to the experimental buffer [125].

However, these principles put some limitation on the system and moreover do not completely prevent non specific interactions of biomolecules with the walls. For this reason we tried a method of neutralization of the glass surface charge by coating the walls with lipids. This technique has already proved its efficiency in the case of solid-state pores [57] and nanocapillaries [91].

To coat the walls of nanocapillaries with lipids we followed the protocol adapted from [91]. We dissolved 2-oleoyl-1-palmitoyl-sn-glycero-3-phosphocholine (POPC) (Sigma-Aldrich) in chloroform to a concentration of 3.25 mM. The solution was let to evaporate under the hood and afterwards dissolved in 150 mM KCl, 10 mM HEPES, pH 7.5 to a final concentration of 2 mM. Small unilamellar vesicles (SUVs) were formed by ultrasonication of the solution for 30 min using Vibra Cell (Sonics & Materials Inc.) and filtered through an Anotop 20 filter (Whatman) with 20 nm pores. The obtained SUVs were added to a cis chamber of a nanocapillary and incubated for 5-10 min at room temperature. Afterwards the solution in the cis chamber was exchanged to an experimental buffer. Successful coating of nanocapillaries decreased its conductance due to the decrease of the size of the opening and increased the force acting on DNA due to the decrease in the electroosmotic flow (Fig. 2.6) [57, 91, 114].

However, we found several drawbacks in the coating procedure. First, the success rate was below 50 %. In half of the cases we did not see coating. Second, after coating the current signal became noisy resulting in a decrease of the signal-to-noise ratio. Third, we observed that the lipid layer was not particularly stable. Based on the conductance characteristics it could get detached after several minutes of experiments. Lastly, in the successfully coated capillaries we still observed sticking of some DNA-protein complexes to the walls.

Due to these reason we have not used lipid capillaries in experiments with DNA-protein complexes. It is worth noting that the further methods of passivation of nanocapillary walls
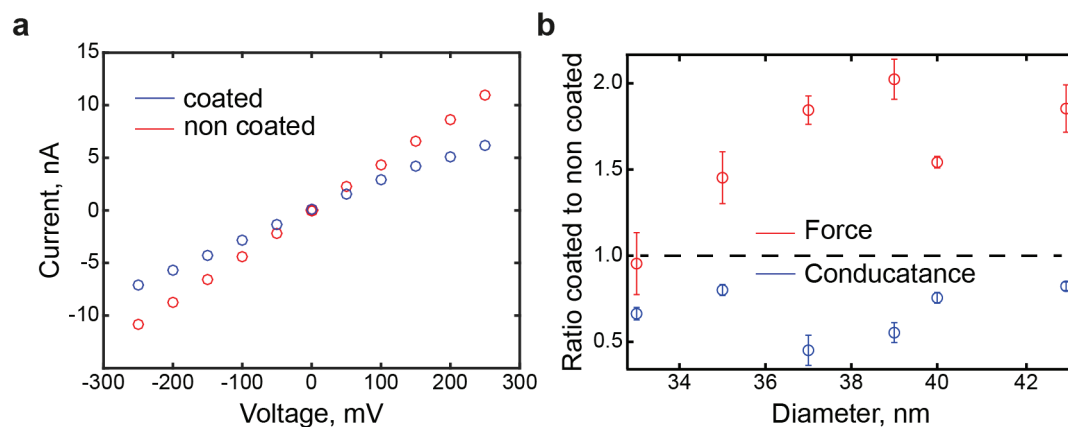
Figure 2.6 – **Lipid coating of nanocapillaries.** (a) IV curves of a non coated (red) and coated with lipids (blue) nanocapillary 33 nm in diameter. The conductance decreased from 43 to 27 nS after coating. (b) Change in the conductance and force on DNA in 6 nanocapillaries in the range of 33-43 nm in diameter. Y axis is represented as a ratio between coated and non coated capillary. Coating of nanocapillaries resulted in simultaneous decrease of conductance and increase of electrophoretic force acting on DNA.

have to be developed. Experiments on coating glass capillaries with polymers to prevent non specific interactions with biomolecules are described in Ref. [126] and can potentially be adapted in our system.

2.2 Combination of nanocapillaries with optical tweezers

To perform experiments a fluidic cell, containing a nanocapillary with a desired size, was mounted on the system that combines optical tweezers and current preamplifier. In the cis chamber of the fluidic cell, beads covered with DNA were used to liaise optical tweezers and nanocapillaries. In this section we provide a description of the setup, protocol for formation of DNA-coated beads and calibration of optical tweezers.

2.2.1 Setup description
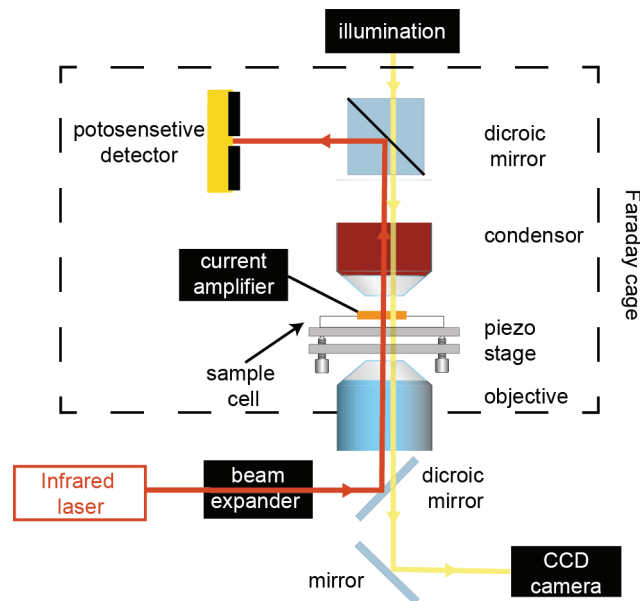
Figure 2.7 – **Schematic of the setup combining nanocapillaries and optical tweezers.** The figure is adapted from [127].

The setup combines optical tweezers and current preamplifier, whose head is enclosed in a Faraday cage (Fig. 2.7). Two types of lasers were used in this thesis: a Nd:YVO4 solid-state laser (Coherent, 2.5 W, λ = 1064 nm) and a Nd:YAG fibre-coupled laser (Sacher Lasertechnik, 1 W, λ = 830 nm). The exchange of the lasers took place due to requirement of the Nd:YVO4 laser for another setup in the laboratory. The lasers were aligned prior to experiments to have symmetric shape of the beam and maximal power at focal plane. They were operated at the maximal power to have the highest stability. The laser beam was expanded by a telescope (3x) to slightly overfill the back aperture of the water immersion microscope objective (Nikon, 60x, 1.2 NA). The transmitted light was collected by a condenser (Olympus, 0.8 NA) and deflected onto a photosensitive detector (PSD) (Pacific Silicon Sensor Inc.) (Fig. 2.7). The PSD allowed to measure the signals in X, Y directions (dX and dY, respectively) and its sum. Before experiments dX and dY signals on PSD were aligned to zero and sum was maximised. A sample cell was positioned on a piezoelectric nanopositioning stage (Mad City Laboratories) and illuminated

by a white light source (Thorlabs) from the top. An image was formed on a CCD camera (Thorlabs) and projected on a computer screen. Ag/AgCl electrodes (see section 2.1.3) were inserted in cis and trans chambers of the sample cell and connected to an Axopatch 200B current amplifier (Molecular Devices), used for applying the potential and measuring the ionic current. The sample cell was enclosed in an aluminium Faraday cage, which blocks the influence from external electric fields. Current and force signals were recorded using a custom-made LabVIEW program at the sampling frequency of 10 KHz (Fig. 2.8). This frequency was chosen as a trade off between the size of the recorded file and time resolution. For the experiments with optical tweezers we did not need to record fast events since the DNA was trapped inside the nanocapillary and pulled out at a controlled speed of 100-800 nm/sec. Positioning of a bead and controlled translocation of DNA was performed using a joystick operated through the LabVIEW program. The analysis of the data was performed using a custom-made Igor or Matlab script.
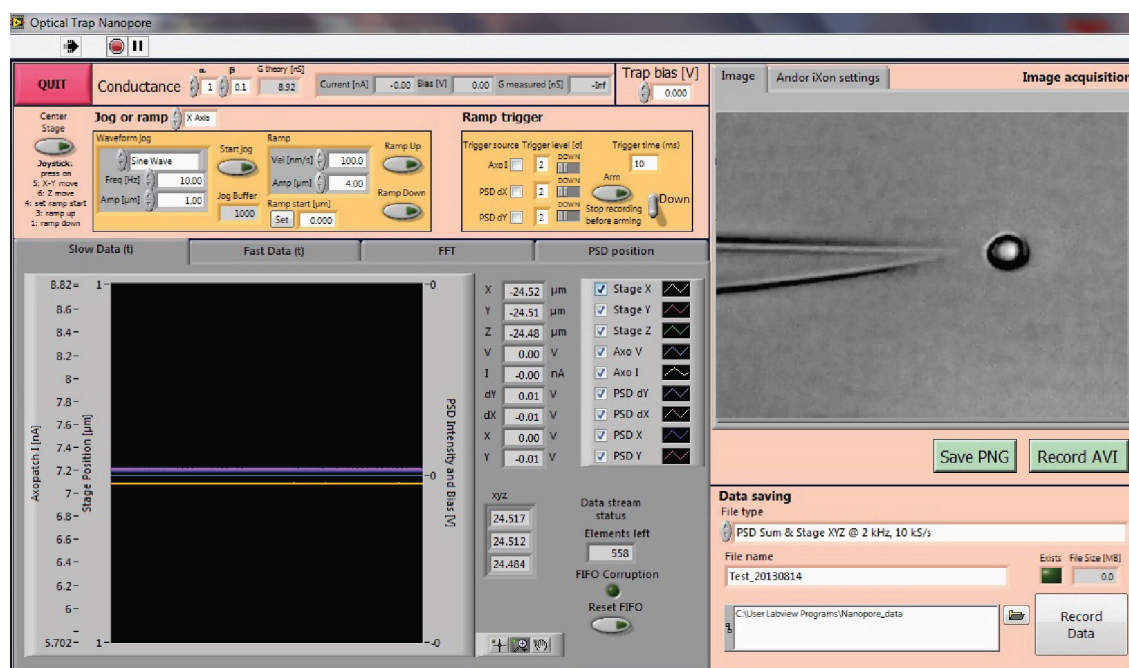
Figure 2.8 – **Screenshot of a LabVIEW program used in experiments.**

2.2.2 Formation of bead-DNA complexes

Bead-DNA complexes serve as a connector between optical tweezers and nanocapillaries. The DNA part of the construct is inserted in a nanocapillary whereas the bead is held by an optical trap. In order to make DNA-coated beads, we incubated 3 μm polystyrene streptavidin-coated beads (Bangs Laboratories) with DNA molecules biotinylated only from one end. Two types of DNA molecules were used: λ-DNA and a PCR fragment of DNA of different lengths. To attach a biotin tag to λ-DNA (New England BioLabs), we ligated it with a 3'-end biotinylated oligonucleotide complementary to the *cos2* overhang of λ-DNA accordingly to [128]. A PCR

fragment with a biotin from one end was obtained by performing PCR using one 18-25 nt long primer (Microsynth) with a biotin tag on a 5' end and the second primer without biotin (see details in Table 2.2). Both primers had similar length and melting temperatures. PCR was performed from a template dsDNA (plasmid or linear, see details in Table 2.2) using Taq polymerase (New England BioLabs) and following the protocol from the manufacturer. The Macherey-Nagel purification kit was used to purify a PCR product. Its concentration was measured using a NanoDrop 1000 Spectrometer.

Table 2.2 – **Primers and template DNA used in PCR.** PCR fragments used in section Results and discussion were obtained using listed primers and templates. The sequences of template DNA are shown in Appendix. (B) in the primer sequences means biotin.

thesis section	template	primers	PCR fragment length, kb
3.1	genomic DNA of phage T7	ATC GAC CCT GAG GAA CTC ATC (B)CAC CAT (B)CT(B)A ACA GTC CCA TCA	5.5
3.2	genomic DNA of phage T7	TGG GAA GGC TTT AGG TGT AGC TGT (B)GGG GAC CTC CTT CTT GGG TTC	9.0
3.3	plasmid pRL574	CGG TGA TGA CGG TGA AAA CC (B)CTT TTC GGG GAA ATG TGC GC	7.4
		AGG CAC CTA TCT CAG CGA TCT (B)AGC GTC AGA CCC CGT AGA AA	7.3
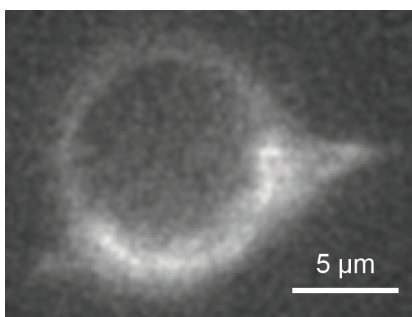
Figure 2.9 – **Image of a bead-DNA complex under fluorescent microscope.** 10 μm streptavidin-coated beads were modified with λ-DNA stained with a fluorescent intercalating dye YOYO.

We incubated 3 μm streptavidin-coated beads with a DNA construct in ratio 100-1000 DNA molecules per 1 bead (depending on the DNA length) in the buffer, containing 100 mM KCl, 1-10 mM Tris/HCl, pH 7-8 during 15-90 min. Afterwards we washed the beads 2-3 times in the incubation buffer to remove non bound DNA molecules using a centrifugation step and resuspended them in the buffer used in experiments. A sample of 1-3 μl of 0.1-1 mg/ml DNA-coated beads was added to the buffer in the cis chamber, and the solution was carefully mixed to avoid breaking a capillary tip and shearing DNA molecules. We found that this is an optimal concentration of beads for our experiments since it allows us relatively quickly find and trap a bead not risking to observe frequent displacement of one trapped bead by another

one.

2.2.3 Calibration of optical tweezers
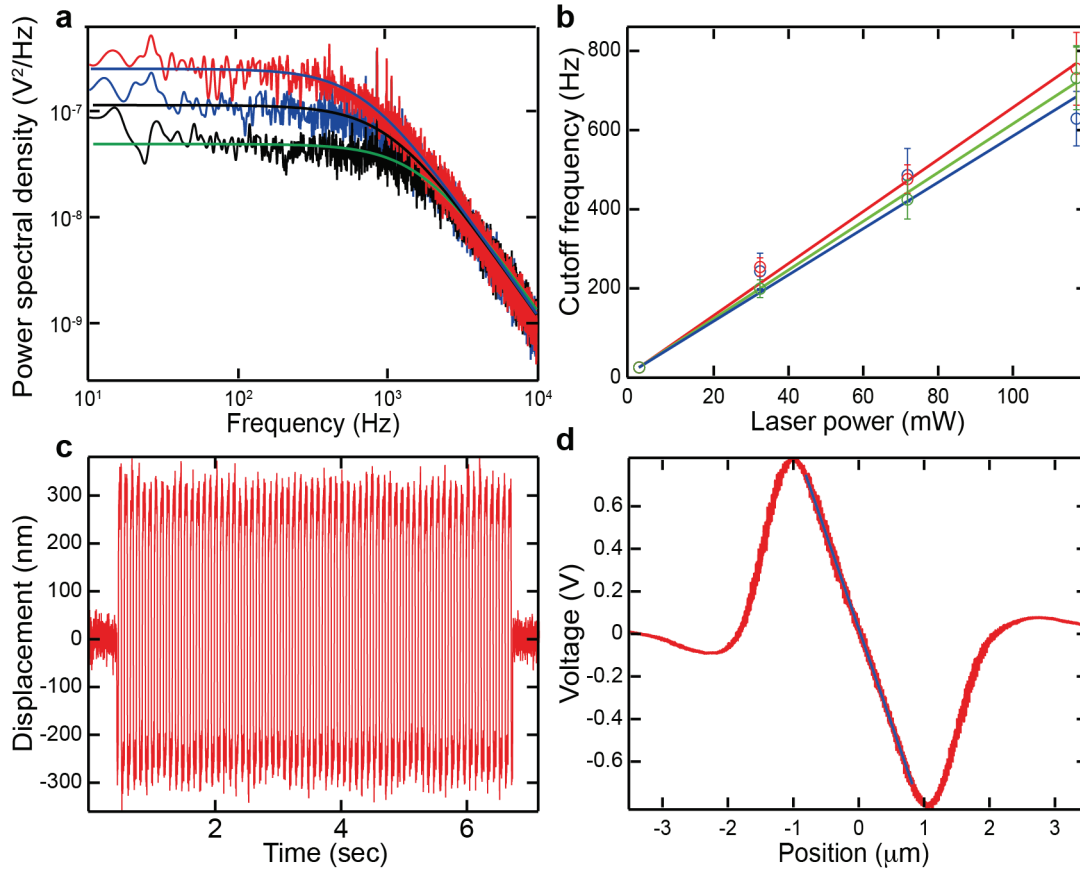
Figure 2.10 – **Calibration of optical tweezers.** Calibration performed on 3 μm polystyrene beads. (a) Power spectral density as a function of frequency for an optically trapped bead. The laser power at sample plane was 95 mW (red), 150 mW (blue), 250 mW (black). (b) Comparison of cutoff frequencies for non-coated beads (red), beads incubated with 5.5 kb DNA in ratio 1:500 (green), beads incubated with λ-DNA in ratio 1:500 (blue). The cutoff frequency was 12 % higher for non-coated beads than for λ-DNA coated beads, and 7 % higher than for 5.5 kb DNA coated beads. The cutoff frequency was estimated at each power on 5-6 different beads at least 5 μm away from any surface. The laser power was measured at sample plane. (c) A displacement of an optically trapped bead induced by the flow applied due to the movement of the nanopositioning stage with triangular pulses at a frequency of 10 Hz and with an amplitude 4 μm. Measuring the displacement allows to extract the stiffness of the trap using a Stokes method (eq. 1.2). (d) Estimation of sensitivity (V/μm) of optical tweezers by scanning a bead stuck to a cover slide. The position of the laser was changed using the nanopositioning stage and voltage was recorded on the position sensitive detector. The voltage response of the position sensitive detector is linear (blue line) within approximately 750 nm from a bead centre. During the experiments we did not observe the displacement of the bead from the trap centre higher than 500 nm. The figure is taken from [127].

Calibration of optical tweezers is required to convert a signal measured on PSD (Volts) to the force (Newtons) as it is described in section 1.1.1. We used the power spectrum density

(PSD) and Stokes methods for calibration of optical tweezers [32]. In the first case thermal fluctuations of a 3 μm trapped bead were recorded at 500 kHz during 5-10 s, and afterwards the cutoff frequency was extracted by fitting a Fourier transform of the fluctuations to Lorenzian function (Fig. 2.10 a, eq. 1.1). The cutoff frequency scaled linearly with the laser intensity (Fig. 2.10 b). Remarkably, the cutoff frequency was less for beads coated with DNA molecules due to their additional friction [112]. The Stokes method was used to calibrate the optical tweezers based on the measurement of the displacement of a trapped bead induced by a movement of a nanopositioning stage (Fig. 2.10 c). The conversion from the signal measured by the position sensitive detector to the displacement was performed on a stuck bead (Fig. 2.10 d) or using thermal fluctuations of a bead according to the section 1.1.1. Calibration was performed on several beads (usually more than 5) and at least 5 μm from any surface to avoid any proximity effects. The error in the stiffness estimated by PSD and Stokes methods did not exceed 20%.

2.3 Sensing of biomolecules in nanocapillaries

We performed sensing of biomolecules in nanocapillaries during their free and controlled (in combination with optical tweezers) translocations. In the first case we detected DNA, proteins and DNA-protein complexes and in the second DNA and DNA-protein complexes. Free transactions were carried out to support the results observed in experiments with optical tweezers.

2.3.1 Free translocations

In contrast to controlled translocations, free translocations were carried out in the system without optical tweezers. In this case, biomolecules diffuse to the area close to a nanocapillary opening and afterwards they are driven inside by electrostatic forces. Before performing translocations of biomolecules IV curves of nanocapillaries were measured (Fig. 2.6 a). For experiments we used only capillaries that demonstrated the right conductance values, low noise and current rectification characteristics [87]. Free transactions of biomolecules (DNA, proteins and DNA-protein complexes) were performed in glass nanocapillaries with diameters of 10-50 nm in the buffer containing 0.4 or 1 M KCl, pH 7-8. Translocation events took place at 150-500 mV. They were recorded using an Axopatch 200B current amplifier (Molecular Devices) at 100 KHz and a custom-made LabVIEW program in accordance with Steinbock et al. [87]. The events were analysed using the OpenNanopore software [129]. One of the examples of free translocations is demonstrated in Fig. 2.11.

2.3.2 Controlled translocations

During voltage-driven translocation through a nanocapillary a DNA molecule experiences the electrophoretic force (F_{ep}) consisting of the bare electrostatic force (F_{bare}) opposed by the drag force (F_{dr}) [131]:

$$F_{ep} = F_{bare} - F_{drag} \tag{2.1}$$

where F_{dr} is originated from the electroosmotic flow of counter ions that screen the negatively charged DNA backbone and glass walls of a nanocapillary. In order to measure the electrophoretic force acting on DNA inside nanocapillaries, we used optical tweezers and DNA-coated beads as a force transducer (Fig. 2.12 a). The force obtained in such a system - stalling force is in balance with the electrophoretic force $F_{stal} = -F_{ep}$.

In a typical experiment, we optically trapped a bead and positioned its surface 3-4 μm from the capillary opening. Next, we applied a positive potential of 50-250 mV in the trans chamber. The voltage attracted DNA molecules attached to the optically trapped bead and forced it to
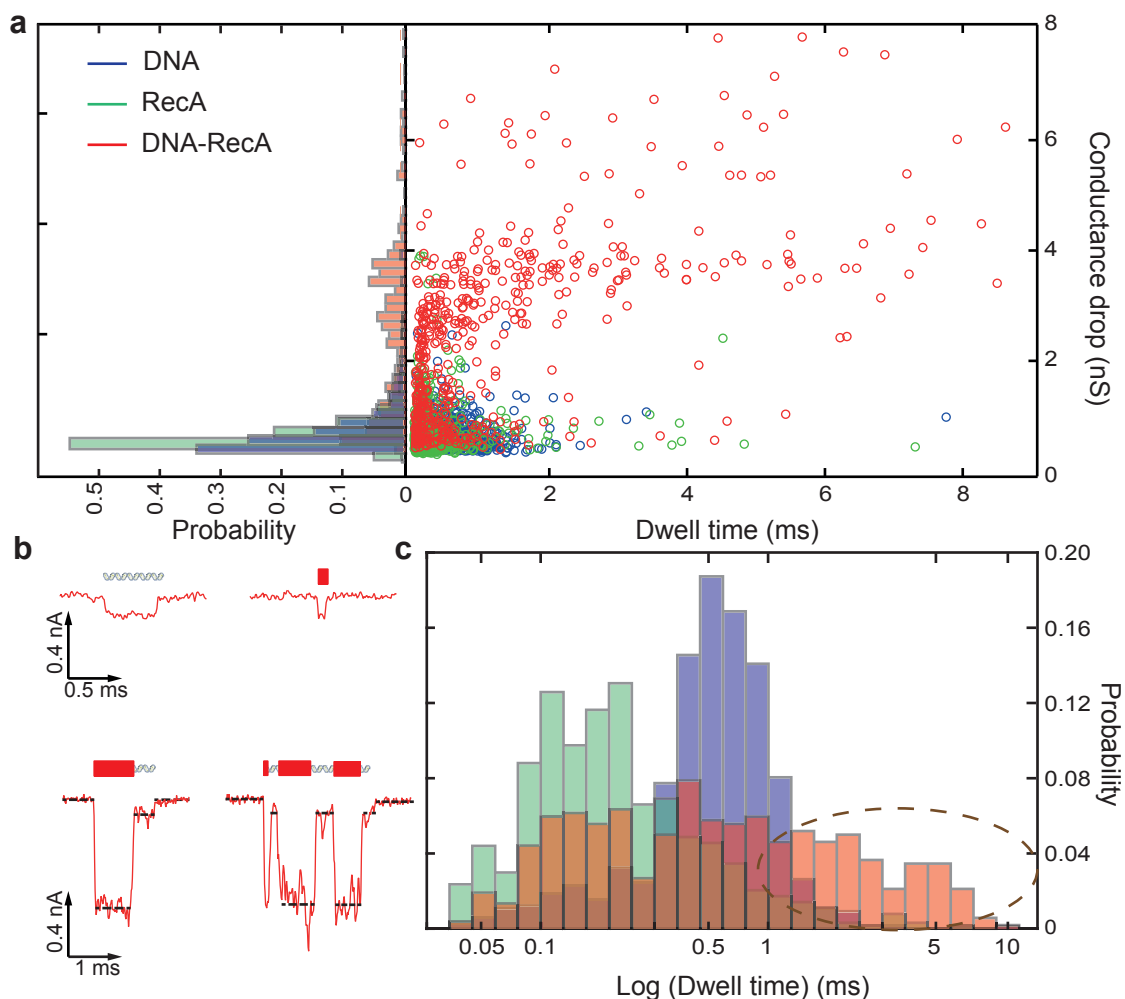
Figure 2.11 – **Translocation of DNA partially coated with RecA in a glass nanocapillary.** (a) A scatter plot and conductance histogram recorded for λ-DNA, RecA and λ-DNA partially coated with RecA. We obtained 646 events for the DNA, 636 for RecA and 520 for DNA-RecA. Molecules were consequently translocated through the same glass nanocapillary and after recording of the data for each molecule the *cis* chamber was flushed with a buffer solution. The theoretical coverage of λ-DNA with RecA was $\approx 25\%$. Based on the conductance drops and dwell times we observed a mixture of RecA not bound to DNA, non modified DNA and DNA-RecA in the solution. RecA proteins and DNA were characterised by similar conductance drops, whereas a DNA-RecA complex had an additional peak with a higher conductance drop. (b) Selected translocation events of λ-DNA, RecA and λ-DNA partially coated with RecA. Noteworthily, the presented time scale for DNA and RecA translocation events is twice shorter than for DNA-RecA. Conductance drops of DNA partially coated with RecA had two levels corresponding to the bare DNA and DNA-protein complex. (c) A dwell time histogram of the scatter plot in (a). In the case of DNA-RecA there were events corresponding to translocation of free RecA and DNA and events with longer dwell times (marked with a brown ellipse). High distribution of dwell times of DNA-RecA could be attributed to partially coating of the DNA with the protein. Lower electrophoretic force acting on the nucleoprotein filaments can be the reason for slower translocation of DNA-RecA than DNA, although we cannot exclude the possibility of its stronger interactions with glass walls. 1.5 times extension of partially coated λ-DNA could not result in the presence of events with much longer dwell times [96]. All data were acquired in a 35 nm glass nanocapillary at 250 mV in 1M KCl, pH 7.4. The figure is taken from [130].

27
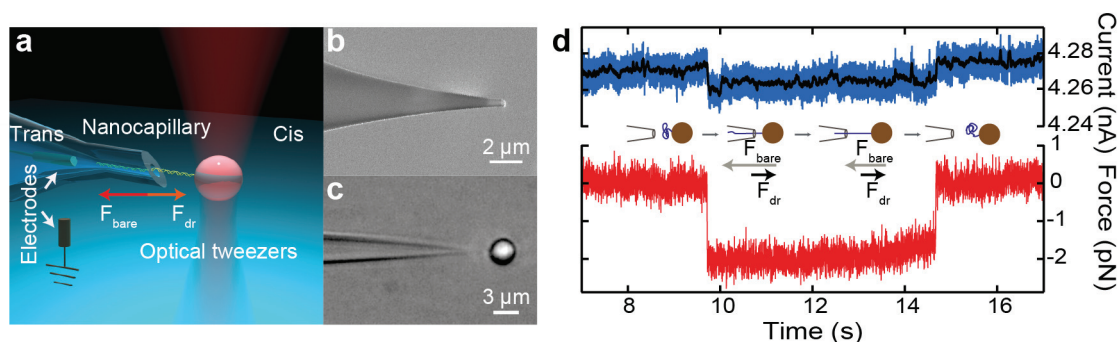
Figure 2.12 – **Detection of DNA in the setup.** (a) Schematic of the setup (not to scale). A DNA-coated bead is optically trapped, and after application of the positive voltage to the trans chamber, a DNA molecule is stalled inside a nanocapillary. (b) An SEM image of a pulled nanocapillary. (c) An image of an optically trapped DNA-coated bead positioned in front of a nanocapillary. (d) Data from a typical experiment in which a single DNA molecule is inserted inside a nanocapillary, followed by reverse translocation of the DNA. The simultaneous change of the current and the stalling force signals corresponds to the capturing of a DNA molecule. After 12 sec, reverse translocation of the DNA is activated using a nanopositioning stage with a velocity of 250 nm/sec. The simultaneous restoring of the stalling force and the current to the initial levels corresponds to the extraction of the single DNA molecule from the nanocapillary. The schematic represents the consecutive steps of the experiment. The arrows represent the direction of the bare electrostatic force (F_{bare}) and the drag force (F_{dr}) simultaneously acting on DNA. The experiment was conducted with a 32 nm nanocapillary, in 1 M KCl, pH 8.7, at 100 mV using a 5.5 kb DNA fragment. The figure is taken from [127].

displace towards the capillary opening. If we did not observe a capture of the DNA within 90 sec, we decreased the distance between the bead and the tip by using a piezoelectric nanopositioning system. Normally, the λ-DNA capturing events took place at a distance of 1.5-3.5 μm from the bead surface to the capillary opening, whereas in the case of a short 5.5 kb DNA fragment we had to decrease the distance down to 0.5-1.5 μm. This observation can be explained by the difference in gyration radius of these DNA fragments [132] and was previously demonstrated [108]. The translocation of a DNA molecule attached to a bead resulted in a simultaneous change in the stalling force and nanocapillary conductance (Fig. 2.12 d). Controllable insertion of only one molecule inside a glass nanocapillary was achieved by adjusting the number of DNA molecules on the bead surface, the distance between the beads and glass nanopores, and the applied voltage. After stalling DNA inside a nanocapillary, its reverse translocation was performed by using the piezoelectric nanopositioning stage at a velocity of 100-800 nm/sec with a single step of 1.5 nm (Movies 1 and 2, see section 3.1.5). At the distance corresponding to the length of DNA, we observed restoration of the conductance

and stalling force to their initial levels (Fig. 2.12 d).

It is worth mentioning, in the case of pulling DNA-protein complexes outside of a nanocapillary the same protocol was used. Although the force and current traces were characterised by additional peak corresponding to a protein (Fig. 3.8).

2.4 Formation and detection of DNA-protein complexes

In this section we will discuss different DNA-protein complexes that were used in this work; the reasons for choosing them, conditions for formation of the complexes and occupancy observed in experiments with optical tweezers and nanocapillaries. In the second part of the section we will describe techniques that we used to detect the formation of DNA-protein complexes as reference methods to our setup.

2.4.1 Formation of DNA-protein complexes

In this thesis 8 different DNA binding proteins were tested in the system combining nanocapillaries and optical tweezers (Table 2.3, Fig. 2.13). Such proteins as ComEA, SpoIIIE, nucleosomes and dCas9 were provided by collaborators whereas all others were purchased. We sought for proteins that bind to specific sites on DNA and form stable complexes that can be observed in experiments with high frequency. Two proteins non specifically binding to DNA RecA and ComEA were tested first due to the ability to get high concentration of DNA-protein complexes on a random DNA strand. All other tested proteins had specific sites on DNA and bound to these locations. Noteworthily, SpoIIIE and nucleosomes having preferences to specific regions still had strong affinity to non specific regions of DNA. However, in all cases we observed non specific binding events. Another important criterium is an ability of the protein to form stable complexes with DNA. This fact would allow to observe the complexes during long period of time and get large statistics of events. For both non specifically binding proteins RecA and ComEA high occupancy of complexes was observed. Only for such specifically binding proteins as ComEA, RecA, RNAP (only T7A1 promoter) and dCas9 we observed relatively high occupancy, meaning that more than 20 % of different DNA molecules taken out of the capillary contained a formed complex. The choice of RecA and EcoRI proteins allowed us to compare our system with the setup combining optical tweezers with nanopores [118]. The localisation results obtained with dCas9 and RNAP specifically bound to their sites will be discussed in the section 3.3 of Results and discussion.

Table 2.3 – **DNA-binding proteins and their characteristics.** Specificity shows if there are specific binding sites for the protein on DNA; occupancy corresponds to the probability to detect the complex in the system.

protein name	specificity	occupancy
RecA	no	high
EcoRI	yes	low
RNAP	yes	high
ComEA	no	high
SpoIIIE	yes/no	moderate
EcoRV	yes	low
Nucleosomes	yes/no	moderate
dCas9	yes	high
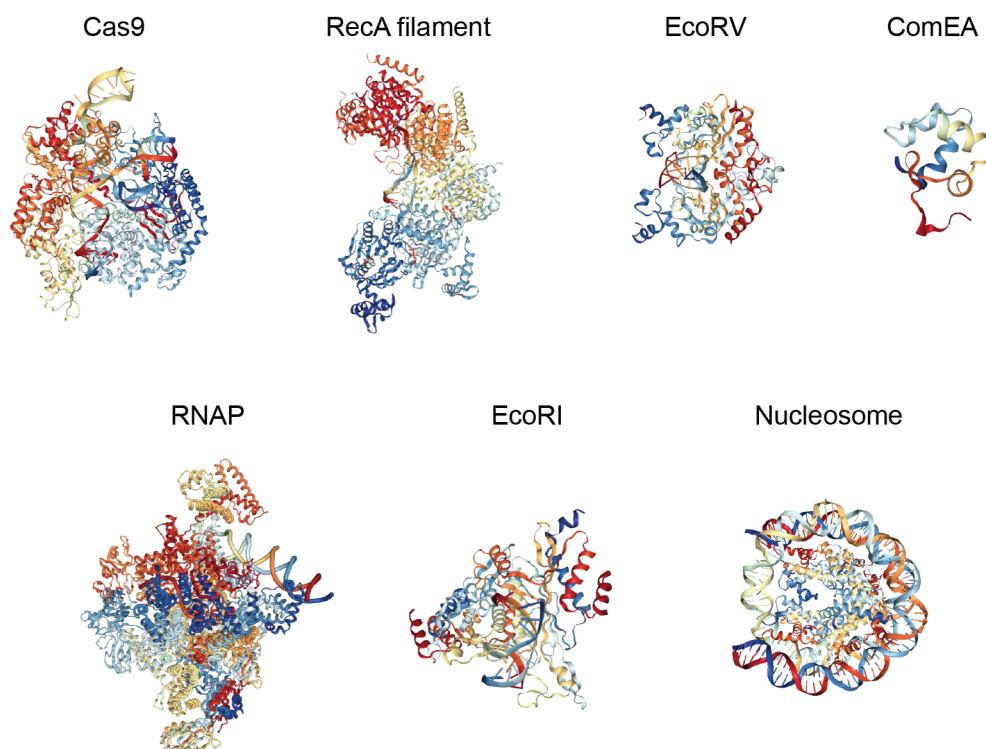
Figure 2.13 – **Structures of DNA-protein complexes used in this thesis.** The structures were taken from PDB (Protein Data Bank). Note that there was no available structure of SpoIIIE and ComEA in the complex with DNA (only protein).

Conditions used during complex formation are described in Table 2.4. It is worth noting that different conditions (buffer composition, temperature, incubation time) have been tried for the same protein in preliminary experiments. Table 2.4 demonstrate the conditions in which the most successful results were achieved. The main results of the work were obtained on dCas9, RNAP, RecA and EcoRI proteins and therefore detailed protocols for formation of their complexes will be outlined below.

DNA-RecA complexes were formed by incubating 50 pM of λ-DNA with 100 nM-6.6 μM of RecA (New England BioLabs) and 85 μM-5.75 mM of ATPγS (Sigma-Aldrich) in the buffer containing 70 mM Tris/HCl, 10 mM MgCl$_2$, 5 mM DTT, pH 7.6 at 37 °C, 60 min. The ratio of DNA to RecA and ATPγS was adjusted depending on the required coverage of DNA molecules.

To form DNA-EcoRI complexes 50 pM of λ-DNA (New England BioLabs) was incubated with 50 nM EcoRI (Invitrogen) in the buffer, containing 150 mM NaCl, 10 mM HEPES, 50 μM DTT, 1 mM EDTA, 100 μg/ml BSA at 30 °C, 30 min.

In the case of dCas9, first, 140 nM of guide RNA was mixed with $\approx$ 7 nM of dCas9 in the buffer containing 20mM HEPES, pH 7.5, 100mM KCl, 5mM MgCl$_2$, 1mM DTT, 5% glycerol and in the presence of 0.5 units of RNAse inhibitors (Roche) for 15 min at 37°C, 250 rpm. It is worth mentioning, we used a modified version of Cas9 with an attached GFP protein and that

binds to a location site and does not cut it (dCas9). After formation of a dCas9-RNA complex λ-DNA was added to the mixture (normally in ratio 1 molecule of DNA to 140 molecules of the complex) and incubated for 30 min at 37°C.

Table 2.4 – **Conditions for formation of DNA-protein complexes**

protein name	buffer composition	time	temp., °C
RecA	70 mM Tris/HCl, pH 7.6,10 mM MgCl$_2$, 5 mM DTT	60	37
EcoRI	10 mM HEPES, 150 mM NaCl, 50 μM DTT, 1 mM EDTA, 100 μg/ml BSA	30	30
RNAP	25 mM Tris/HCl, pH 8.0, 100 mM KCl, 4 mM MgCl$_2$, 1 mM DTT, 3 % glycerol, 0.15 mg/ml BSA	30	37
ComEA	3 mM Tris/HCl, PH 7.5, 150 mM KCl, 1 mM EDTA	15	22-25
SpoIIIE	50 mM Tris/HCl, pH 7.5, 7.5 mM NaCl, 10 mM MgCl$_2$, 3 % glycerol, 0.15 mg/ml BSA	15	30
EcoRV	20 mM imidazol, pH 6.2, 100 mM NaCl, 2 mM DTT, 0.1 mM EDTA, 50 μg/ml BSA	180	22-25
Nucleosomes	dialysis from 10 mM Tris, pH 7.5, 2 M KCl to 10 mM Tris, pH 7.5, 10 mM KCl	over-night	4
dCas9	20 mM HEPES, pH 7.5, 100 mM KCl, 5 mM MgCl$_2$, 5 % glycerol	30	37

For formation of a DNA-RNAP complex two promoters were used: 1) promoter C of bacteriophage T7 and 2) promoter T7A1 of E.coli. 1) 60 pM of 9 kb DNA molecules with a biotin tag from one end and containing a promoter C were mixed with 20 nM of RNAP (Affymetrix) in the presence of 1 mM NTP (Thermo Scientific), except for UTP, in the buffer composed of 150 mM KCl, 10 mM MgCl$_2$, 40mM Tris/HCl, 1 mM DTT, 0.01% TritonX, pH 7.5 at 37°C, 90 min. In the absence of UTP RNAP forms a paused transcription complex on a DNA promoter [133]. 2) Similarly, in the absence of UTP in the solution, RNAP stalls on DNA 20 bp downstream [134] of a T7A1 promoter. A 7.2 kb ds DNA fragment containing a biotin tag on one end was obtained by PCR of the plasmid pRL574 kindly provided by Landick's lab. 50 nM RNAP (New England Biolabs) was mixed with $\approx$ 500 pM of DNA with a single T7A1 promoter, 500 μM ApU (TriLink), 100 μM of ATP, CTP and GTP (Invitrogen) in a buffer, containing 25 mM Tris/HCl, pH 8.0, 100 mM KCl, 4 mM MgCl$_2$, 1 mM DTT, 3 % glycerol, 0.15 mg/ml BSA for 30 min at 37°C, 250 rpm.

In the case of RNAP (promoter T7A1) and dCas9 DNA-protein complexes were formed first and afterwards they were incubated with beads (section 2.2.2). In the case of other proteins, first bead-DNA complexes were formed and then they were incubated with the proteins. A sequence of steps for formation of bead-DNA-protein complexes was tested experimentally in order to achieve the highest occupancy of proteins on their binding sites. All DNA-protein complexes were prepared on the day of experiments except for DNA-RNAP (T7A1 promoter) that demonstrated high stability during several days of storage at +4 °C.

2.4.2 Methods for detection of DNA-protein complexes

Before testing DNA-protein complexes in the setup combining nanocapillaries and optical tweezers, all of them were probed using a reference method. That could be atomic force microscopy (AFM), electrophoretic mobility shift assay (EMSA) or pyrophosphate method. Protocols of these methods with some examples are listed below.

2.4.2.1 Atomic Force Microscopy (AFM)

AFM is a technique widely used for detection of DNA-protein complexes [135, 136, 137]. We would like to emphasise three advantages of AFM for studying DNA-protein complexes: 1) it is a rather fast method; 2) one can directly visualise DNA, proteins and DNA-protein complexes and 3) for majority of proteins the protocol of a sample preparation does not significantly vary. The main drawback of AFM in this application is that the majority of proteins also bind to mica during DNA deposition. Consequently it can make an impression of false bound proteins to DNA (Fig. 2.15 b, c). In addition, some complexes can be destroyed during sample preparation and require additional efforts for their visualisation under AFM [138]. For example, in the case of nucleosomes bound to DNA we did not observe any complexes unless the sample was fixed with glutaraldehyde beforehand (Fig. 2.14).
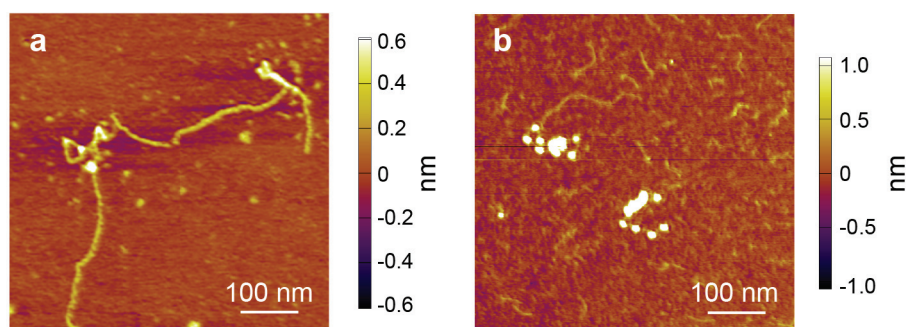
Figure 2.14 – **AFM images of DNA-nucleosome complexes.** (a) DNA-nucleosomes not fixed and (b) fixed with glutaraldehyde before AFM. In (a) no clear DNA-nucleosome complexes were observed in comparison to (b). In both cases DNA-nucleosome complexes were formed on a 2 kb DNA fragment containing 12 nucleosome positioning sites (NPS). There was a 1.5 excess of nucleosomes in relation to one NPS. The protocol of complex formation is described in Table 2.4.

To prepare DNA-protein complexes for AFM, they were diluted in 10 mM $MgCl_2$, deposited on freshly cleaved mica and afterwards rinsed thoroughly with ddH2O for two minutes. The AFM images were acquired in air in tapping mode using an Asylum Research Cypher microscope. We used Olympus silicon cantilevers (Olympus OMCL-AC240TS-R3) with a spring constant of 1.7 N/m and a resonant frequency of 70 kHz. A typical scan rate was 1- 2 Hz.

In Fig. 2.15 a bare 809 bp DNA was imaged. In Fig. 2.15 b and Fig. 2.15 c a non specifically binding protein ComEA was added to the DNA and complexes were visualised under AFM. One can observe proteins bound to DNA as well as to mica. The number of DNA-protein

complexes increases with increasing the protein concentration (Fig. 2.15 b and c).
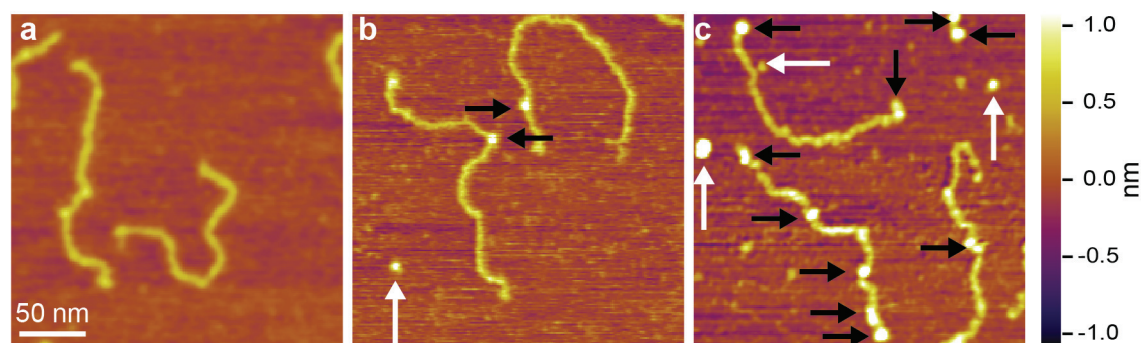
Figure 2.15 – **AFM images of bare DNA and DNA-ComEA complexes.** (a) Bare DNA fragments (DNA to protein ratio 1:0). (b) DNA-protein complex at a molecular ratio of 1:2.5. (c) DNA-protein complex at a molecular ratio of 1:10. The proteins bound to the DNA are marked with black arrows; unbound proteins are labeled by white arrows. The height or Z scale is shown on the right and is the same for all three panels displaying 270 nm x 270 nm scan areas. The figure is taken from [139].

2.4.2.2 Electrophoretic mobility shift assay (EMSA)

Another method used to verify binding of proteins to DNA is an electrophoretic mobility shift assay (EMSA). This method allows to try different ratios of DNA to protein at the same time and make a conclusion regarding the right concentration of the protein. EMSA was performed accordingly to [140] using 4-8 % polyacrylamide gel, 0.5 X TBE (45 μM Tris/boric acid, pH 8.2, 1mM EDTA) as a running buffer, voltages in the range of 100-150 V and running time 60-90 min. Gels were stained using 1 X SYBR safe in 0.5X TBE for 30-40 min. Photographs were taken using an UV transilluminator.

EMSA method was used to verify binding of EcoRI, EcoRV, RNAP and ComEA proteins to DNA. Since all mentioned proteins except for ComEA bind specifically to DNA, a DNA fragment (200-600 bp) was designed to contain a single specific binding site. The DNA used for studying of binding of ComEA contained a random sequence. On Fig. 2.16 increase in the ratio of ComEA to DNA led to the higher displacement of the DNA band due to the higher number of protein molecules formed a complex with it. Moreover, the intensity of the DNA band was lower with increasing concentration of ComEA due to higher accumulation of the complex in the gel wells. In the case of SpoIIIE and RNAP a similar trend with inability of complexes to enter the gel at high excess of proteins was observed.

2.4.2.3 Pyrophosphate method

Motor proteins moving on DNA use the energy from hydrolysis of NTP to NMP and pyrophosphate (Pi). In the EnzChek Phosphate Assay Kit (Molecular Probes) the enzyme purine nucleoside phosphorylase (PNP) converts a certain substrate in the presence of pyrophosphate to a product that absorbs at 360 nm. The accumulation of this product due to the enzymatic
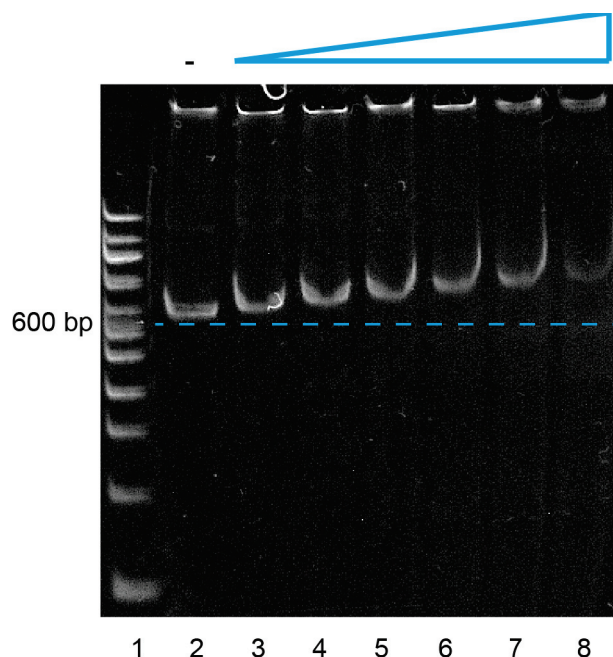
Figure 2.16 – **Electrophoretic mobility shift assay of a ComEA protein on DNA.** lane 1 - ladder, lane 2:8 contain 32 nM 570 bp DNA fragment and 0, 0.35, 0.70, 0.105, 0.14, 0.21 and 0.28 μM of ComEA, respectively. The gel was made out of 6 % polyacrylamide.

reaction will result in the increase of the absorbance at this wavelength (Fig. 2.17). Thus, the method is an easy way to test the protein activity. However, it is applicable only to enzymes using the energy of NTP and could not be used for testing of the complexes of ComEA for instance. Moreover, the presence of proteins activity does not prove that they form stable complexes with DNA. This method was used for SpoIIIE and RNAP proteins to check their activity after long storage or transportation.
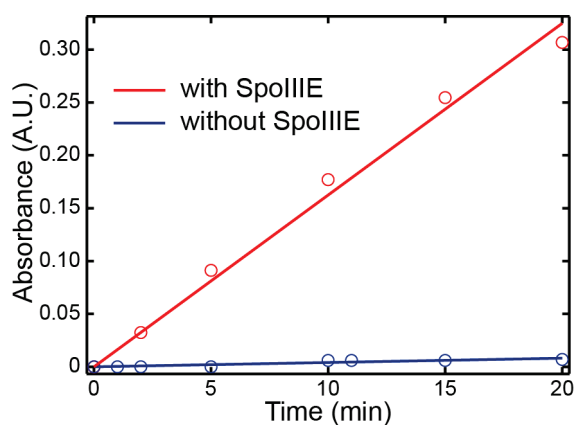
Figure 2.17 – **Pyrophosphate detection method to study activity of SpoIIIE on DNA.** Absorbance is measured at 360 nm.

2.5 Model of a nanocapillary

To better understand the translocation dynamics of DNA inside nanocapillaries we made a numerical and analytical model of it. The models provide the expressions for the potential, electric field and fluid velocity inside a nanocapillary. We compared the two models and checked their validity on experimental results in section 3.1.3.

2.5.1 Analytical calculations of the potential

The potential inside nanocapillaries is not uniform due to their elongated shape. Below we provide a derivation of a position-dependent potential profile inside nanocapillaries. The derived equation was used throughout the whole thesis.

According to [141] and neglecting a small influence of the DNA molecule captured outside a nanocapillary the position-dependent electric field $E(x)$ can be related to the ionic current I:

$$E(x) = \frac{I}{\sigma \pi R(x)^2} \tag{2.2}$$

where σ - the specific conductivity of the solution and $R(x)$ - the position-dependent radius of a nanocapillary. Taking into account that for a nanocapillary with conical shape $R(x)=R_0 - x\,tan\alpha$ (Fig. 3.5 a, please note that x values are negative), where R_0 - the radius of a nanocapillary opening, α - the opening angle of a nanocapillary (Fig. 3.5 a), the position-dependent electric field can be expressed as:

$$E(x) = \frac{I}{\sigma \pi \, tan^2 \alpha (\frac{R_0}{tan\alpha} - x)^2} \tag{2.3}$$

or

$$E(x) = \frac{a_1}{(b - x)^2} \tag{2.4}$$

where $a_1 = \frac{I}{\sigma \pi tan^2 \alpha}$ and $b = \frac{R_0}{tan\alpha}$. Since the potential $\Phi(x) = -\int E(x)\,dx$ integrating of equation 2.3 results in:

$$\Phi(x) = \frac{a_1}{b - x} - d_1 \tag{2.5}$$

where d_1 is an integration constant. From another hand, this equation can be represented in the following way:

$$\Phi(x) \sim \frac{1}{(1 + x/\xi)} \tag{2.6}$$

with ξ the electrostatic decay length and x growing inside the capillary with the origin at the opening.

2.5.2 COMSOL finite element model

The most successful approach for modelling physics at this scale includes coupling of Poisson-Nernst-Planck-Stokes equations. A finite element method for modelling fluid flows and electric potentials in nanocapillaries was previously implemented in [122]. We reproduced this model using an axially symmetric system in COMSOL Multiphysics (version 4.4) represented by a quartz nanocapillary in a salt solution. Electrostatic interactions between bound (quartz surface) and free charges (salt solution) were modelled using the Poisson equation for the electrostatic potential $\phi(\mathbf{r})$ as a function of the space coordinate $\mathbf{r}$:

$$\nabla^2 \phi(\mathbf{r}) = -\frac{\rho(\mathbf{r})}{\epsilon_0 \epsilon_r} \tag{2.7}$$

with $\rho(\mathbf{r}) = eN_a \sum_i z_i c_i(\mathbf{r})$ - the density of free charge carriers, where z_i - the valency, $c_i(\mathbf{r})$ - the density in mol/m^3 of the ion i at a position $\mathbf{r}$, ϵ_0 - the vacuum permittivity, ϵ_r - the relative permittivity of the material (80 for water, 3.8 for quartz), N_a - the Avogadro constant and e - the elementary charge. The free charge densities $c_i(\mathbf{r})$ were subject to the Nernst-Planck equation for the ion flux $\mathbf{J}_i$ of species i with convection due to the fluid flow with a velocity $\mathbf{u}(\mathbf{r})$:

$$\mathbf{J}_i = -D_i \nabla c_i(\mathbf{r}) - \frac{D_i}{k_B T} z_i e c_i(\mathbf{r}) \nabla \phi(\mathbf{r}) + c_i(\mathbf{r}) \mathbf{u}(\mathbf{r}) \tag{2.8}$$

where D_i are the diffusion coefficients of potassium and chloride ions ($D_1 = D_2 = 2 \cdot 10^{-9}\ m^2/s$).

The fluid flow was obtained using the Stokes equation with an electric body force $\rho(\mathbf{r}) \nabla \phi(\mathbf{r})$ and pressure gradient ∇p:

$$\eta \nabla^2 \mathbf{u} = \rho(\mathbf{r}) \nabla \phi(\mathbf{r}) + \nabla p \tag{2.9}$$

where η – the dynamic viscosity of water.

The mesh was constructed similar to previous works [122] using boundary layer refinement with minimal size at the boundaries of 0.1 nm and growth ratio of 1.2[122]. Near the nanocapillary opening the mesh was additionally refined until convergence was obtained. First we

a

b
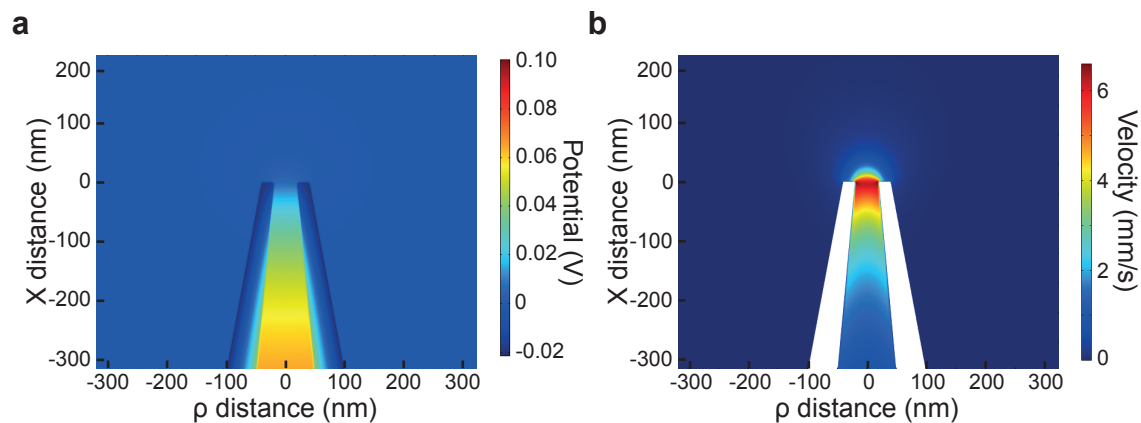
Figure 2.18 – **Surface plots of the potential drop and electroosmotic flow velocity in a nanocapillary.** (a) Surface plot of the electrostatic potential near the nanocapillary tip. (b) Surface plot of the liquid flow velocity near the nanocapillary tip. Parameters used in the model were opening angle $\alpha = 5°$, opening radii $R_0 = 20$ nm, salt concentration $c_0 = 150$ mM, potential $\Delta\Phi = 100$ mV, and the surface charge density of glass walls $\sigma = -20 \ mC/m^2$. The figure is taken from [130].

solved the Poisson-Nernst-Planck equations (without a flow) on a 1D domain, which was then mapped as the boundary condition for the general (3D) problem [122]. Fig. 2.18 shows surface plots of the electrostatic potential and electroosmotic flow profiles in a nanocapillary.

2.6 Model of a DNA-protein complex inside a nanocapillary

The major part of this thesis deals with the measurement and characterisation of the forces on DNA-protein complexes inside nanocapillaries. In this section we describe analytical and numerical models that were introduced in order to explain protein force profiles and extract physical parameters from the observed results. All the models were developed by Sanjin Marion.

2.6.1 Calculation of the drag force on proteins in COMSOL

We observed that the effective charge of DNA-RecA complexes is more positive than of bare DNA (section 3.2) . Since this observation contradicts with the fact that the linear charge density of DNA-RecA is ~ 2 times higher than for the bare DNA [115], we postulated a hypothesise that the drag force (F_{drag}) has a strong impact to the total force (F_p) on the DNA-RecA complexes inside nanocapillaries. In order to quantify it we used numerical simulations in COMSOL Multiphysics. We modelled the system using the Poisson-Nernst-Planck-Stokes equations accordingly to section 2.5.2. A DNA-protein complex was modelled as a charged rod with a sphere with different charge density coaxial to the nanocapillary (Fig. 2.19). The force on the protein originated from the fluid flow was calculated using a COMSOL built-in reaction for different distances x from the nanocapillary opening. From the simulations we concluded that the EOF-induced drag force on the proteins is well approximated by the Stokes drag equation $F_{stokes} \propto R_p u \eta$, where R_p - the protein hydrodynamic radii, u - the fluid velocity, and η - the dynamic viscosity. For the general geometry used in the model the drag force can be as high as several pN, i.e. sufficient to significantly influence the total force on the protein F_p. The EOF-induced drag force will consequently renormalise the real value of the charge of a DNA-protein complex.

2.6.2 Stochastic model of controlled translocations

We modelled the evolution of the force acting on DNA-protein complexes during pulling them outside of a nanocapillary. In other words, we simulated an experiment of reverse translocation (section 2.3.2). In this section firstly, we laid out a general expression for the free energy of the system. Secondly, we wrote down an explanation of each component of the expression. Lastly, we derived an expression for the free energy of DNA and protein in three geometries: nanopore, nanocapillary approximated as a single cone and double cone. The derived model allowed us to explain the observed protein force profiles and extract the charge of the complexes (section 3.2 and 3.3).
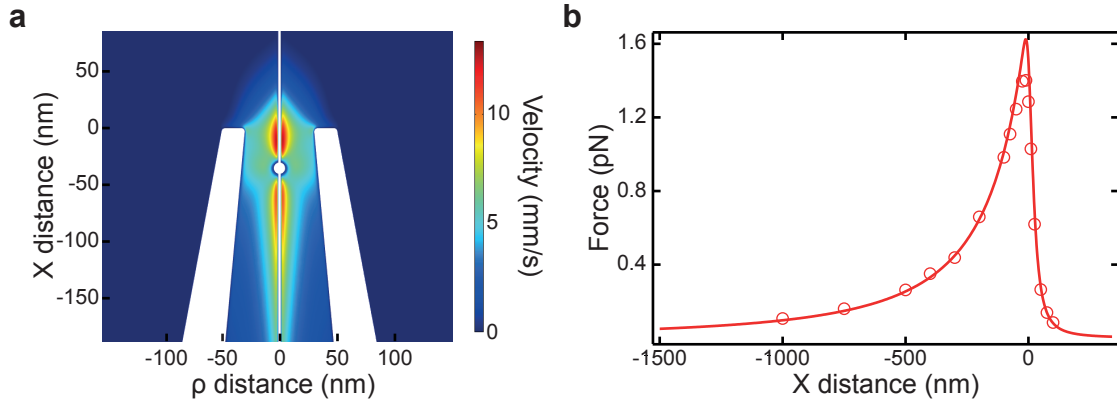
Figure 2.19 – **COMSOL simulations of the drag force acting on DNA-protein complexes in nanocapillaries.** (a) Surface plot of a flow velocity $u(x)$ obtained with COMSOL inside a nanocapillary, containing a DNA-protein complex. DNA was modelled as a rod with the surface charge density $\sigma_{DNA} = -136.2 \ mC/m^2$ and the protein as a sphere with a radii $R_p = 5 \ nm$ and surface charge density $\sigma_p = -25 \ mC/m^2$. All other parameters were kept the same as in Fig. 2.18. (b) Comparison of the EOF-induced drag on a spherical DNA-protein complex (circles) and the Stokes drag $F_{drag} \sim R_p \eta u(x)$ obtained from Fig. 2.18 b knowing the velocity profile $u(x)$ (line). The force calculated using a COMSOL built-in reaction on the protein and the Stokes drag force are related via a proportionality constant. The figure is adapted from [130].

Coupled Langevin equations

We used a stochastic modelling scheme [142] previously implemented to explain controlled translocation events in nanopores [118]. The model is based on two coupled Langevin equations for two state variables of the system, the bead position away from equilibrium at the stage position z, denoted r, and the length of the DNA contour located between the bead and the capillary opening s (Fig. 2.20). Thus we solved two Langevin equations with an external force determined by the total free energy $G(r, s)$. For the position of the bead $r = y - \rho$, with

Figure 2.20 – **Notations used in a stochastic model.** r - the distance from the centre of the bead to the opening, z - the distance from the centre of the optical trap to the opening, s - the contour length of the DNA, s_p - the contour length of the DNA until the position of the protein, $L - s$ - the length of DNA inside the capillary. The figure is adapted from [130].
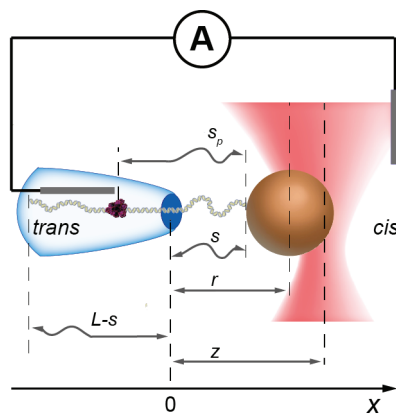
the bead radius $\rho = 1.5\ \mu m$, the temporal evolution is given by:

$$\eta_b \dot{r} = -\frac{\partial G(r,s)}{\partial r} + \sqrt{2 k_B T \eta_b}\, g(t), \tag{2.10}$$

and for the contour length of DNA s:

$$\eta_p \dot{s} = -\frac{\partial G(r,s)}{\partial s} + \sqrt{2 k_B T \eta_p}\, g(t). \tag{2.11}$$

Here $g(t)$ is a random, time-dependent, Gaussian, δ-correlated noise of magnitude unity. The constants $\eta_b = 5 \cdot 10^{-5}\, pNs/nm$ and $\eta_p = 1 \cdot 10^{-5}\, pNs/nm$ are values for the Stokes friction for the bead and polymer, respectively, and $k_B T \approx 25.7$ meV is the thermal energy at room temperature. The total free energy is:

$$G(r,s,z) = G_{DNA}(s) + G_{wlc}(r,s) + G_{ot}(r,z) + G_p(r,s), \tag{2.12}$$

and it consists of contributions from the optical trap $G_{ot}(r,z)$, the entropic free energy of a worm-like chain of DNA $G_{wlc}(r,s)$, the free energy of a charged DNA molecule in the nanocapillary $G_{DNA}(s)$, and the free energy contribution from a protein bound to the DNA $G_p(s)$ at the position s_p. We numerically solved the two coupled equations while slowly varying the stage position z with a speed $v \approx 500$ nm/s, from the DNA being almost completely inside the capillary, until it exits. In order to determine any numerical parameter we made ~ 100 averages of pulling out protocols with random starting conditions. The time step was $\Delta t \sim 10^{-5}\, s$ with additional refinements when the force terms $\partial G/\partial s$ and $\partial G/\partial r$ were larger than the contribution from thermal fluctuations.

Free energy of the system

We presented an expression for each component of the free energy of the system shown in eq.2.12.

The elastic-entropic free energy G_{wlc} for extending a DNA strand [143] is

$$G_{wlc}(r,s) = \frac{k_B T}{L_p} \left\{ \frac{s}{4} \left[\frac{1}{1-(r-\rho)/s} - 1 \right] - \frac{r-\rho}{4} + \frac{(r-\rho)^2}{2s} \right\}, \tag{2.13}$$

with $L_p \approx 50$ nm the persistence length of DNA. In our regime, the force on a DNA persistence length segment is much larger than the thermal energy, resulting in a full extension of the DNA of contour length s from the bead surface to nanocapillary opening. In the case of much longer capillary tips ($\xi \gg 100\ nm$) it might be necessary to include the details of the DNA extension (parameter ξ is introduced in section 2.5.1).

Additionally, we have the free energy from the harmonic pulling force of the optical trap:

$$G_{ot}(r) = \frac{1}{2}\kappa(z-r)^2, \tag{2.14}$$

where κ is the optical trap spring constant $\kappa \approx 0.05$-0.1 pN/nm. The bead equilibrium position z was taken to be a function of time $z = vt$, where $v \approx 500$ nm/s was the experimental pulling speed.

The DNA electrostatic free energy is directly calculated from the electrostatic potential distribution $\Phi(z)$ inside the nanopore/capillary by approximating that the DNA is a charged extended rod with the effective linear charge density λ, with a constant contribution coming from the DNA contour length s being on the energetically unfavourable side of the opening [118]

$$G_{DNA}(s) = \lambda_{DNA} \int_{-(L-s)}^{s} \Phi(x)dx. \tag{2.15}$$

Here the position $x = 0$ is the location of the nanocapillary opening (exit). The effective linear charge density of the DNA λ_{DNA} includes both effects of counter ion condensation and drag force from any electroosmotic flow [144, 113, 118]. Similarly to the DNA we can obtain the free energy for a point-like charged protein at a position s_p along the DNA contour from the bead:

$$G_p(s) = \int \Phi(x) q^* \delta(x - (s - sp))dx, \tag{2.16}$$

here q^* is the effective charge of the protein with both electrostatic and electroosmotic flow contributions [118].

Below we derived analytical expressions for forces acting on DNA and proteins in nanopores and nanocapillaries(cone and double cone geometry).

Electrostatics of nanopores

In the case of nanopores, the electric field acting on the DNA and protein is mostly localised around the pore opening [145]. We approximate the electrostatic potential in nanopores by using:

$$\Phi(x) = V(\tanh(x/l_{eff}) + 1)/2, \tag{2.17}$$

because when the effective electrostatic thickness of the nanopore l_{eff} goes to 0 the potential transforms into a step function. Here V is the driving electrostatic potential. From this the free energy of a DNA strand is:

$$G_{DNA}^{np} = -\frac{1}{2} l_{eff} \lambda_{DNA} V \left(\log\left(\cosh\left(\frac{L-s}{l_{eff}} \right) \right) - \log\left(\cosh\left(\frac{s}{l_{eff}} \right) \right) - L \right), \tag{2.18}$$

and the resulting force $F_{DNA} = -\partial G_{DNA}/\partial s$:

$$F_{DNA}^{np} = -\frac{1}{2} \lambda_{DNA} V \left(\tanh\left(\frac{L-s}{l_{eff}} \right) + \tanh\left(\frac{s}{l_{eff}} \right) \right). \tag{2.19}$$

For a protein represented as a point at location s_p of charge q, the free energy is:

$$G_p^{np} = qV(\tanh((s-s_p)/l_{eff})+1)/2, \tag{2.20}$$

leading to a force on the protein of:

$$F_p^{np} = \frac{qV}{2l_{eff}}(1-\tanh^2((s-s_p)/l_{eff})). \tag{2.21}$$

Electrostatics of nanocapillaries (cone geometry)

The simplest model for the spatial dependence of the electrostatic potential valid inside a nanocapillary approximates the capillary as a cone:

$$\Phi(x) = \frac{V}{1-x/\xi}\theta(-x) + V\theta(x), \tag{2.22}$$

with $\theta(x)$ the Heaviside step function. The first contribution comes into consideration when DNA is being pulled outside of the nanocapillary, giving a specific decay in the force profile (section 3.1.2). The second contribution is the driving potential on the DNA due to its negative charge.

From the electrostatic potential of a nanocapillary follows the free energy of a DNA strand:

$$G_{DNA}^{ncp1} = V\lambda_{DNA}\left(\ln\left(1 + \frac{L-s}{\xi}\right) + s\right), \tag{2.23}$$

and subsequently the force on the DNA:

$$F_{DNA}^{ncp1} = -\lambda_{DNA}V\left(1 - \frac{1}{1 + \frac{L-s}{\xi}}\right). \tag{2.24}$$

The free energy of a point protein at location s_p with charge q^* is:

$$G_p^{ncp1} = -q^*V\frac{1}{1 + \frac{s-s_p}{\xi}}\theta(s_p - s) + q^*V\theta(s - s_p), \tag{2.25}$$

and the force on the protein:

$$F_p^{ncp1} = -\frac{q^*V}{\xi}\frac{1}{\left(1 + \frac{s-s_p}{\xi}\right)^2}. \tag{2.26}$$

Modelled force profiles for DNA-protein complexes and DNA coiling in the geometries of nanopores and nanocapillaries is presented in Fig. 2.21.
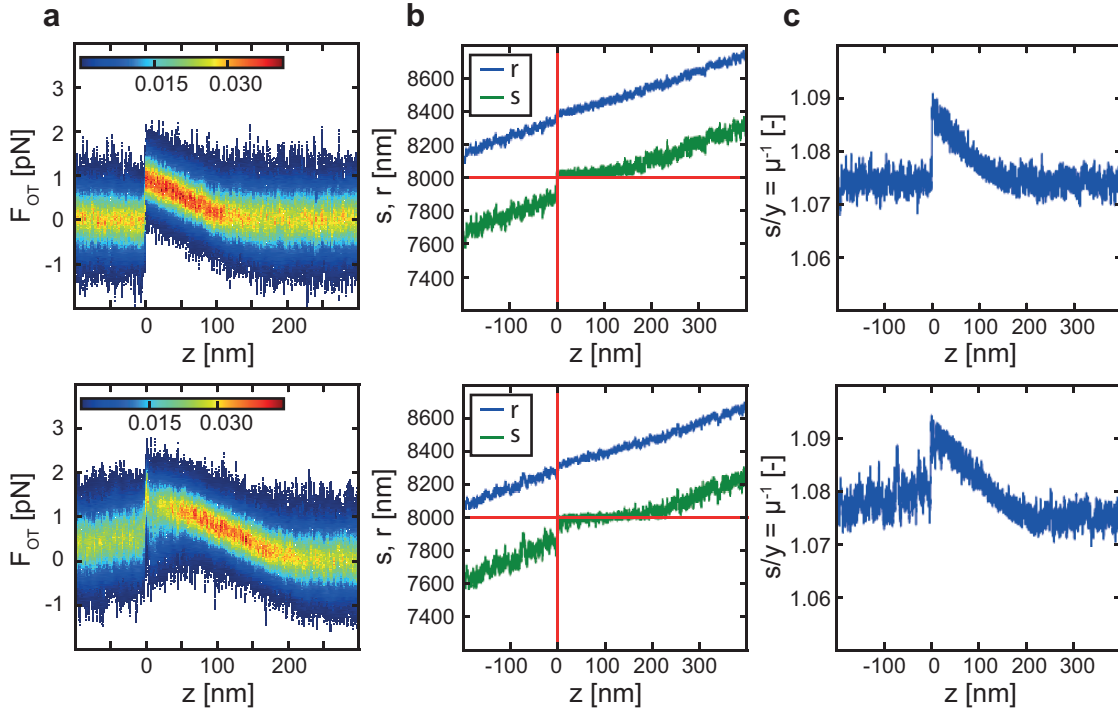
Figure 2.21 – **Comparison of characteristic DNA-protein jumps during controlled translocation in nanopores (top row) and nanocapillaries with cone geometry (bottom row).** (a) Force versus stage position z averaged for 100 different starting conditions and normalised so that the total probability for each z is equal to 1 (scale on the density plot shows this probability). (b) Internal state variables r, s versus stage position z. A single experiment is demonstrated with the horizontal red line marking the protein position s_p and vertical red line the protein location which corresponds to $z = 0$, (c) DNA coiling s/y (inverse extension) versus stage position z. The parameters used were $\lambda_{DNA} = -0.04\ e/bp$ and $V = 200\ mV$ with the electrostatic decay length $\xi = 200\ nm$ for nanocapillaries and thickness $l_{eff} = 10\ nm$ for nanopores, the protein charge was $q^* = 10\ e$. The figure is taken from [146].

Electrostatics of nanocapillaries (double cone geometry)

A more accurate description of nanocapillaries can be made modelling it as two truncated cones [89, 87] (Fig. 2.4). It is worth mentioning, usually in double cone geometry the main impact on biomolecules is done by the smallest cone and therefore the second cone, which does not contain a nanocapillary opening, can be often neglected. Nevertheless, to have a full picture of the system we provided equations for the free energies of DNA and protein in this geometry as well.

The total potential in double cone geometry consists of the same functional dependence inside both parts with different characteristic lengths and boundary conditions [141, 127]. We defined t and T as the cone taper lengths, α and β - the opening angles, d and $D = d(1 + 2t \tan \alpha / d)$ - the smallest base diameter for the small and large cone, respectively (Fig. 2.4). The electrostatic potential $V(x)$ can be obtained from the continuity condition for the electric field and potential

as:

$$V_1(x) = V\frac{Ax}{(1-\frac{x}{\xi})\xi} + V \tag{2.27}$$

in the small cone, and in the large cone as:

$$V_2(x) = V\frac{B}{1-\frac{x+t}{\zeta}} \tag{2.28}$$

with two constants A and B expressed as:

$$A = \frac{(t+\xi)^2}{t^2 + t\xi + \zeta\xi} \tag{2.29}$$

$$B = \frac{\zeta\xi}{t^2 + t\xi + \zeta\xi}. \tag{2.30}$$

We have defined the constants $\xi = d/2\tan\alpha$ and $\zeta = D/2\tan\beta$ as the characteristic decay lengths of the potential. The total potential in space can thus be written as:

$$\Phi(x) = V\theta(x) + V_1(x)\theta(-x)\theta(x+t) + V_2(x)\theta(-x-t). \tag{2.31}$$

Due to different compartments in this geometry, the integration of these equations is performed separately for each part. Thus for DNA:

$$G_{DNA}^{ncp2}(s) = \begin{cases} V\lambda A\xi\ln\left(1+\frac{L-s}{\xi}\right) + V\lambda(1-A)(L-s) + V\lambda s & \text{for } L-s < t \\ V\lambda B\zeta\ln\left(1+\frac{L-s-t}{\zeta}\right) + VA\xi\ln\left(\frac{t+\xi}{\xi}\right) + V\lambda t(1-A) + V\lambda s & \text{for } L-s > t. \end{cases} \tag{2.32}$$

while for a protein:

$$G_p^{ncp2}(s,s_p) = \begin{cases} qV & \text{for } s > s_p, \\ qV\frac{A(s-s_p)}{(1-\frac{s-s_p}{\xi})\xi} + V & \text{for } -t < s - s_p < 0, \\ qV\frac{B}{1-\frac{s-s_p+t}{\zeta}} & \text{for } s - s_p < -t. \end{cases} \tag{2.33}$$

The forces can be obtained by taking a derivative of the free energy. It is omitted here for simplicity.

An example of a solution in this geometry is shown in Fig. 2.22 for a typical choice of parameters. Notice the change of the shape and mirroring of the force curves for oppositely charged

proteins. We made a stochastic model in this geometry for the results described in section 3.2, however modelling in one cone geometry would also produce accurate fits.
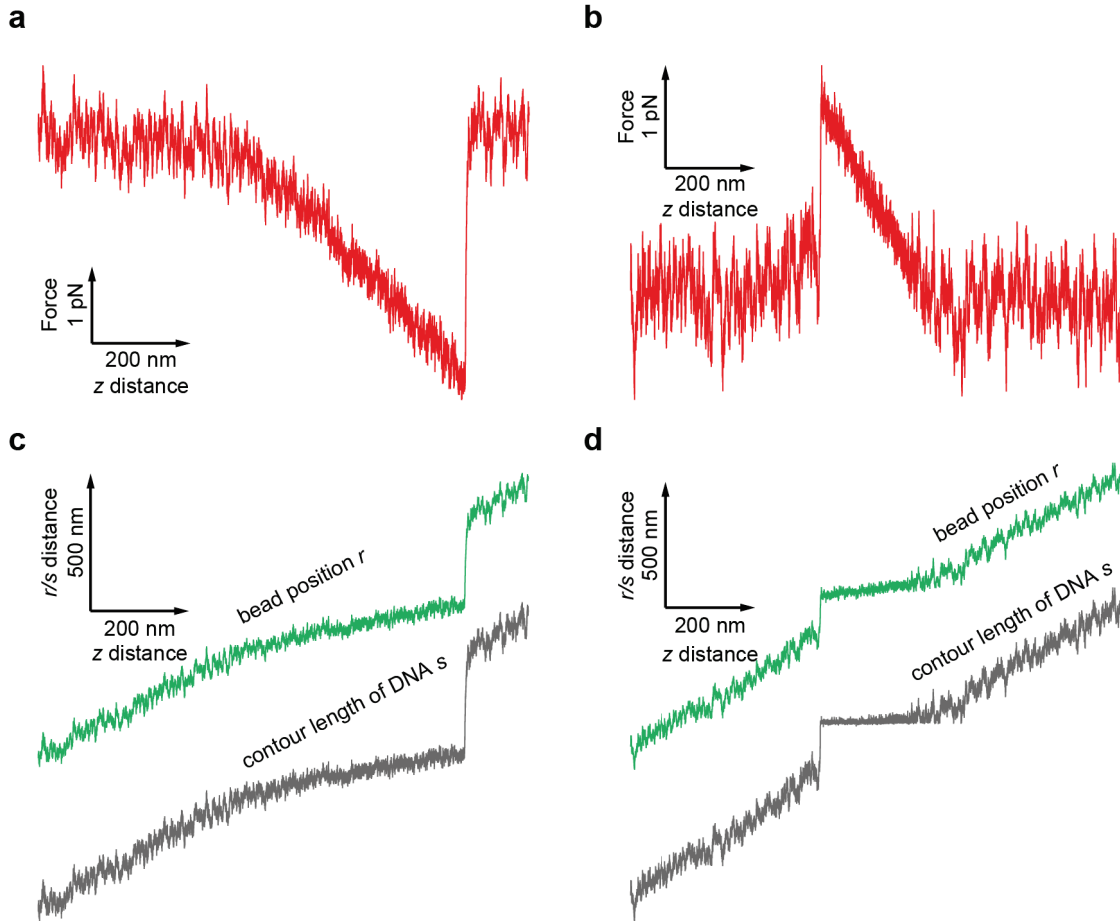
Figure 2.22 – **Modelled force curves with corresponding state variable** (s, r) **curves for controlled translocation of negatively and positively charged DNA-protein complexes in a nanocapillary with double cone geometry.** Force $F(z)$ (a) and lengths s and r (c) as a function of the bead equilibrium position z obtained using the stochastic model for parameters $\Delta\Phi = 100\ mV$, $q = -30e$, $\xi = 100\ nm$, $\zeta = 200\ nm$, $s_p = 2500\ nm$, $\kappa = 0.01\ pN/nm$ and $\lambda = -0.1e/0.34\ nm$. (b) and (d) were obtained at the same parameters except the sign of the protein charge was changed, *i.e.* $q = +30e$. The figure is taken from [130].

2.6.3 Analytical solution for a protein localisation shift

In our setup the measured position of protein DNA-binding sites deviated from the theoretical ones (see section 3.3). Therefore we made an analytical model to account for the measured shift. We connected the measured position of the protein at y_p to the internal coordinate at s_p, also taking into account that we measure relative distances in respect to the DNA exit point at y_x (all variables are noted on Fig. 3.16). The measured protein position is the distance

between the locations of the protein at y_p and the DNA exit at y_x:

$$\Delta y_p = y_x - y_p. \tag{2.34}$$

The shift between the measured and theoretical position (s_p) is expressed as:

$$\Delta_{shift} = (L - s_p) - \Delta y_p, \tag{2.35}$$

where $L - s_p$ comes from the fact that the experiments measure from the free end at $s = L$, while we measure contour distances from the bead at $s = 0$.

It remains to determine the relation between the DNA contour length s and the distance between the bead and capillary opening y. This is, for any s, given by the extension μ:

$$\mu(s) = \frac{y}{s}, \tag{2.36}$$

and is always in the regime that $\mu(s) < 1$, i.e. the DNA is never "completely" extended. We can now calculate Δy_p by transforming the bead to capillary distances into internal strand coordinates,

$$\Delta y_p = s_x \mu(s_x) - s_p \mu(s_p), \tag{2.37}$$

where s_x is the contour length between the bead and capillary at which the DNA exits. Without fluctuations this exit will happen when all the DNA is used for coiling at the tension and bead-opening distance such that $s_x = L$ and $y_x^0 = L\mu(L)$. In practice, as it is a single molecule experiment, the DNA will exit earlier due to fluctuations such that $y_x^0 = L\mu(L) > y_x = s_x\mu(L)$.

The length of a DNA strand that jumps out Δs_x is not accessible for binding site localisation as the DNA jumps out even without the presence of the protein. This inaccessible length at the free end is the difference between the length at the moment of the ideal exit without fluctuations and the real exit:

$$\Delta s_x = s_x^0 - s_x = L - s_x. \tag{2.38}$$

Here, the relationship between the length of strand where the jump took place and the experimental distance is:

$$y_x = s_x \mu(s_x). \tag{2.39}$$

So that the experimental (or numerical) position is related to the inaccessible length Δs_x through:

$$\Delta y_x = L\mu(L) - s_x \mu(s_x), \tag{2.40}$$

or

$$\Delta y_x = L\mu(L) - (L - \Delta s_x)\mu(s_x). \tag{2.41}$$

In practice the unprobable region Δs_x is not a significant problem since one can easily attach a piece of DNA to the end of the probed region thus rendering the DNA of interest wholly probable. We also note here that the process of threading the free end of DNA is harder to predict and thus the entrance of DNA cannot be used instead of the exit as a reference point [108, 69].

It remains to determine the DNA extension. In the strong stretching regime [143] the relation between the force extending the DNA, $F_{DNA} = \lambda_{DNA}\Delta V f(s)$, and the extension μ can be derived as:

$$\mu(s) = \frac{y}{s} = 1 - \frac{1}{\sqrt{A f(s)}}, \tag{2.42}$$

with

$$f(s) = \begin{cases} 1 & \text{nanopore} \\ 1 - \frac{1}{1 + \frac{L-s}{\xi}} & \text{nanocapillary,} \end{cases} \tag{2.43}$$

and

$$A = \frac{4\lambda_{DNA}V L_p}{k_B T}. \tag{2.44}$$

by taking into account the known force profile inside nanocapillaries (2.5.1). Here λ_{DNA} is the effective DNA linear charge density, V the driving potential, L_p the persistence length of DNA and $k_B T$ the thermal energy at room temperature. Equations (2.35), (2.37) and (2.42) enable the conversion from the measured positions to the internal positions on the strand for bare DNA controlled translocation.

The previous equations neglect that the protein changes the force extending the DNA at the moment of the jump. In the regime where the force on the protein is small comparable to the force that is pulling the DNA into the nanocapillary, we can assume that, at the moment when the jump happens, the force extending the DNA is changed by the presence of the protein. We can approximate the force as $F_{ext} = F_{DNA} - F_p(s = s_p) = F_{DNA} - qV/\xi$ and obtain the corrected extension relation at s_p

$$\mu(s_p) = \frac{y}{s_p} = 1 - \frac{1}{\sqrt{4L_p F_{ext}/k_B T}}, \tag{2.45}$$

with which we can predict the measured protein localisation shift for small forces on the protein. This formula is valid until the force on the protein becomes comparable to the force extending the DNA when we are no longer in the strong extension regime.

2.6.4 Equilibrium information from protein jump events

One of the objectives of the thesis was to discriminate different DNA-bound proteins based on their characteristic force profiles (section 3.3). We calculated the works invested in movement of the complexes away from the opening and using the Jarzynski equality (JE) extracted corresponding free energies. Knowing the value of free energies we were able to calculate effective charges of the complexes inside nanocapillaries. Here we provide derivation of equations for extraction of the charge from the free energies. It is worth mentioning, even though JE have been extensively used in the experiments with optical tweezers [147], it has never been applied in combination with nanocapillaries.

The Jarzynski equality [148] enables us to determine the free energy difference $\Delta G_{AB} = G(r_B, s_B, z_B) - G(r_A, s_A, z_A)$ between two positions before and after the protein jump with $G(r, s, z)$ the total free energy of the system (see Fig. 3.16 for notations and an example of a protein jump). The system is considered to be in an equilibrium state before the jump happens at state variables (r_A, s_A, z_A). After the non-equilibrium jump it relaxes into a new equilibrium state at (s_B, r_B, z_B). The work W_i measured for the individual protein jump was averaged over different experimentally realised trajectories $\langle W_i \rangle = \bar{W} \geq \Delta G_{AB}$, where the equality sign is valid when the number of samples goes to infinity. We obtained the difference between the two states with the JE:

$$e^{-\frac{\Delta G_{AB}}{k_B T}} = \langle e^{-\frac{W_i}{k_B T}} \rangle. \tag{2.46}$$

In order to use the JE to obtain a meaningful physical quantity related to the protein we computed the difference between the free energy before and after the jump. We assumed that the measured force before and after the jump event is the same $F_{ot}(r_A, z_A) = F_{ot}(r_B, z_B)$, which implies that differences between stage and bead coordinates are the same $\Delta z = \Delta r$ and that the free energy of the optical trap does not change $\Delta G_{ot} = 0$. What remains is the free energy of the DNA worm-like chain (2.13), DNA electrostatic free energy (2.15) and protein free energy (2.16).

The difference of free energies for the DNA before and after the jump for thin nanopores ($l_{eff} \ll 10nm$) is:

$$\Delta G_{DNA} = V \lambda_{DNA} \Delta s, \tag{2.47}$$

and for nanocapillaries:

$$\Delta G_{DNA} = V \lambda_{DNA} \Delta s - V \lambda_{DNA} \xi \log \frac{\xi + L - s_B}{\xi + L - s_A}. \tag{2.48}$$

Nanocapillaries have the additional term which is relevant when the DNA's free end is near the opening so that it is influenced by the characteristic potential (2.22). If the protein location is far away from the DNA free end ($s_p \ll L$) this is negligible.

The protein free energy difference is $\Delta G_p = q^* V$ for nanopores, and

$$\Delta G_p = q^* V - \frac{q^* V}{1 + \frac{s_p - s_b}{\xi}}, \tag{2.49}$$

for nanocapillaries. We can assume that the DNA strand position after the jump is the same as the protein position, $s_B \approx s_p$. This is confirmed by our stochastic model in Fig. 2.21 where $s_B \approx s_p$ even after the DNA has again extended and the force level has returned to its value before the jump. We can then further simplify by also writing $s_A \approx s_p - \Delta s$ leading to

$$\Delta G_p = q^* V \frac{\Delta s}{\xi + \Delta s}. \tag{2.50}$$

If the protein is far away from the free end, the change in DNA extension before and after the jump is negligible so that $\mu_A \approx \mu_B = \mu$. This is valid, unless we are dealing with proteins positioned near to the free end of the DNA for nanocapillaries. Finally the change in the free energy of the DNA worm like chain is:

$$\Delta G_{wlc} \approx \frac{k_B T}{L_p} \frac{\Delta z}{4} \left[\frac{\mu}{1 - \mu} - (1 - 2\mu) \right], \tag{2.51}$$

which amounts to $\Delta G_{wlc} \ll 1 \ k_B T$ and is negligible for discrimination of proteins.

To summarise, the change of the free energy before and after the jump can be approximated by eq. (2.50) which can be further simplified with $\Delta s \approx \Delta z$, valid for short jumps as the extension which links the two coordinates $\mu \approx 1$. With this equation we are able to use the free energy difference obtained from non-equilibrium work analysis (JE) and connect it to the effective charge of the bound protein.

3 | Results and discussion

3.1 Measurement of the position-dependent electrophoretic force on DNA in a glass nanocapillary
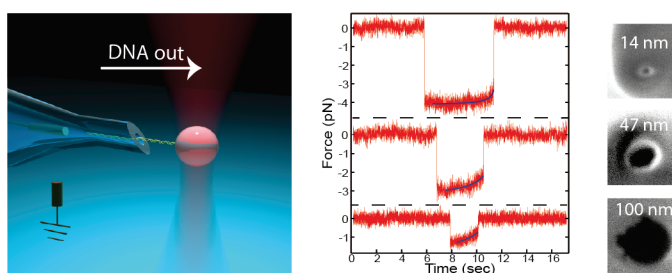
We started the project by characterising the system that combines nanocapillaries and optical tweezers. We inserted and controllably pulled out DNA of different lengths in nanocapillaries of different sizes and at different applied voltages. We mapped out position-dependent force profiles at different parameters of the system. We supported the obtained results based on the model of a nanocapillary. This step was required to get a detailed overview of the system before studying DNA-protein complexes in it.

The results of this chapter have been published in the manuscript:

"Roman D. Bulushev, Lorenz J. Steinbock, Sergey Khlybov, Julian F. Steinbock, Ulrich F. Keyser, and Aleksandra Radenovic. Measurement of the Position-Dependent Electrophoretic Force on DNA in a Glass Nanocapillary. *Nano Letters*, 14(11):6606-6613, 2014."

3.1.1 Effect of the nanocapillary size and DNA length on the force magnitude

During the first stage of this thesis, we investigated the magnitude of the electrophoretic force on DNA as a function of the size of a nanocapillary and length of DNA handle. For this purpose we used a setup, combining nanocapillaries and optical tweezers (see section 2.3.2).

Glass nanocapillaries were fabricated using programs 1 and 2 from Table 2.1 and shrunken to diameters 9 to 165 nm by exposing them to electron irradiation accordingly to section 2.1.2. The experimental buffers contained either 40 mM or 1 M KCl, pH 8.0 or 8.7. Streptavidin-coated beads were modified with either biotinylated 48.5 kb (16.5 μm) λ-DNA or biotinylated 5.5 kb (1.85 μm) DNA PCR fragment accordingly to section 2.2.2. The trap stiffness used in the experiments was in the range of 9-20 pN/μm (see section 2.2.3).

After capturing a single DNA molecule (see section 2.3.2), we ensured that in the range of 40-150 mV the stalling force increases linearly with the voltage (Fig. 3.1 a). On the next step, we investigated the magnitude of the conductance and stalling force drops caused by inserting a DNA molecule in nanocapillaries of different diameters. In 1 M KCl solution, the conductance change was higher for the nanocapillaries of smaller diameters (Fig. 3.1 b) in accordance with [87]. However, in 1 M KCl solution sometimes we observed sticking of DNA to glass walls inside a nanocapillary (data not shown). The repulsion between two negatively charged surfaces of DNA and glass can be decreased due to the significant effect of screening at high salt concentration [124]. On the other hand, in the buffer with low ionic strength (40 mM KCl) we did not observe nonspecific interactions of DNA with glass walls. This is a promising result, particularly in the context of experiments that aim to probe protein-DNA interactions and thus require low ionic strength. In 40 mM KCl solution the stalling force is increased with decreasing of nanocapillary size (Fig. 3.1 c, movies 1 and 2 in section 3.1.5), which is consistent with solid-state nanopores [113]. The negatively charged backbone of DNA trapped inside a nanocapillary induces an opposite flow of counter ions, resulting in additional drag force on a DNA molecule. The drag force depends on the nanopore diameter and is of smaller magnitude in smaller nanopores. We fit the stalling forces as a function of a nanocapillary opening by using the equation:

$$F(R) \sim \frac{1}{ln(\frac{R}{1.1})} \tag{3.1}$$

where R is the radius of a nanocapillary and 1.1 represents the radius of dsDNA in nm [113, 144]. However, the stalling forces in nanocapillaries were smaller than those in solid-state nanopores (Fig. 3.1 c) [113, 114]. To explain this observation, a nanocapillary can be considered as a sequence of ultra thin nanopores with continuously increasing diameters. The increase in the size of the pore will lead to an increase in the drag force generated from the DNA backbone, as mentioned before, resulting in a smaller total stalling force. Another aspect affecting the magnitude of the stalling force is the electroosmotic flow acting on DNA, which is caused by the negatively charged glass walls. The presence and characterisation of an electroosmotic nanojet produced by the glass walls of nanocapillaries has been previously shown by calculating the rotation frequency of slightly asymmetric beads trapped in front of the openings [52]. The effect of electroosmotic flow on DNA translocation was also demonstrated for solid-state nanopores [114]. In this work the modification of a pore surface with neutrally charged

3.1. Measurement of the position-dependent electrophoretic force on DNA in a glass nanocapillary
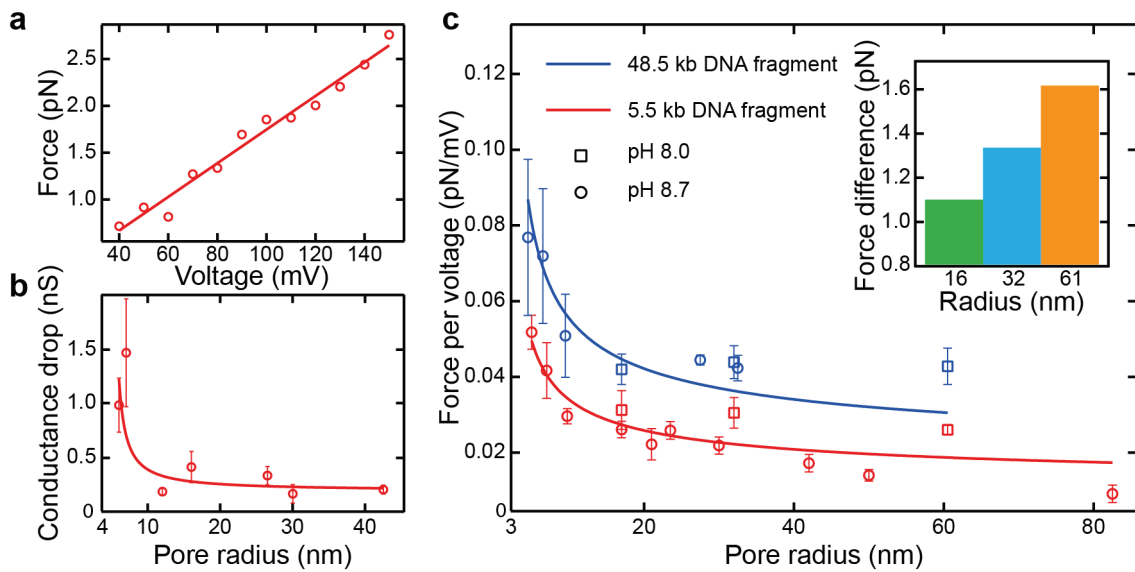
Figure 3.1 – **Investigation of the stalling force and conductance drop in nanocapillaries of different sizes.** (a) Stalling force as a function of applied potential. The data was acquired with a 53 nm nanocapillary, in 1 M KCl, pH 8.7, using the 5.5 kb long DNA fragment. The data was fit to linear function. (b) Measured conductance drop versus nanocapillary radius in 1 M KCl, pH 8.7, using the 5.5 kb long DNA fragment. Data was fit to equation (3) from Ref. [87]. (c) Measured stalling force versus nanocapillary radius. The data was acquired in 40 mM KCl, pH 8.7 (circles) or pH 8.0 (squares) for the 5.5 kb DNA fragment (red) and λ-DNA (48.5 kb) (blue). The data was fit to equation 3.1. The length of DNA inside a nanocapillary varied in the range 0.4-1.35 μm for a 5.5 kb DNA fragment and $\approx$ 12-14.5 μm for λ-DNA. The inset shows the difference in the stalling force for the λ-DNA and 5.5 kb DNA fragments in 40 mM KCl, pH 8.0 (see text for details). The stalling force acting on the longer DNA was higher, and the difference is represented in pN. The figure is taken from [127].

lipids almost doubled the magnitude of the stalling force. The effect of the drag force on biomolecules inside nanocapillaries will be also discussed in the next section.

In addition to the diameter of nanocapillaries, DNA length also influenced the magnitude of the stalling force. In general, the stalling forces for 48.5 kb λ-DNA, were higher than those for the 5.5 kb DNA fragment (Fig. 3.1 c). For the nanocapillaries with the diameters of 32, 64 and 121 nm, we first measured the stalling force acting on the 5.5 kb DNA fragment. Afterwards we removed the DNA-coated beads by rinsing the cis chamber with a 40 mM KCl buffer. In the next step λ-DNA-coated beads were injected, and we were able to measure the stalling force acting on longer λ-DNA molecules.

We observed that the stalling force acting on the λ-DNA was higher, especially for nanocapillaries exceeding 60 nm in diameter (Fig. 3.1 c inset). The length-dependent behaviour of the stalling force can be attributed to the fact that for shorter DNA the optically trapped bead has to be positioned closer to the opening and consequently it experiences higher electroosmotic flow [52]. In addition, for longer DNA the increased number of basepairs inside the nanocapillary leads to the higher bare electrostatic force (F_{bare}) due to the extended electric field. A

more detailed explanation will be discussed later.
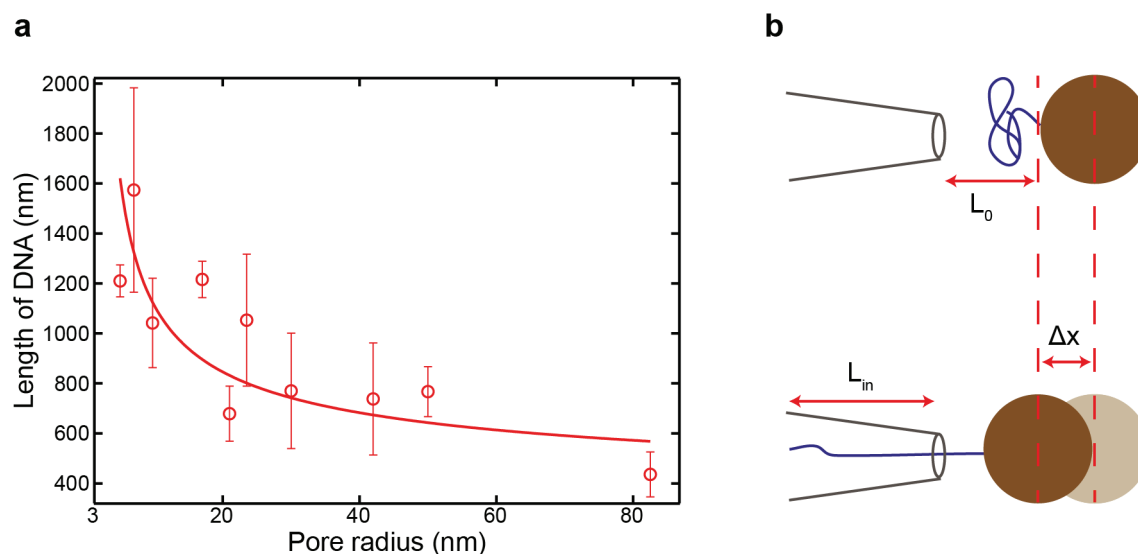
Figure 3.2 – **Length of DNA captured inside nanocapillaries as a function of a nanocapillary open-ing.** The length of DNA trapped inside a nanocapillary (L_{in}) was calculated based on the change of the position of the nanopositioning stage during pulling the DNA out. Noteworthily, L_{in} depends on the distance from the bead surface to the opening at which the event took place (L_0) and displacement of the bead caused by the event (Δx). The higher L_0, the shorter piece of DNA is trapped inside a nanocap-illary. The higher Δx, the longer piece of DNA is trapped inside a nanocapillary. The displacement of the bead depends on the force (F) pulling a DNA molecule and stiffness of the trap (k): F=-kΔx. To compare the results of L_{in}, obtained for different nanocapillary openings, the captured length of DNA was recalculated taking into account the stiffness of 11 pN/μm for all experiments. Although initial distances between the nanocapillary tip and the bead surface cannot be assumed identical for different nanocapillaries, we observed a trend of increasing of the DNA length captured inside nanocapillaries of smaller diameters. This finding could be explained by the higher magnitude of the stalling force acting in smaller nanocapillaries. The data were fit to equation 3.1. The experiments performed in the buffer, containing 40 mM KCl, pH 8.7, at 100 mV, using the 5.5 kb DNA fragment, and stiffness of optical trap in the range of 10-14 pN/μm. The figure is taken from [127].

3.1.2 Measurement of position-dependent force profiles

The dependence of the stalling force on the length of the DNA handle prompted us to continu-ously vary the length of DNA captured inside the nanocapillaries by performing its reverse translocation. This method, implemented on the 5.5 kb DNA fragment allowed to measure the DNA length trapped inside a nanocapillary (Fig. 3.2) and to record the position-dependent stalling force profiles (later in the terms "position-dependent force profiles/force profiles/force decays" the word "stalling" is omitted for simplicity). The profiles varied in the magnitude and shape with the size of the nanocapillaries (Fig. 3.3 a). In the case of nanocapillaries less than 20 nm in diameter, the force decay was insignificant and took place only in the final part of the nanocapillaries, close to the opening. This profile closely resembles the data reported for solid-state nanopores, where the stalling force is kept constant along the entire nanopore

length [114, 117]. However, the increase of the nanocapillary size leads to longer decays of the force profiles. For example, in a 100 nm nanocapillary the decay in the stalling force was pronounced along the entire length of DNA (Fig. 3.3 a). There was no visible difference between the profiles recorded in the same nanocapillary for the 5.5 kb DNA and λ-DNA (Fig. 3.4). The smaller stalling force acting on shorter DNA could be attributed to the already mentioned higher electroosmotic flow on a bead, heating effects of the laser and small uncertainties in the force calibration regarding the trap stiffness.
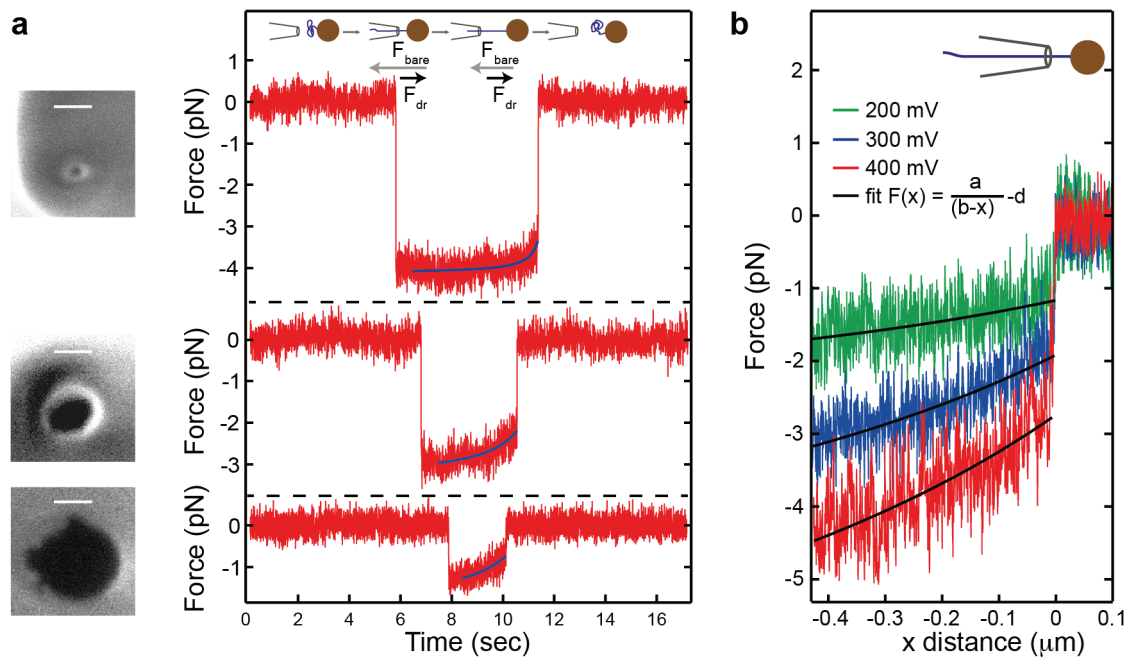
Figure 3.3 – **Mapping the gradients of stalling force inside nanocapillaries of different sizes and at different voltages.** (a) Stalling force profiles for nanocapillaries with diameters 14, 47 and 100 nm (from top to bottom). SEM images of the nanocapillaries are represented on the left (scale bars, 50 nm). The schematic represents the consecutive steps of the experiment. The arrows show the direction of the bare electrostatic force (F_{bare}) and the drag force (F_{dr}) simultaneously acting on DNA. The experiments were performed in 40 mM KCl, pH 8.7, at 100 mV, using the 5.5 kb DNA and a stage velocity of 250 nm/sec. The electrophoretic force profiles recorded during activation of the nanopositioning stage were fit to equation 3.3, where coefficient b was fixed in accordance with the opening radius, and coefficients a and d were used as fitting parameters. (b) Measured stalling forces as a function of the distance inside a nanocapillary recorded at 200, 300 and 400 mV. The schematic shows the orientation of the nanocapillary. The experiments were performed with the 165 nm nanocapillary, in 40 mM KCl, pH 8.7, using the 5.5 kb DNA fragment. The figure is taken from [127].

In addition to the size-dependent behaviour in the range of diameters of 9-165 nm, we investigated the influence of applied voltage on the position-dependent force profiles. We pulled the DNA molecule out of the 165 nm nanocapillary under applied voltages of 200, 300 and 400 mV (Fig. 3.3 b). We observed a variation in the slope of the position-dependent force while increasing the applied voltage.
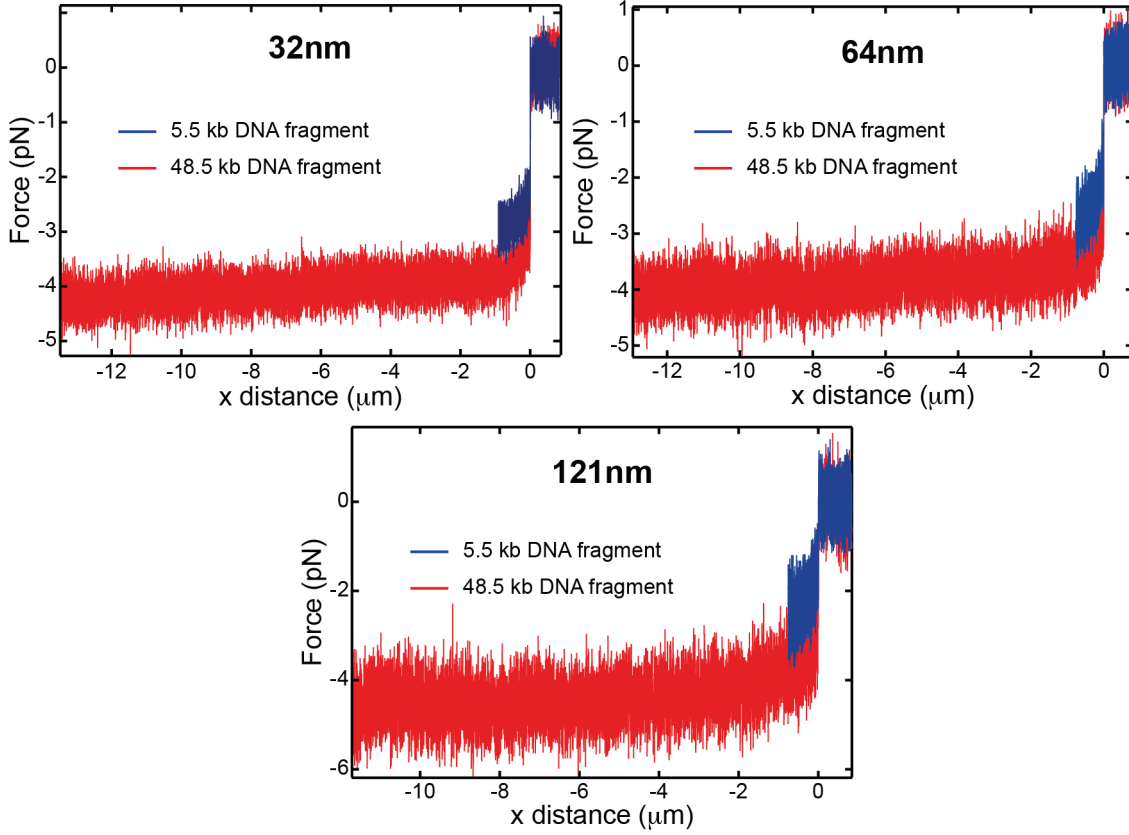
Figure 3.4 – **Comparison of the position-dependent force profiles for DNA of different length.** Reverse translocation of trapped DNA molecules (5.5 kb and 48.5 kb) was performed in nanocapillaries with diameters of 32, 64 and 121 nm in 40 mM KCl, pH 8.0. Direction of a nanocapillary is represented in the same way as in Fig. 3.3 b. The position-dependent force profiles were similar for DNA of different length, however the stalling force magnitude was higher for the longer DNA. The figure is taken from [127].

3.1.3   Explanation of position-dependent force profiles

To provide an explanation for the size- and voltage-dependent behaviour of the force profiles, we performed analytical and numerical calculations. Based on Ref. [107], the position-dependent force F(x) inside a nanocapillary is proportional to the position-dependent potential $\Phi(x)$:

$$F(x) = -\frac{q_{eff}}{l}\Phi(x) \tag{3.2}$$

where q_{eff} is the effective charge of a DNA base pair and l represents the distance between two base pairs. We modelled $\Phi(x)$ and $E(x)$ inside a nanocapillary with finite element analysis using COMSOL Multiphysics software (section 2.5.2). We represented a nanocapillary as a

3.1. Measurement of the position-dependent electrophoretic force on DNA in a glass nanocapillary
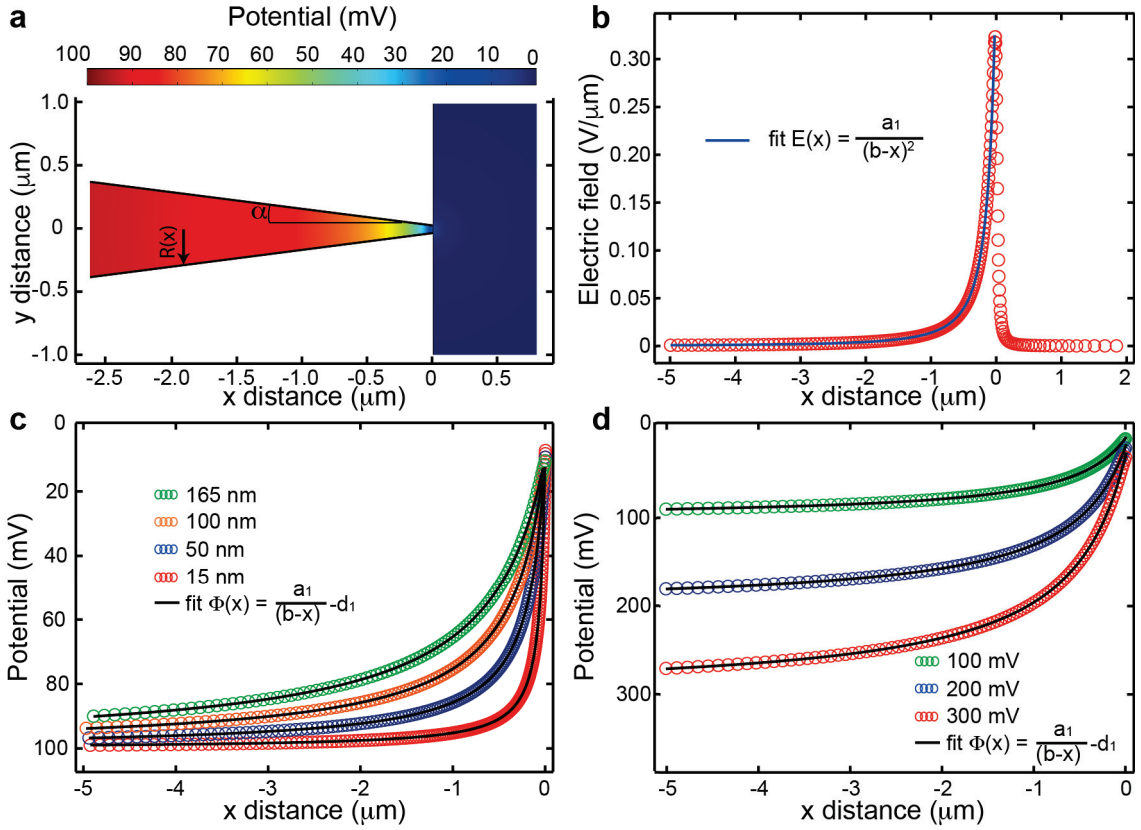
Figure 3.5 – Modelling of the position-dependent potential and electric field in nanocapillaries.
(a) Finite element analysis of the position-dependent potential in the conical nanocapillary with an opening radius R_0=30 nm, and an opening angle $\tan\alpha$=0.133. The modelling was simulated in 40 mM KCl at 100 mV. (b) The position-dependent electric field for the nanocapillary shown in (a). The data was fit to equation (2.4), coefficient b was fixed in accordance with the radius of the nanocapillary and a_1 as a fitting parameter. (c) The position-dependent potentials in nanocapillaries with diameters 15, 50, 100 and 165 nm, calculated in 40 mM KCl at 100 mV. The data was fit to equation (2.5), coefficient b was fixed in accordance with the radius of the nanocapillary, coefficients a_1 and d_1 as fitting parameters. (d) The position-dependent potentials for a 165 nm nanocapillary, calculated in 40 mM KCl at 100, 200 and 300 mV. Data was fit to equation (2.5), coefficient b was fixed in accordance with the radius of the nanocapillary, coefficients a_1 and d_1 as fitting parameters. All fitting parameters are shown in Table 3.1. The figure is taken from [127].

cone with an opening angle $\tan\alpha$=0.133 and varying radii R_0 (Fig. 3.5 a). A typical profile of the position-dependent electric field $E(x)$ in the 60 nm nanocapillary is shown in Fig. 3.5 b. We compared the distance-dependent potentials $\Phi(x)$ extracted from the finite element model for 15, 50, 100 and 165 nm nanocapillaries. The $\Phi(x)$ profiles were steeper for smaller nanocapillaries. Almost 90% of the applied potential drops within the first micrometer from the opening inside the 15 nm nanocapillary, whereas for the 165 nm nanocapillary this value was only ≈ 60%. This finding explains the difference in the position-dependent force profiles for nanocapillaries of different sizes (Fig. 3.3 a) and is one of the reasons of the higher stalling

force exerted on the 48.5 kb DNA versus 5.5 kb DNA (Fig. 3.1 c). Since the component of the electrophoretic force acting on a tethered DNA molecule from the outside of a nanocapillary is much less than from the inside (Fig. 3.6), it was not taken into account in the following analysis.

Table 3.1 – **Fitting parameters of the data represented in Fig. 3.5.**

figure	radius, nm	voltage, mV	a_1, V/μm	b, μm	d_1, V
3.5 b	30	100	$0.02 \pm 1.5\times10^{-5}$	0.23	0
3.5 c	7.5	100	-0.005 ± 10^{-6}	0.057	$-0.1 \pm 5.0\times10^{-6}$
3.5 c	25	100	$-0.017 \pm 3.6\times10^{-6}$	0.19	$-0.1 \pm 6.9\times10^{-6}$
3.5 c	50	100	$-0.035 \pm 7\times10^{-6}$	0.38	$-0.1 \pm 7.7\times10^{-6}$
3.5 c	82.5	100	$-0.057 \pm 4\times10^{-5}$	0.63	$-0.1 \pm 3.2\times10^{-6}$
3.5 d	82.5	100	$-0.057 \pm 4\times10^{-5}$	0.63	$-0.1 \pm 3.2\times10^{-6}$
3.5 d	82.5	200	$-0.11 \pm 8.2\times10^{-5}$	0.63	$-0.2 \pm 6.3\times10^{-5}$
3.5 d	82.5	300	$-0.17 \pm 1.2\times10^{-4}$	0.63	$-0.3 \pm 9.5\times10^{-5}$
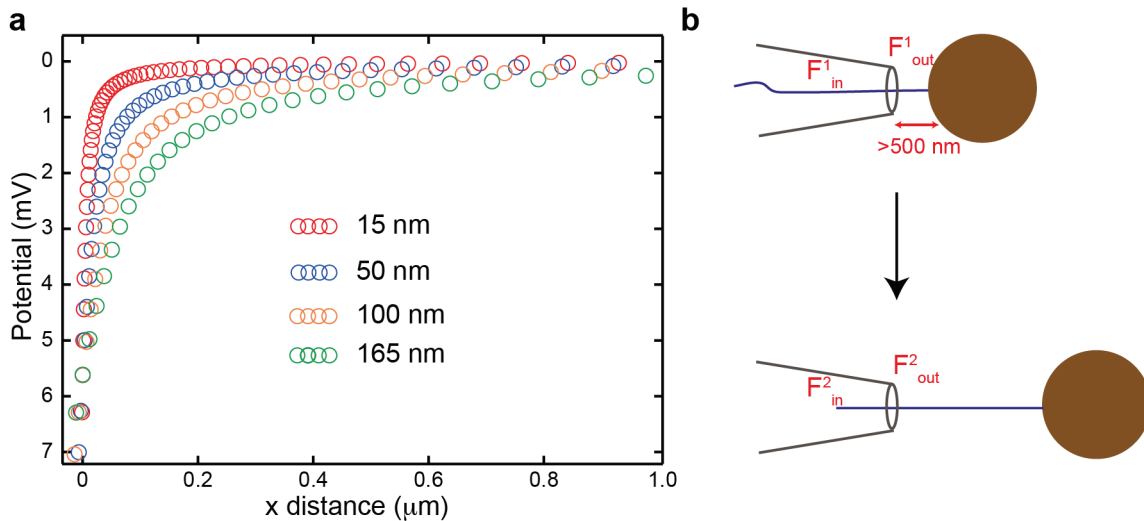
Figure 3.6 – **Potential distribution outside of a nanocapillary.** (a) Finite element analysis of the position-dependent potential outside of nanocapillaries of different sizes. The analysis was performed in 40 mM KCl at 100 mV for nanocapillaries with an opening angle tanα=0.133. X-axis is represented in the same way as in Fig. 3.3 b. Around 5-10 % of the total potential drops outside of nanocapillaries and majority of it is in the first 500 nm close to the tip. (b) The total electrophoretic force acting on tethered DNA can be assumed as a superposition of forces acting on DNA inside and outside of a nanocapillary: $F_{total}=F_{in}+F_{out}$. When a DNA molecule is pulled out of a nanocapillary the DNA length outside increases. This fact leads to the increase in the electrophoretic force acting on DNA from outside of the nanocapillary $F_{out}^2>F_{out}^1$, whereas $F_{in}^2<F_{in}^1$. Accordingly to the experiments the initial distance between DNA and a bead surface was not less than 500 nm. These data were extracted based on the length of DNA (1.85 μm) and the change in the position of the nanopositioning stage. Thus, the change in F_{out} during pulling a DNA molecule out of a nanocapillary was neglected in the analysis of the position-dependent force profiles. The figure is adapted from [127].

Accordingly to the analytical model, $E(x)$ inside nanocapillaries decays proportionally to x^{-2} (equation (2.3)), whereas $\Phi(x)$ obeys simple hyperbolic behaviour (equation (2.5)). To validate

the finite element analysis simulations, we fit $E(x)$ and $\Phi(x)$ acquired in COMSOL to equations (2.4) and (2.5), respectively as shown in Fig. 3.5 b, c and d. We observed an almost perfect fit of the COMSOL results to the analytical model.

Based on equations (3.2) and (2.5), the position-dependent force can be described by a hyperbolic expression:

$$F(x) = (\frac{a}{b-x}) - d \qquad (3.3)$$
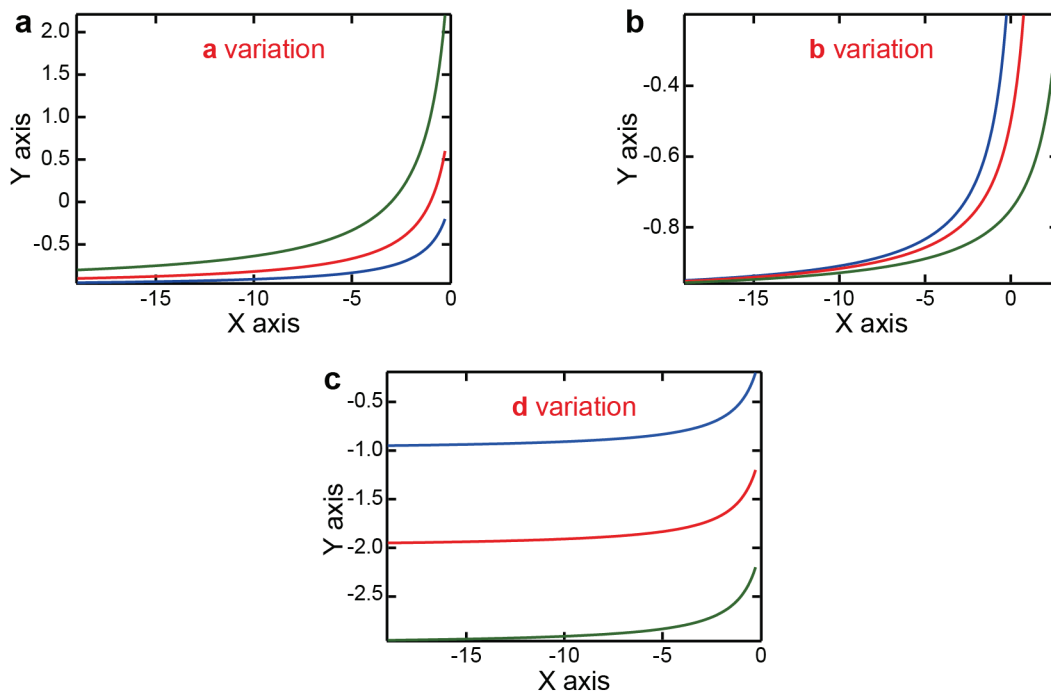
Figure 3.7 – **Representation of the role of parameters** a, b **and** d **in the function** $y(x) = \frac{a}{(b-x)} - d$ **(eq. (3.3)).** On all pictures the blue curve represents the function $y(x) = \frac{1}{(1-x)} - 1$. For clarity only the curve corresponding to negative values of x is shown. (a) Parameters $b=d=1$, $a=2$ (red curve), $a=4$ (green curve). The variation in a parameter results in change of the slope. (b) Parameters $a = d=1$, $b=2$ (red curve), $b=4$ (green curve). The variation in b parameter results in horizontal displacement of the curve. (c) Parameters $a = b = 1$, $d=2$ (red curve), $d=3$ (green curve). The variation in d parameter results in vertical displacement of the curve. The figure is taken from [127].

where a, b and d are parameters, which do not depend on the distance x inside a nanocapillary. Equation (3.3) represents a hyperbolic function, where coefficients b and d correspond to horizontal and vertical displacements of the curve, respectively, and coefficient a describes the slope of the curve (Fig. 3.7). Equation (3.3) demonstrates, that the electrophoretic force acting on different parts of a translocating DNA molecule decays with the distance inside a nanocapillary. A part of DNA close to the nanocapillary opening experiences higher electrophoretic force than one already further away from the entrance. Moreover, the electrophoretic force

decay depends on the geometry of a nanocapillary and it is steeper for the nanocapillaries of smaller diameters. While coefficient d in equation (3.3) is responsible for the magnitude of the stalling force, coefficients a and b describe the behaviour of the decay of the electrophoretic force on DNA with the distance inside nanocapillaries of different sizes.

Table 3.2 – **Coefficients used to describe the position-dependent force profiles for nanocapillaries of different sizes**. The force profiles were fit to equation (3.3), where coefficient b was fixed in accordance with the radius of a nanocapillary, and coefficients a and d were used as fitting parameters. The data were acquired in 40 mM KCl, pH 8.7, at 100 mV.

pore radius, nm	a, pN × μm	b, μm	d, pN
5	0.03 ± 0.0003	0.038	5.01 ± 0.001
7	0.037 ± 0.001	0.05	4.08 ± 0.002
23.5	0.17 ± 0.002	0.18	2.86 ± 0.004
30	0.19 ± 0.002	0.23	2.32 ± 0.004
42.5	0.27 ± 0.003	0.33	1.74 ± 0.01
50	0.33 ± 0.004	0.38	1.55 ± 0.01
82.5	0.49 ± 0.01	0.63	1.16 ± 0.01

Table 3.3 – **Coefficients used to describe the position-dependent force profiles for nanocapillaries at different voltages**. The force profiles were fit to equation (3.3), where coefficient b was fixed in accordance with the radius of a nanocapillary, and coefficients a and d were used as fitting parameters. The data was acquired in 40 mM KCl, pH 8.7, for the 165 nm nanocapillary.

voltage, mV	a, pN × μm	b, μm	d, pN
200	0.93 ± 0.01	0.63	2.55 ± 0.02
300	2.05 ± 0.01	0.63	5.13 ± 0.01
400	2.97 ± 0.02	0.63	7.38 ± 0.02

We fit our experimental data for nanocapillaries of different sizes to equation (3.3). The results are shown in Table 3.2 . Coefficient b, which represents the size of the capillary opening, was estimated from SEM images. During the fitting procedure, coefficient b was fixed and only coefficients a and d were used as fitting parameters. We noticed a trend of increasing of coefficient a for larger nanocapillaries. Coefficient a allows for the quantitative comparison of force profile slopes for nanocapillaries of different diameters. In contrast, coefficient d tended to decrease while increasing the size of nanocapillaries, due to the dependence of the stalling force on the opening size (Fig. 3.1 c). In addition, we analysed the voltage-dependent behaviour of force profiles inside a 165 nm nanocapillary using the same approach. The data was fit to equation (3.3) and represented in Table 3.3. We observed that the absolute values of coefficients a and d increase almost linearly at higher applied voltages.

However, there are some simplifications in our model, which we would like to emphasise below. First of all, the geometry of a laser pulled nanocapillary deviates from the shape of an ideal cone (Fig. 2.4) [87]. Shrinking of nanocapillaries under SEM leads to an additional

change of the shape close to the tip, especially for small nanocapillaries [89]. Moreover, the proposed model does not explicitly take into account the drag force (F_{dr}) on DNA and relies only on the bare electrostatic force (F_{bare}) through the assumption of a constant effective charge. Nevertheless, our model provides a good qualitative explanation of the experimental results and enables comparison of the force profile slopes recorded in nanocapillaries of different sizes and at different voltages.

3.1.4 Conclusions

We investigated the electrophoretic force on DNA in glass nanocapillaries shrunken under SEM. We demonstrated that the electrophoretic position-dependent force profiles depend on the nanocapillary size and the applied voltage. The results of this work provide a better understanding of the translocation behaviour of charged molecules through nanocapillaries. Compared to nanopores in a membrane, conical glass nanopores represent a system that can be easily tailored to simultaneously apply forces of different magnitude on different parts of tethered biomolecules.

3.1.5 Supplementary movies

The movies can be found following the links:

http://lben.epfl.ch/files/content/sites/lben/files/Movie1_10nm_nanocapillary.avi

http://lben.epfl.ch/files/content/sites/lben/files/Movie2_100nm_nanocapillary.avi

Movie S1 (Movie1_10nm_nanocapillary.avi) and Movie S2 (Movie2_100nm_nanocapillary.avi) show the capture of DNA molecules inside nanocapillaries followed by their reverse translocation. Initially, the DNA-coated beads are positioned in front of the nanocapillary openings and the positive voltage is applied in the trans chambers. In Movie S1 on the 3-4th second the bead suddenly jumps towards the opening, which represents the translocation and stalling of a DNA molecule. The DNA is pulled out from the nanocapillary using a nanopositioning stage. On the 11-12th second the bead suddenly jumps back towards the trap centre after pulling the DNA completely out of the nanocapillary. The second movie (Movie2_100nm_nanocapillary.avi) features the 100 nm nanocapillary. The translocation of DNA took place on the 3rd second and it was pulled out of the nanocapillary 4 seconds later.

Both experiments were carried out in the buffer containing 40 mM KCl, pH 8.7, at 100mV, using the 5.5 kb DNA fragment and nanopositioning stage at a velocity of 250 nm/sec. The stiffness used in the experiments was almost the same: 9.9 and 11.4 pN/μm for the 10 and 100 nm nanocapillary, respectively. However, in the case of the 10 nm nanocapillary the displacement of the bead is more pronounced. Consequently, the stalling force in the 10 nm nanocapillary is higher than in the 100 nm one.

3.2 Relevance of the drag force during controlled translocation of a DNA-protein complex through a glass nanocapillary
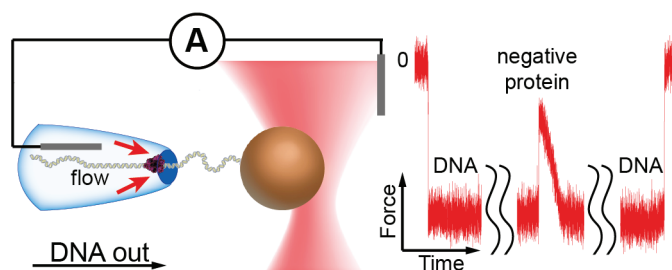
On the next step we moved to detection and characterisation of DNA-bound proteins in the system combining nanocapillaries and optical tweezers. We used 3 proteins RecA, EcoRI and RNAP. The first two proteins have been studied in nanopores combined with optical tweezers and therefore allowed us to reveal the effect of the capillary geometry on the protein force profiles. We characterised DNA-protein complexes at different buffer conditions, voltages by translocating them back and forth through the nanocapillary. In addition, we developed a model of controlled translocation that provided us an explanation of the observed force profiles and allowed to extract the effective charges of the proteins. This chapter is broken down into results, where we present force and current DNA-protein profiles, and discussion, where we give explanations of the observed phenomenon.

The results of this chapter have been published in the manuscript:

"Roman D. Bulushev, Sanjin Marion, and Aleksandra Radenovic. Relevance of the Drag Force during Controlled Translocation of a DNA-Protein Complex through a Glass Nanocapillary. *Nano Letters*, 15(10):7118-7125, 2015."

3.2.1 Detection of DNA-bound proteins with nanocapillaries and optical tweezers

In the system combining nanocapillaries and optical tweezers (section 2.3.2) we studied three DNA-protein complexes with EcoRI, RecA and RNA polymerase (RNAP). In this work nanocapillaries were pulled using program 3 from Table 2.1. The composition of experimental buffers is shown in Table 3.4. The stiffness of the trap was in the range of 30-80 pN/μm. Protocols for formation of DNA-protein complexes are summarised in section 2.4.1.

All chosen proteins have different physical-chemical characteristics (Table 3.5) and also differ in their way of interaction with DNA. EcoRI binds to the DNA as a dimer, RecA forms long polymeric fibres and RNAP interacts with the DNA as a single protein. While RecA binds nonspecifically to the DNA, EcoRI and RNAP recognise and interact with specific sequences. It is worth mentioning, the complex of EcoRI and RecA with the DNA was previously detected in the system combining nanopores in membranes and optical tweezers, and the choice of

Table 3.4 – **Buffers used in experiments and corresponding conductance changes due to translocation of DNA-bound proteins.**

application	[KCl], mM	[Tris/HCl], mM	[Tris/ Boric acid], mM	[EDTA], mM	pH	conductance change
Detection of DNA-EcoRI with nanocapillaries and optical tweezers	400	10	-	1	8.1	increase
	150	3	-	1	7.5	-
	40	-	3	1	8.7	-
Detection of DNA-RecA with nanocapillaries	1000	3	-	1	7.4	decrease
Detection of DNA-RecA with nanocapillaries and optical tweezers	1000	3	-	1	7.4	decrease
	150	3	-	1	7.2	decrease
	150	3	-	1	9.0	decrease
	150	10	-	-	8.0	decrease
	100	10	-	-	8.0	decrease
	40	3	-	-	8.0	decrease
Detection of DNA-RNAP with nanocapillaries and optical tweezers	40	3	-	1	8.1	decrease
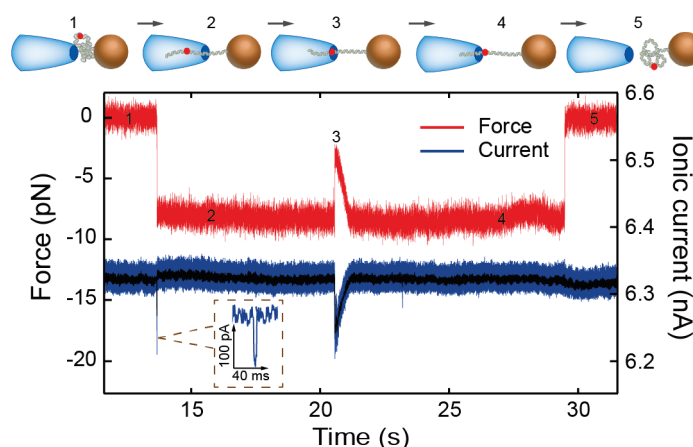
Figure 3.8 – **Measurement of force and current signals during controlled translocation of DNA-protein complexes through a nanocapillary.** The cartoon above explains consequent steps of the experiment. The inset shows the current signal corresponding to free translocation of a DNA-protein complex. Afterwards this complex was detected during controllable pulling of the DNA molecule out performed with a nanopositioning stage. Thus, it was possible to compare the current signatures of the same attached proteins during free and controlled translocation through the same nanocapillary opening. The amplitude of the conductance drops was similar, whereas the current profiles had different shapes. Movement of the nanopositioning stage initiated after entrance of the DNA molecule with a velocity of 800 nm/s. The experiment was performed with RecA bound proteins in a 44 nm nanocapillary at 150 mV in 150 mM KCl, pH 7.2. The figure is adapted from [130].

such proteins allowed us to directly compare the impact of the geometry of nanocapillaries on the force profiles of the DNA-bound proteins [118].

In a general case a controlled translocation of DNA continued smoothly with a change of

Table 3.5 – **Isoelectric points and sizes of DNA-EcoRI, RecA and RNAP complexes.**

protein	diameter of DNA-protein, nm	isoelectric point (pI)
EcoRI	≈5 [137]	≈6.4 [149]
RNAP	≈10 [150]	≈5.3 [151]
RecA	≈7 [98]	≈5.6 [98]

Figure 3.9 – **Illustration of a positively charged DNA-protein complex passing through a nanocapillary opening.** Cartoons on the left represent consequent steps of the experiment, whereas graphs on the right demonstrate corresponding force signals measured in the system. F_{ot} - the force measured with optical tweezers, F_{ep} - the electrophoretic force acting on the DNA, F_p - the force acting on the protein. The red circle represents a protein with a positive effective charge. Once such a protein is approached to the nanocapillary opening additional force F_p causes its "jump" to the lowest-energy state. This fast displacement can be observed by the change in the force and current signal and results in relaxation of the DNA outside of the nanocapillary. The figure is taken from [130].
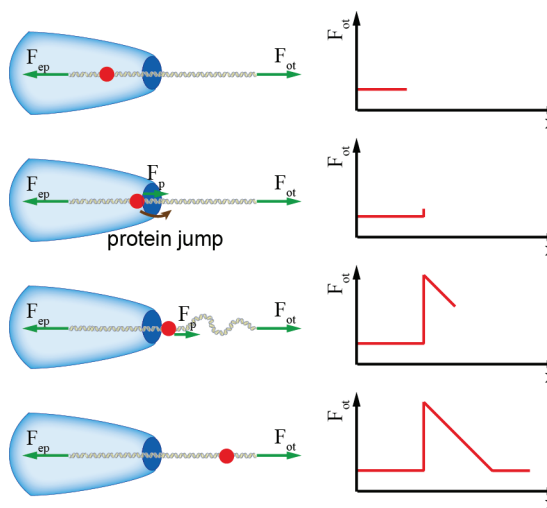
the stage position, marked by a flat force profile (Position 2 on Fig. 3.8), until a DNA-protein complex reached the opening of the capillary. At the opening there is the largest gradient of the electrostatic potential and the largest electroosmotic flow, and thus the largest force on the complex. When the force exerted by the external potential on the DNA strand is comparable to the force exerted on the DNA-protein complex F_p, it will be energetically more favourable for the protein to abruptly displace (jump) to a position where it experiences lower total force (Fig. 3.9). This is identified by a characteristic peak in both force and current (Position 3 on Fig. 3.8). A positively charged complex will jump outside the nanocapillary (positive work) followed by an increase in the length (coiling) of DNA between the capillary opening and the bead (Fig. 2.22 a, 3.9). As the stage position is increased, the complex stays at the same position until the extension of the DNA returns to the pre-jump level. After that a change in the stage also displaces the protein with the DNA. An effectively negatively charged complex first causes a coiling, before jumping when the DNA has accumulated sufficiently resulting in a mirrored jump shape (negative work) [118] (Fig. 2.22 b).

3.2.1.1   Detection of a DNA-EcoRI complex

EcoRI is a restriction enzyme that is known to cut DNA at the specific sequence GAATTC [152]. However, in the absence of Mg^{2+} ions EcoRI forms a stable complex with DNA without cleaving it [153, 154, 155]. After insertion of a single DNA molecule with attached EcoRI inside a nanocapillary, the DNA was pulled out through the opening until the specific peaks in force
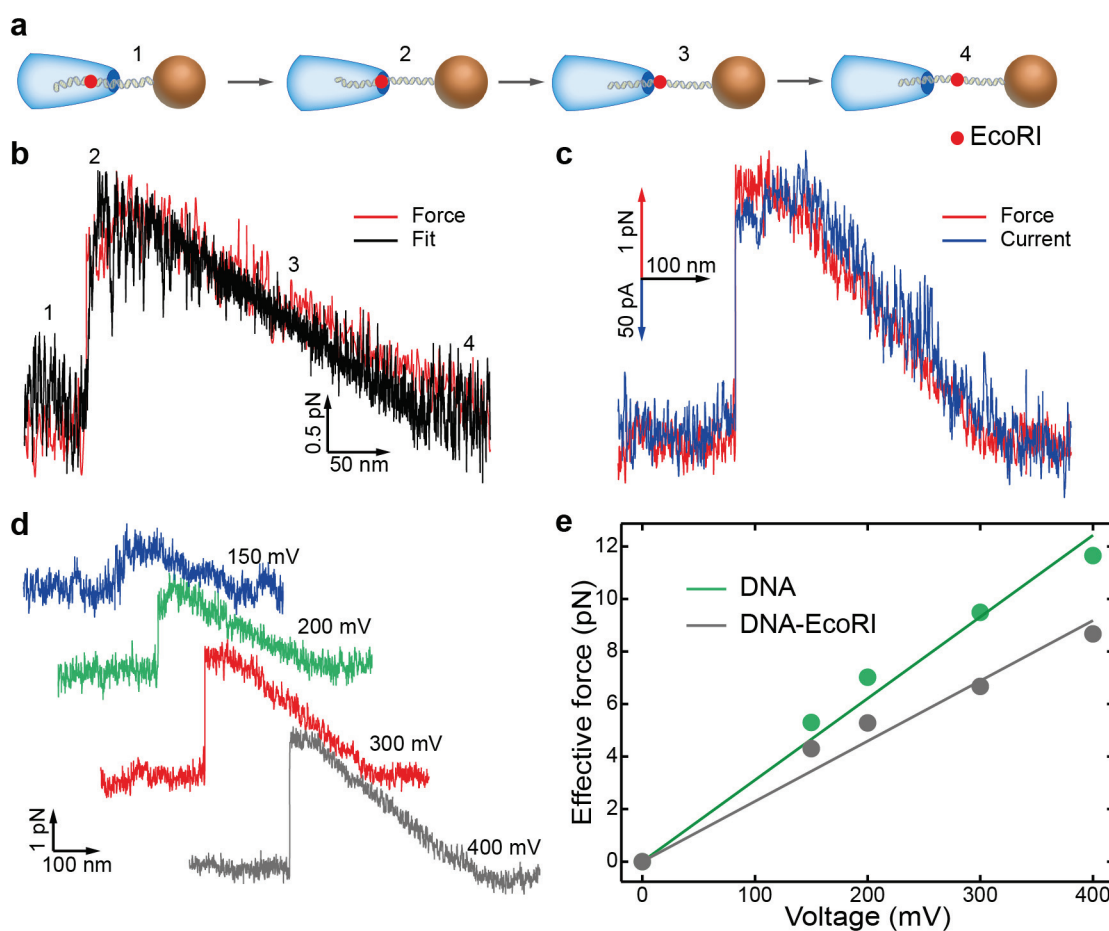
Figure 3.10 – **Detection of a DNA-EcoRI complex with glass nanocapillaries and optical tweezers.** (a) The cartoon represents the consequent steps of the experiment, where a red circle is an EcoRI protein. The orientation of the nanocapillary used in all experiments presented in this figure was the same as shown here. (b) Force profile of an EcoRI protein bound to DNA (red curve) and its fit to the analytical model (black curve) obtained at 200 mV. (c) Force (red curve) and current (blue curve) signals detected for the same EcoRI at 300 mV. (d) Force profiles of a DNA-EcoRI complex recorded at different voltages. (e) Comparison of the effective force acting on DNA and DNA-EcoRI complex at different voltages. In the case of the complex the force was measured at the peak maximum and data were fit to a linear function. All data in this figure were acquired in a 42 nm nanocapillary in 400 mM KCl, pH 8.1. The figure is taken from [130].

and current signals corresponding to the DNA-protein complex were revealed (Fig. 3.10 b, c). Experiments with DNA-EcoRI complexes were performed in different nanocapillaries and under various buffer conditions with the concentration of KCl 40-400 mM and pH 7.5-8.7 (Table 3.4, Fig. 3.11). The same EcoRI protein was detected at different potentials applied across the nanocapillary opening (FIg. 3.10 d). In general, the measured force on a DNA-EcoRI complex was lower than the one on the bare DNA, and it was linearly dependent on the voltage (FIg. 3.10 e). At higher potentials the surface area under the protein force curve linearly increased, corresponding to higher work required to pull the DNA-protein complex outside of the nanocapillary. Protein force signatures, and their dependence on the voltage were similar

to the results obtained with nanopores combined with optical tweezers [118].
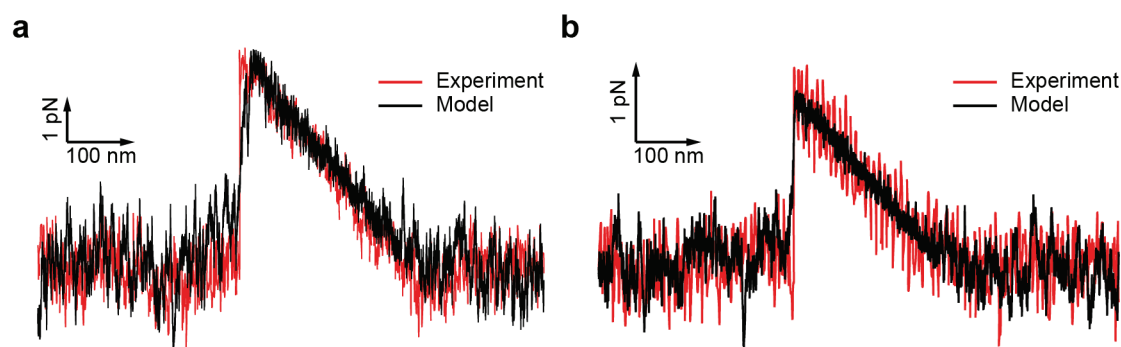
Figure 3.11 – **Force profiles of single DNA-EcoRI complexes in different conditions.** Experimentally obtained results (red) and their fits to the stochastic model (black). (a) The data obtained in a 43 nm nanocapillary at 200 mV in 150 mM KCl, pH 7.5. (b) The data obtained in a 42 nm nanocapillary at 150 mV in 40 mM KCl, pH 8.7. The figure is taken from [130].
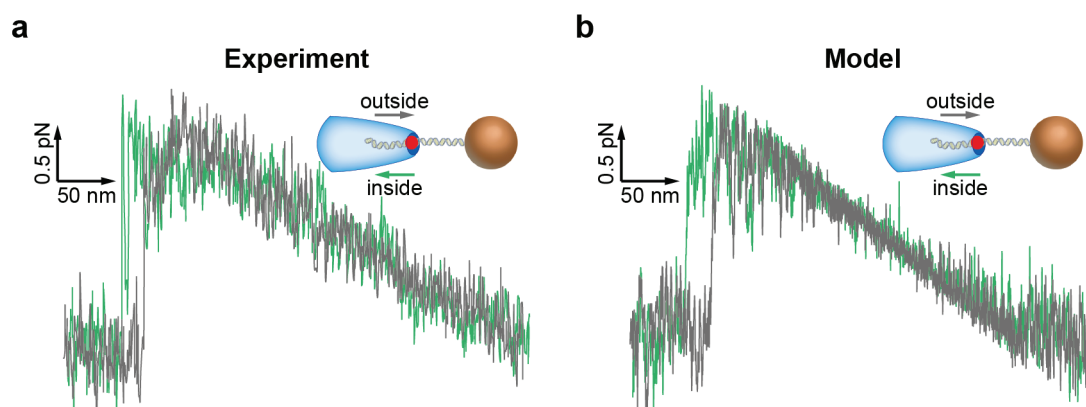
Figure 3.12 – **Threading/unthreading of a DNA-EcoRI complex through a nanocapillary.** Experimentally (a) and theoretically (b) obtained force curves of a DNA-EcoRI complex pulled outside (grey curve) and inside (green curve) the nanocapillary opening. The experimental data were acquired in a 42 nm nanocapillary at 200 mV in 400 mM KCl, pH 8.1. The figure is taken from [130].

The experimental data were fit to the stochastic model in the geometry of two truncated cones (Fig. 2.4, section 2.6.2). The effective charge q of a DNA-EcoRI complex was estimated to be +10-30 e in 40-400 mM KCl, pH 7.5-8.7, which is in the range of the values obtained in Ref. [118] in 20 mM KCl, pH 8.0. Pulling DNA-EcoRI back and forth through a nanocapillary opening revealed a hysteresis in the force profiles of ≈8 kT at 200 mV (Fig. 3.12). We attribute this value to an energy barrier for a jump from the cis to the trans state.

The current signature of a DNA-EcoRI complex (Fig. 3.10 c) shows a similarity to the force profile as both are related to the position of the protein inside the nanocapillary. To detect the current signature of EcoRI we increased the concentration of charge carriers to get 400 mM KCl, providing better signal-to-noise ratio. However, we did not detect many DNA-

protein complexes in such conditions due to their probable denaturation. We cannot make a conclusion on the direction of the conductance change, however the event demonstrated in Fig. 3.10 c had an increase in the conductance.

3.2.1.2 Detection of DNA-RecA and DNA-RNAP complexes

Next we studied a DNA-RecA complex, also previously detected in the system with nanopores and optical tweezers [115, 118]. This protein plays a key role in recombination, DNA repair and UV-induced mutagenesis in bacteria [156]. In the presence of ATPγS disassembly of RecA from DNA is drastically decreased resulting in a stable nucleoprotein complex [157]. Due to positive cooperativity RecA forms long filaments on DNA extended by 50% comparing to the DNA molecule [98]. The linear charge density of such filaments is approximately twice higher than those for the bare DNA [115]. In accordance with theory, the electrophoretic force on RecA-coated DNA inside nanopores and measured with optical tweezers was 2-4 times higher compared to the DNA [115]. In addition, force profiles of local RecA structures on the DNA in nanopores exhibited different behaviour than for an EcoRI protein due to the different charge of the complex [118].

However, in glass nanocapillaries DNA-RecA filaments experienced higher electrophoretic force than the bare DNA (Fig. 3.13 a) in 40 mM-1 M KCl, pH 7.2-9.0 (Table 3.4). To perform experiments we first introduced DNA-coated beads in the cis chamber and the force acting on the bare DNA inside nanocapillaries was recorded. Afterwards the chamber was flushed and beads covered with DNA-RecA were used. The theoretical coverage ratio of the DNA with RecA was 100 %, however we almost never observed fully covered DNA entering nanocapillaries. We assume that the observation of patches of bare DNA is due to low kinetics of RecA polymerisation at neutral pH [158] and high stiffness of the nucleoprotein filaments (persistence length ≈ 950 nm [98]), which could complicate their threading. Indeed, using atomic force microscopy (AFM) we observed stiff DNA-RecA filaments not always fully coated with RecA (Fig. 3.14). In our system a more flexible end of DNA not covered with RecA usually entered the nanocapillary first in accordance with Ref. [96] (Fig. 3.15).

In order to investigate local RecA structures on DNA we used the theoretical ratio of RecA to DNA that allows covering 20-60 % of the DNA molecule. We detected different segments of RecA on the DNA - long filaments and separate patches (Fig. 3.13 c). The electrophoretic force acting on such structures was lower than the one on the bare DNA, which is different from the results obtained in nanopores in membranes [118].

Comparison of the experimentally obtained curve in Fig. 3.13 b with the stochastic model in the double cone geometry (section 2.6.2) showed that the RecA segment has a length of 1850 nm with an effective linear charge density λ of -0.03 e/nm. Since λ of DNA was -0.15 e/nm in this experiment, RecA forms a complex with the DNA that causes a reduction in its effective linear charge density. As a consequence, such a complex produces a jump characteristic for positively charged proteins from the trans to the cis direction (Fig. 3.13 b). These results
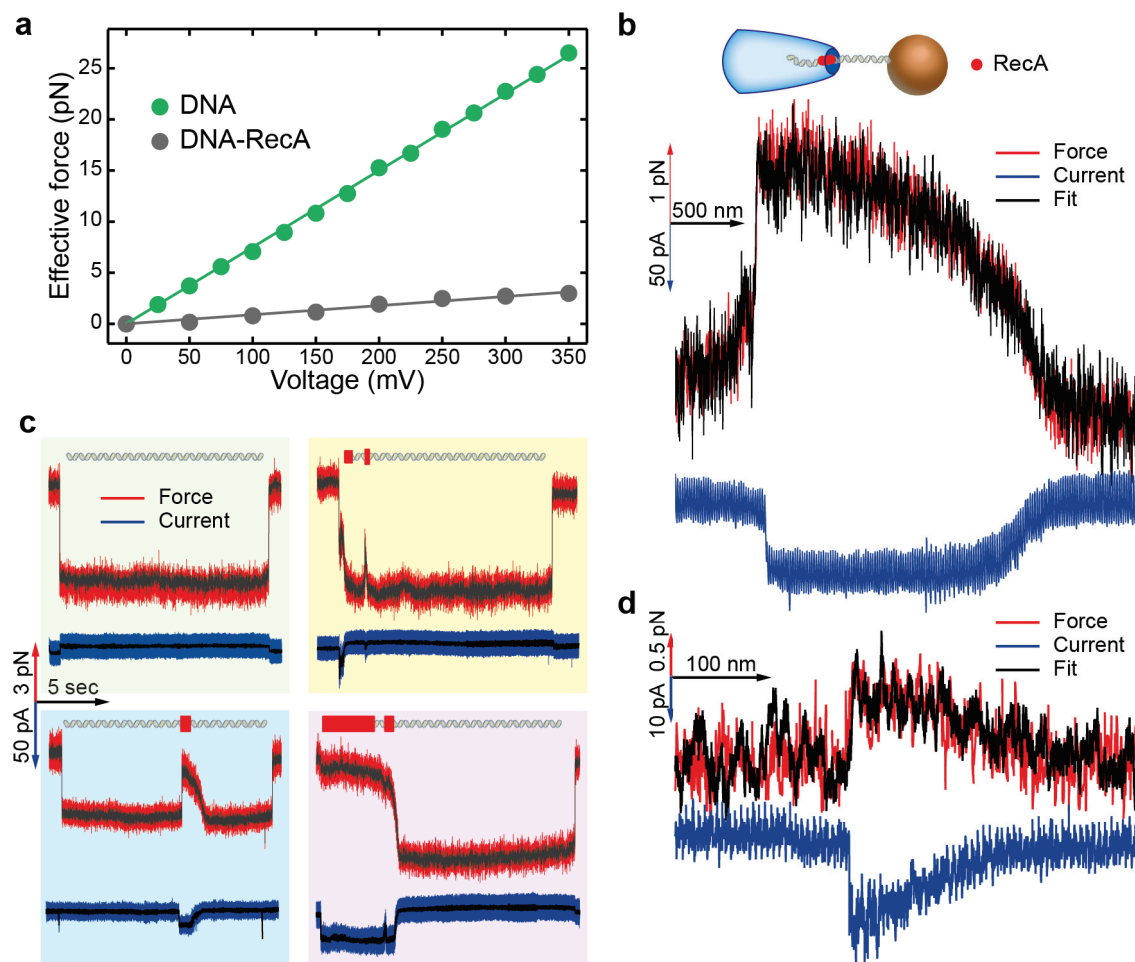
Figure 3.13 – **Detection of DNA-RecA and DNA-RNAP complexes with glass nanocapillaries and optical tweezers.** (a) Measured force versus voltage acting on DNA and DNA-RecA. The studied fragment of DNA-RecA experienced constant force at least during 500 nm. Data were acquired in a 21 nm nanocapillary in 150 mM KCl, pH 7.5 and fit to a linear function. (b) Force and current signals corresponding to a local RecA structure on DNA, where the red curve - the force signal, the blue curve - the current signal, the black curve - fit to the model. The cartoon illustrates the orientation of the nanocapillary used in all experiments presented in this figure. Data were acquired in a 108 nm nanocapillary at 150 mV in 150 mM KCl, pH 7.2. (c) Force and current signals corresponding to DNA and DNA partially covered with RecA, where the red curve - the force signal and the blue curve - the current signal. The red rectangles on the DNA above the graphs correspond to local structures of RecA. The data were acquired in two different 59 nm nanocapillaries at 100 mV (left bottom graph) and 150 mV (all other graphs) in 150 mM KCl, pH 7.2. (d) Force and current profiles of a DNA-RNAP complex, where the red curve - the force signal, the blue curve - the current signal, the black curve - fit to the model. The data were acquired in a 44 nm nanocapillary at 150 mV in 40 mM KCl, pH 8.1. The figure is taken from [130].

contradict to the fact that DNA-RecA complexes have higher linear charge density than DNA [115] and lead us to the conclusion that the electrophoretic driving force inside nanocapillaries cannot be based only on electrostatic interactions.

a

b
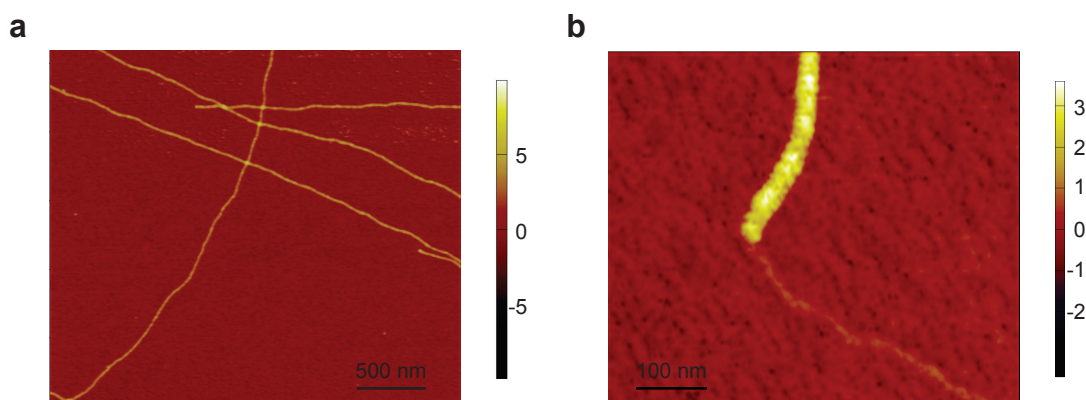
Figure 3.14 – **AFM images of DNA-RecA complexes.** (a) DNA-RecA complexes form stiff filaments. (b) Even though the theoretical coverage of DNA molecules was 100% we found fragments of the DNA that did not form a complex with the protein. Relatively flexible ends of uncovered DNA could facilitate entrance inside nanocapillaries. The figure is taken from [130].
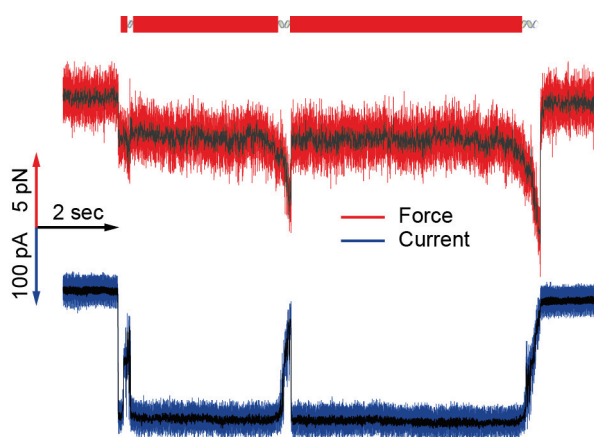
Figure 3.15 – **Force and current profiles of a DNA-RecA complex in a nanocapillary with a small diameter.** Cartoon above represents coverage of the DNA with RecA (red rectangles). There are three parts of the DNA not completely covered with RecA. One can see additional details of the DNA-protein complex provided by the current signal. The data were acquired in a 21 nm nanocapillary at 150 mV in 150 mM KCl, pH 7.5. A nanopositioning stage was activated after entrance of the DNA with a velocity of 800 nm/s. The figure is taken from [130].

To eliminate the possibility of RecA fibre structures influence the measured force we also studied a complex of a single RNA polymerase (RNAP) with DNA. RNAP is responsible for transcription using nucleoside triphosphates (NTP). In the absence of one of NTPs it forms a paused transcription complex on the DNA [133, 159]. Although the charge of RNAP was estimated to be negative, i.e. equal to -77 e at pH 7.0 [58], we found that a DNA-RNAP complex also reduces the effective local charge of the DNA (Fig. 3.13 d). Using the stochastic model in the double cone geometry we estimated the effective charge of the DNA-RNAP complex to be +10 e at 40 mM KCl, pH 8.1. In the same experiment λ of the DNA was -0.06 e/nm. Notably, different experimental conditions (buffers and nanocapillaries) cause different linear charge density of DNA due to the difference in the drag force. Considering that RNAP covers a length of DNA of ≈10 nm leads us to a local linear charge density of the complex +0.94 e/nm. Thus, the effective charge of the DNA-RNAP complex is locally positive inside nanocapillaries.

3.2.2 Discussion of force profiles of DNA-protein complexes

In the system combining nanocapillaries and optical tweezers we observed that negatively charged proteins bound to DNA experience lower electrophoretic force than the bare DNA. In the previous experiments with nanopores and optical tweezers it was shown that the electrophoretic force on a DNA-RecA complex was higher than on the DNA and opposite for a DNA-EcoRI complex [115, 118]. We proposed an explanation of this phenomenon based on the high impact of the drag force during controlled translocation of a DNA-protein complex through a glass nanocapillary.

Nanocapillaries in comparison to nanopores have larger characteristic length where the electrostatic force is enclosed (section 3.1). Based on their shape, nanocapillaries should have a better-formed flow profile, which is known to be directed outwards from the opening, opposing the electrostatic force on negatively charged molecules and producing additional drag [52, 122, 160]. From the other hand, larger penetration of the potential drop inside nanocapillaries leads to the local extension of DNA up to 20-30 persistence lengths inside the nanocapillary compared to just one persistence length inside nanopores [145]. To obtain these numbers we determined when the thermal (random) force $k_B T / L_p$ is stronger than the electrostatic force $E(x)L_p\lambda$ at the position x using a COMSOL simulation (Fig. 2.18). Longer rod-like DNA could also influence better flow formation resulting in higher drag force. Experimentally this drag can be seen in a 2-5 times smaller effective electrophoretic force on DNA in nanocapillaries than in nanopores [127, 113, 114, 161].

Another argument supporting the strong impact of the EOF inside nanocapillaries is the difference in the drag force acting on proteins of different sizes. All proteins we used are negatively charged, some are expected to be even more charged than DNA. However, we observed that the linear charge density of RecA is less than those for DNA, and that the charge density of RNAP even changes the sign. We attribute this fact to the EOF-induced drag force, which renormalises the electrostatic charge of the proteins. Based on the sizes of studied DNA-protein complexes (Table 3.5), we expect RNAP to be subject to the largest drag force and EcoRI - the smallest in identical experimental conditions. From the COMSOL model we concluded that F_{drag} on proteins attached to DNA could be approximated using the Stokes drag equation (see section 2.6.1). Thus, we can relate the ratio of the Stokes drag between these three individual proteins as $F_{stokes}(EcoRI) : F_{stokes}(RecA) : F_{stokes}(RNAP) = 5:7:10$. Based on the flow velocity being in the order of 10 mm/s (Fig. 2.19 a), we can estimate that the drag force on these proteins can be above several pN, e.g. sufficient to overcome the electrostatic force.

To additionally support the hypothesis of importance of the drag force in nanocapillaries we studied free translocation of DNA-RecA complexes. It was previously reported that the force measured with optical tweezers and velocity of translocation are roughly proportional [113, 162]. In solid-state nanopores 20% RecA-coated λ-DNA had similar dwell times as the bare DNA [96]. However, in glass nanocapillaries we observed that there was a population of

events of partially coated DNA with RecA that had much longer dwell times than the bare DNA (Fig. 2.11). This is consistent with the smaller electrophoretic force acting on the nucleoprotein filaments originated from higher drag force.

3.2.3 Discussion of conductance drops of DNA-protein complexes

During DNA translocation through a nanopore the measured conductance can either increase or decrease, depending on the salt concentration [162]. It was considered that at low salt concentration (<300 mM KCl) DNA enhances the local concentration of charge carriers due to its counter ions and produces an increase in the conductance [162]. While at high salt concentrations (>300 mM KCl) a decrease in the conductance was explained as coming from the reduction of the effective cross sectional area available for conduction (a current blockage) [163, 164]. However, the recent work implies that at all salt concentrations DNA enhances the concentration of local charge carriers and the current blockage model is not applicable [165]. The crossover point at 300 mM KCl is attributed to the dominant frictional forces between the ions and DNA, causing a current drop [165]. In our case, both DNA and protein present microscopically rough surfaces and influence the current modulation.

To date, there are not many results of detection of DNA-protein complexes in nanopores or nanocapillaries at low salt concentration. Usually nanopore experiments are performed in denaturing conditions allowing for detecting only proteins stably bound to DNA [115, 58, 99, 101]. In our system we detected current signatures of DNA-protein complexes in physiological conditions with the concentration of KCl in the range of 40-150 mM (Fig. 3.13 b, c, d). Notably, the current in addition to the force signal increases the resolution for detection of local protein structures on DNA, especially in nanocapillaries of small diameters (Fig. 3.15). Current and force signals have similar shapes since they both are related to the position of the protein in respect to the narrowest part of the nanocapillary (Fig. 3.10, Fig. 3.13 b, c, d).

However, to detect current signatures of a DNA-EcoRI complex we had to increase the concentration to 400 mM KCl. At these non-physiological conditions we did not detect many complexes and were not able to make a conclusion regarding the current profile of DNA-EcoRI. In contrast, for DNA-RNAP and DNA-RecA complexes in the range of 40-150 mM KCl we measured a decrease in the conductance during their controlled translocation (Fig. 3.13 b, c, d, Table 3.4). Our results are different from those obtained for DNA-RecA in the system combining nanopores and optical tweezers, where a conductance drop at 600 mM KCl and a conductance increase at 100 mM KCl were obtained [115]. Comparing these data for DNA-RecA conductance modulation to well-known results for DNA [162], we would also expect a transition point in the conductance in nanocapillaries. As DNA-RecA has a larger diameter than DNA, we could argue that the molecular friction contribution between charge carriers and RecA surface is stronger at larger drag forces, thus more likely reducing the transition point below our experimental range (<40 mM KCl) [165].

DNA-RNAP conductance drops can be attributed both to a current blockage [164] and to

reduction of the current at the surface due to molecular friction [165]. In the context of our experiments, RNAP has low surface charge density, as the drag force is capable to overcome its electrostatic charge. It is even possible that the drop in the conductance happens due to the fact that a DNA-RNAP complex removes the local DNA counter ion charge and thus reduces the number of charge carriers. A similar current drop was detected for a single DNA-2-CysPrx complex during its controlled translocation through nanopores in 20 mM KCl [117]. In our system, it is possible that the EOF contributes to the change of the conductance during translocation of a DNA-protein complex by changing the advective current density [165] - an effect analogous to current polarisation [160]. This phenomenon would also explain a conductance drop for RecA-coated DNA that we observed in nanocapillaries at salt concentration as low as 40 mM KCl.

3.2.4 Conclusions

We demonstrated that glass nanocapillaries combined with optical tweezers is a suitable tool for detection of DNA-bound proteins in physiological conditions. Nanocapillaries showed versatility due to their simple fabrication process and high SNR, allowing for the recording of current signatures of DNA-protein complexes. We observed renormalised effective charge of proteins attached to DNA inside nanocapillaries that we attributed to the EOF-induced drag force. The impact of the drag force during translocation of molecules was demonstrated before in nanopores in membranes [107, 113, 114, 161]. In certain cases the drag force dominated the electrostatic force resulting in translocation of charged molecules in the direction against the electric field [166]. On the example of DNA-protein complexes we showed relevance of the drag force during its translocation through conical nanopores made in glass and estimated the drag force to be higher than in nanopores in membranes.

3.3 Single molecule localisation and discrimination of DNA-protein complexes by controlled translocation through nanocapillaries

Conductance Drop
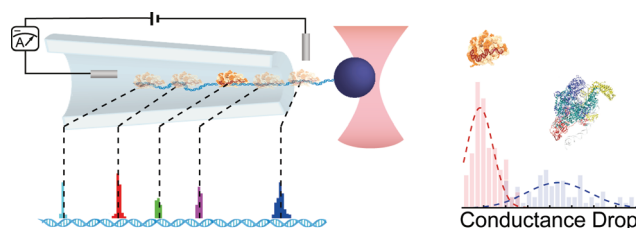
After having DNA-protein complexes characterised in the system we tested the ability to localise and discriminate DNA-bound proteins using our technique. We designed binding sites for two proteins dCas9 and RNAP at certain locations on DNA. During controlled translocation of DNA we measured its exit point and knowing the distance moved by a nanopositioning stage before the exit we mapped out the DNA-protein sites. We observed a displacement of the detected positions compared to the designed (theoretical) ones. We developed a model that explains and accounts for the measured shift. Moreover, while measuring the location of the complexes we also recorded their corresponding works and conductance changes. These data helped us to discriminated between DNA-RNAP and dCas9 complexes.

The results of this chapter have been published in the manuscript:

"Roman D. Bulushev, Sanjin Marion, Ekaterina Petrova, Sebastian J. Davis, Sebastian J. Maerkl and Aleksandra Radenovic. Single Molecule Localization and Discrimination of DNA–Protein Complexes by Controlled Translocation Through Nanocapillaries. *Nano Letters*, 16(12):7882-7890, 2016."

3.3.1 Localisation of protein binding sites on DNA

To study localisation of proteins we used dCas9 and RNAP which are known to bind to specific sites along DNA. In contrast to free translocation experiments [58, 99], we carried out our experiments in physiological ionic and pH conditions. All DNA-protein complexes were probed in the same buffer (100 mM KCl, 10 mM HEPES, 5% glycerol, pH 7.5) barring the addition of 0.01% TWEEN 20 to RNAP to prevent sticking of the protein to the capillary. Glass nanocapillaries were pulled accordingly to program 4 from Table 2.1 and shrunken to diameters 43-58 nm. Applied voltage bias varied between 150-200 mV to optimise the capture rate during bead approach and signal-to-noise ratio of the current measurement. The stiffness was in the range of 60-120 pN/μm. In the case of dCas9 we took advantage of the single guide RNA technique to engineer five distinct sites along the 16.5 μm (48.5 kbp) λ-DNA, whereas for RNAP we probed two distinct sites along a shorter, 2.45 μm (7.2 kbp) DNA (see 2.4.1 for details of complex formation). For dCas9 we performed experiments both with a single RNA guide present in the mixture as well as with several (two and three). The presence of multiple binding site possibilities did not affect the localisation of each individual site and shows the
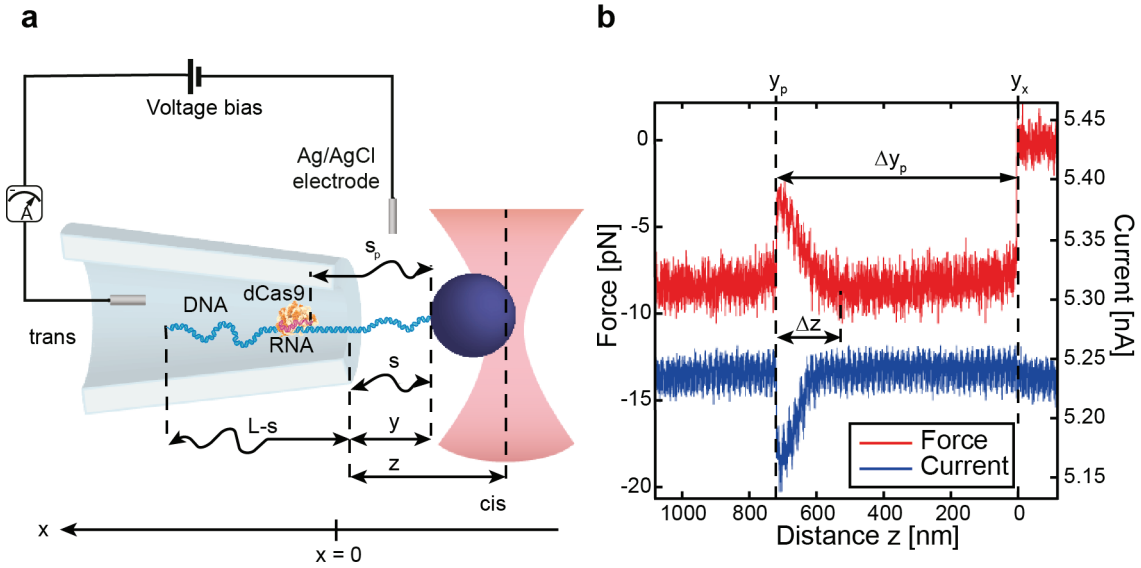
Figure 3.16 – **Notations used during localisation of DNA-protein complexes in nanocapillaries.** (a) Schematic of the experimental setup with notations. The distance between the optical trap equilibrium position and the capillary opening (stage distance) is marked as z, the distance between the capillary opening and the surface of the bead is marked as y. The total length of the DNA is L, while s is the length of the DNA contour between the bead and the capillary opening. The bead to protein distance, as measured along the contour, is marked s_p. (b) Typical force and current curves are shown as a function of the stage z with the jump location marked as y_p and the DNA exit out of the capillary marked as y_x. The protocol used to move the stage and thus pull out the DNA was a linear increase of z with a speed $v \approx 500\ nm/s$. We measured the relative distance Δy_p between two points y_x and y_p, and the protein jump width is marked as Δz. The figure is taken from [146].

potential of using our method to perform multiplexed localisation. Indeed in some cases we were able to observe multiple binding events on the same DNA.

During controlled translocation of DNA we visualised additional peaks in the force and current signals corresponding to DNA-protein complexes (Fig. 3.16, see section 3.2.1 for additional explanations of protein force and current profiles). The binding site position $\Delta y_p = y_x - y_p$ was determined as the distance between the DNA exit out of the capillary (y_x) and the position of the protein jump inside the capillary (y_p) (Fig. 3.16 b). Measured protein binding locations for all sites are shown in Fig. 3.17 as histograms. For each binding site studied we obtained a histogram which included both specific and non specific events with clustering seen at positions close to the theoretically predicted ones (Fig. 3.18).

We eliminated all events which deviated strongly from these clusters as non specific binding by implementing a modified Z score analyses [167]:

$$Z_{score} = \left| \frac{0.6745 \cdot (x_i - \bar{x})}{MAD} \right|. \tag{3.4}$$
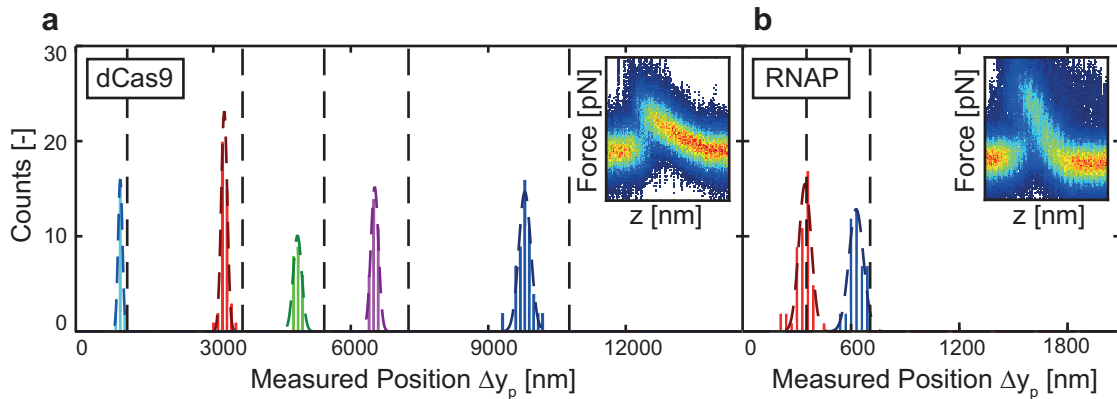
Figure 3.17 – **Localisation of protein binding sites on DNA in physiological conditions.** (a) Localisation histograms obtained from force curves for five dCas9 sites along λ-DNA in 100 mM KCl, 10 mM HEPES, 5% glycerol, pH 7.5. Black, vertical, dashed lines represent expected (theoretical) binding sites at 1100, 3570, 5320, 7120, and 10560 nm from the free end. Different coloured histograms represent different binding sites with only specific events shown. In total 17 different capillaries were used across the five sites and the number of single specific complexes used was 20, 42, 24, 31, and 54 for each site respectively. (b) Localisation of two RNAP binding sites along a 2450 nm long DNA in 100 mM KCl, 10 mM HEPES, 5% glycerol, 0.01% TWEEN 20, pH 7.5. Black, vertical, dashed lines are theoretical binding sites at 400, and 750 nm from the free end. In total 4 different capillaries were used across the two sites and the number of single specific complexes was 49 and 43 for each site respectively. Insets in panel a (b) represents the density plot of 60 (122) averaged force curves for dCas9 at site 1100 nm (RNAP at site 750 nm), which were shifted to the same DNA force level and normalised to a probability of 1 for each z. Force curves also include events without an equal DNA base level before and after the jump that were not used for later non-equilibrium work analysis. The figure is taken from [146].

If Z_{score} was above 3.5 for a given trajectory then that protein event was classified as non specific. Here x_i is the location of the protein for trace i, $\bar{x}$ is the median of the set, and MAD is the median absolute deviation of the set given by the median of $|x_i - \bar{x}|$. The Z score criteria was implemented to identify specific binding in all our cases (see Fig. 3.18).

With larger statistics this method may be able to better assess non specific binding of proteins and determine if any differences are present in size or charge which would hint at variation in binding interactions between specific and non specific binding. Non specific binding has been seen both *in vivo* and *in vitro* [168, 169, 170, 171] and results, for example in the case of dCas9, from mismatching between the RNA guide sequence and the DNA, bulge formations, or transient binding [172]. The obtained localisation has an average standard deviation of 97 nm and 49 nm respectively for dCas9 and RNAP, with a smaller error near the free end of DNA and thus a smaller error for shorter DNAs, as seen with RNAP.

We assume the error comes from a wide distribution of drag forces on the DNA strand, the stochastic nature of the process, unspecific interactions not taken into account by our statistics,
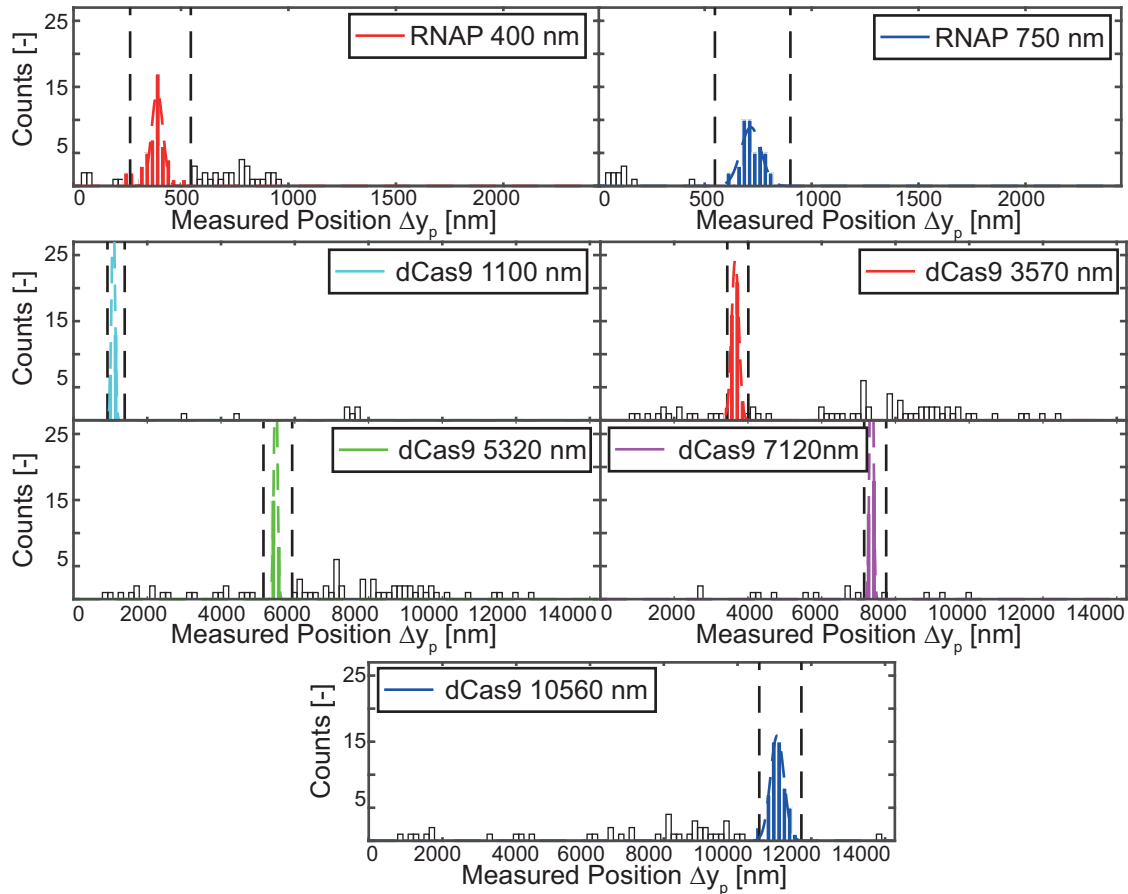
Figure 3.18 – **Histogram of protein localisation including non specific events.** Coloured bins correspond to binding events identified as specific and white bins non specifically bound proteins. Vertical, dashed, black lines represent the limit between specific and non specific binding. See accompanying text for the criteria used to identify specific binding. The figure is taken from [146].

friction between the DNA and the capillary (if the pulling occurs slightly off axis), and a minor contribution also comes from the different voltages used. To verify that there is no dependence on the translocation protocol we performed a reverse protocol (threading the complex into the capillary) but found no difference in the localisation value (Fig. 3.19) which we attribute to a small or negligible hysteresis [118, 130]. This result differed from the one obtained with a DNA-EcoRI complex (Fig. 3.12). We assume that the hysteresis on Fig. 3.19 could be hidden within an experimental error of protein localisation during averaging. This error was 110 (130) bp and 11(14) K_BT for taking the complex out (pulling in).

3.3.2   Analytical model for explaining localisation shifts

Although we localised protein binding sites, both thanks to force and current traces (Fig. 3.20 a), the positions were shifted in comparison to the expected locations (Fig. 3.17 a, b). For positions close to the free end of the DNA strand, the shift is small, or even negligible in the case
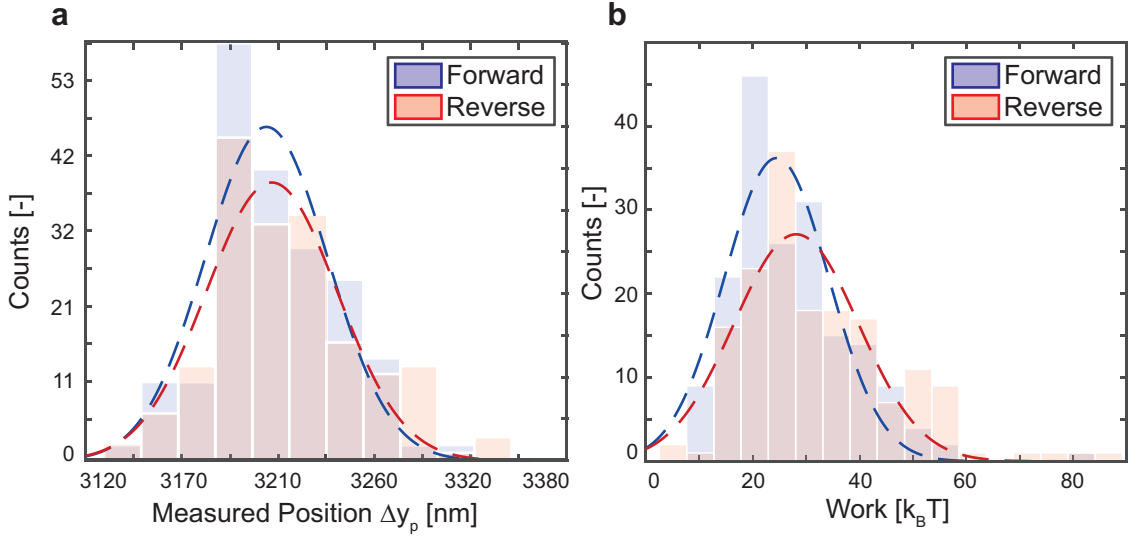
Figure 3.19 – **Localisation and work hysteresis measured for a DNA-protein complex.** (a) Forward (translocation from in- to outside the capillary) and reverse (from out- to inside) histograms of protein localisation Δy_p performed to verify that localisation does not depend on the direction of the translocation protocol. Experiments were performed for dCas9 binding site at 3570 nm with 10 distinct protein-DNA complexes where each complex was probed with a forward and backward protocol multiple times producing from 20 to 40 individual protein jump events. For these experiments we used a sawtooth pattern for the nanopositioning stage, without allowing the DNA to exit. (b) By performing back and forth experiments as described previously we compared the work performed in the forward and reverse events. A difference was observed between forward and reverse works which hints at the hysteresis of the cycle, but it was not significant enough for further analysis. Note that the definition of forward/backwards work will be different for proteins with a different charge sign. The figure is taken from [146].

of one RNAP binding site, and it grows as the expected position is closer to the tethered end of DNA. Fig. 3.20 a shows how the difference between the measured and expected positions for dCas9 and RNAP (inset) $\Delta_{shift} = (L - s_p) - \Delta y_p$ depends on the theoretical location of the complex. This shift can be explained by taking into account that the experimentally measured distance of the protein Δy_p is not the same as its position s_p along the DNA contour. At any distance y between the capillary opening and the bead, the DNA "coil" is extended to a contour length s such that the extension $\mu(s) = y/s < 1$. The shift Δ_{shift} is due to an early exit of the DNA strand out of the capillary (the DNA strand's exit length s_x is shorter than the full length L of the DNA strand), caused by fluctuations, as well as the DNA being extended by the pulling force. For each contour length s there is a corresponding y such that

$$\Delta y_p = s_x \mu(s_x) - s_p \mu(s_p), \tag{3.5}$$

with s_x the contour length corresponding to the DNA exit location y_x. The effect of the localisation shift is to make the apparent protein position smaller than expected.
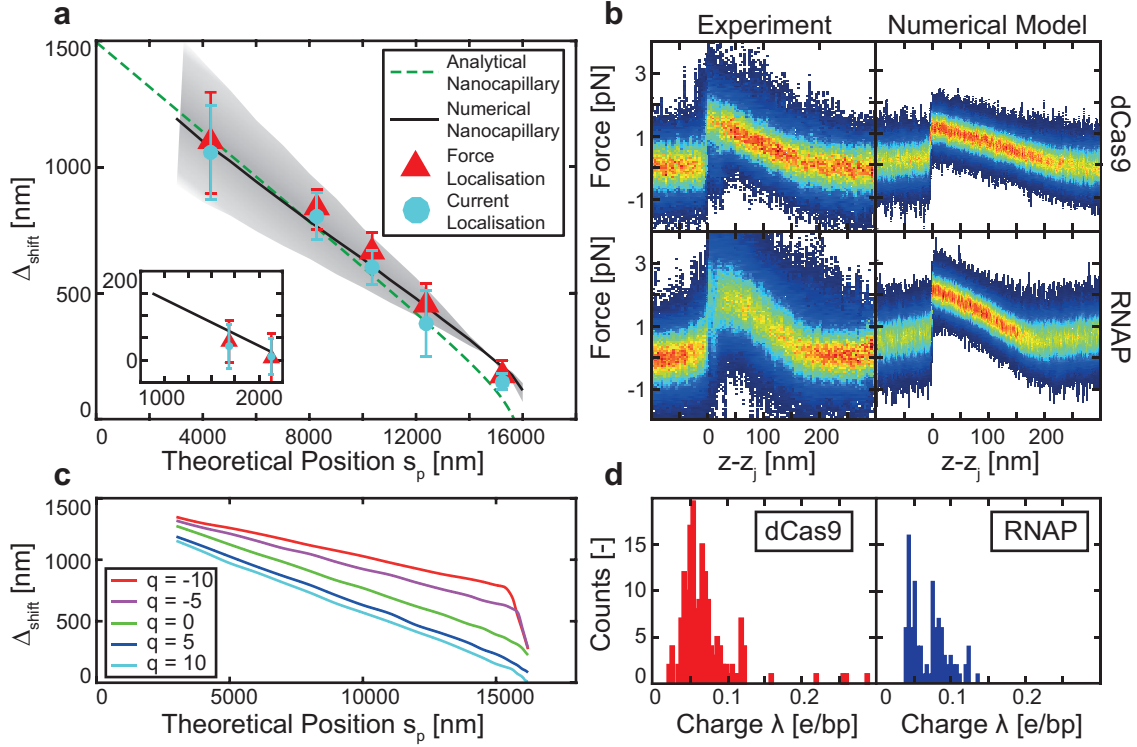
Figure 3.20 – **Protein binding site localisation shift.** (a) Difference between measured and expected location $\Delta_{shift} = (L - s_p) - \Delta y_p$ for dCas9 binding sites on λ-DNA. Red triangles correspond to localisation shift obtained from force curves, and blue circles from current curves, all for 5 tailored binding sites on λ-DNA. Green dashed line represents the best fit obtained with the analytically derived nanocapillary shift formula. Full black line represents the numerically obtained fit with $\xi = 75$ nm, $V = 200$ mV, $\lambda_{DNA} = -0.04\ e/bp$, and the effective protein charge $q^* = 10e$, while shaded area shows the variation of the numerical fit curve if λ_{DNA} varied from $-0.02\ e/bp$ (upper border) to $-0.08\ e/bp$ (lower border) as in panel d. Inset shows the same for two RNAP binding sites on a short 2448 nm DNA with an analytical fit with the same parameters as in the full panel except $\xi = 10$ nm (most likely due to boundary effects). (b) Comparison of 47 and 110 force versus stage position curves plotted as density plots for dCas9 and RNAP respectively (left column) with numerically obtained plots (right column). The sites shown correspond to the same as in the insets of Fig. 3.17 (i.e 1100 nm and 800 nm for dCas9 and RNAP respectively). Before averaging, all curves were shifted so that the jump position is at $z = 0$ and all noisy curves, without a well defined DNA force level before and after the jump, were not taken into consideration. (c) Plot of localisation shift obtained from the numerical stochastic model using different values of the effective charge of the complex for the same parameters as the numerical fit in panel a. Charge $q = 0$ corresponds to no protein, i.e. bare DNA localisation shift. (d) Histograms of measured DNA linear charge density λ_{DNA} for dCas9 and RNAP attributed to changes in the electroosmotic flow induced drag force. The histograms correspond to a total of 10 (2) nanocapillaries used for dCas9 (RNAP) localisation. The figure is taken from [146].

The extension of the DNA molecule, $\mu(s) = y/s$, which is required to explain the shift, can be obtained analytically in the strong stretching regime [143] which corresponds to the range of forces on DNA measured in typical experiments [173, 127] (Fig. 3.1). It is useful to compare how the results change between nanopores and nanocapillaries, as both can be used for localisation. The force on the DNA can be written as $F_{DNA} = \lambda_{DNA} \Delta V f(s)$ where $f(s)$ is a general functional dependence of the potential on the length of DNA inside the capillary, such that $f(s) = 1$ for nanopores and $f(s) = 1 - \frac{1}{1 + \frac{L-s}{\xi}}$ for nanocapillaries (2.5.1). λ_{DNA} is the effective linear charge density of DNA reduced by screening and drag. We assume that the extending force comes from both the force on the DNA and the force exerted by the complex, where, if it is small, we can continue in the strong stretching regime. Approximating that the protein jump is located at the point where the force is largest we can write for the extending force $F_{ext} = F_{DNA} - F_p(s = s_p) = F_{DNA} - q^* V / \xi$. The extension in the high stretching regime is then

$$\mu(s) = \frac{y}{s} = 1 - \frac{1}{\sqrt{4 L_p F_{ext} / k_B T}}, \tag{3.6}$$

with $L_p = 50\ nm$ the persistence length of DNA. Fig. 3.20 a shows the analytically obtained fit (from (3.5) and (3.6)) to the shift for dCas9 assuming a nanocapillary geometry with $\xi = 75\ nm$ and $V = 175\ mV$ (details in 2.6.3). The fit results in $\lambda_{DNA} = -0.06\ e/bp$, $L - s_x = 200 nm$ and the effective DNA-protein complex charge of $q^* = 5e$. The obtained λ_{DNA} is larger than the experimental mean of $-0.04\ e/bp$ (Fig. 3.20 d), which we attribute to the strong stretching regime approximations used.

3.3.3 Numerical model for explaining localisation shifts

Our analytical formulas can predict the shift in the range of small charges, but in order to better fit the shift, and thus accurately predict the localisation, a more precise modelling of how the complex charge affects translocation is necessary. For this reason we performed numerical modelling of the system in the cone geometry accordingly to section 2.6.2. Fig. 3.20 a shows the fit obtained with parameters $\lambda_{DNA} = -0.04\ e/bp$, $V = 200$ mV, $\xi = 75$ nm and an effective charge of the complex $q^* = 10e$ for dCas9 and the same except $\lambda_{DNA} = -0.02\ e/bp$ and $q^* = 12e$ for RNAP. λ_{DNA} values in the fit were taken as the means of the experimentally measured ones. We can also predict the general shape of the force curves using our simplified cone geometry (Fig. 3.20 b). Fig. 3.20 c shows that protein charge influences the shift for both positively and negatively charged bound proteins. The shaded area in Fig. 3.20 a shows the numerical fit variation if the linear charge density of DNA changes from its smallest to its largest experimentally measured value. This can easily account for the large standard deviations seen on the localisation shift as explained by the wide distribution of effective linear charge densities of DNA $\lambda_{DNA} = \lambda_{DNA}^0 - \lambda_{DRAG}$ seen in the DNA force levels (see Fig. 3.20 d).

This is caused by a variability of electroosmotic flow induced drag on the DNA (λ_{DRAG}) in nanocapillaries [53, 52, 160, 122, 130]. Two other reasons that increased the localization error are variation between different nanocapillaries in experiments at different voltages (Fig. 3.21). This error becomes apparent after combining all data acquired across different nanocapillaries. In the ideal case sufficient statistics should be accumulated in one capillary at a certain voltage. Nevertheless, being on initial development stages, our data for localisation of DNA-protein complexes are comparable to those obtained with other single-molecule techniques.
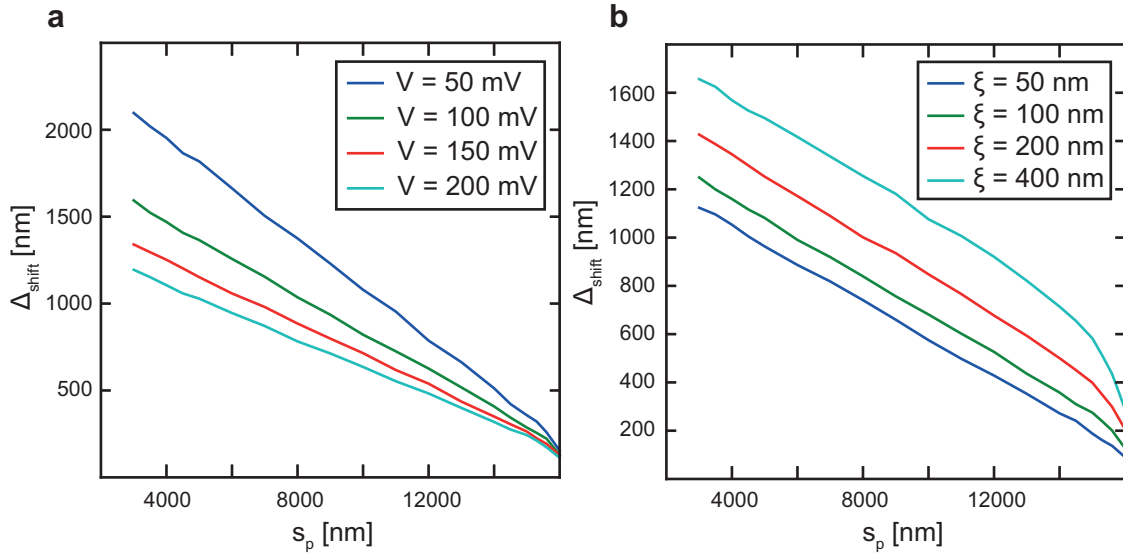
Figure 3.21 – **Dependence of protein localisation shift on the voltage and electrostatic decay length** (a) Effect of different driving voltages on the localisation shift. (b) Effect of different electrostatic decay lengths ξ on the localisation shift. Parameters were λ_{DNA} = -0.04 e/bp, q^* = 5e, ξ = 75 nm (a) and V = 175 mV (b). The figure is taken from [146].

3.3.4 Discrimination of DNA-bound proteins using non-equilibrium work and conductivity

In order to simultaneously discriminate DNA-protein complexes whilst localising, two methods, able to detect differences in charge and size, were used. The first is based on non-equilibrium work analysis of the force curves during the jump [118] while the second uses the characteristic of nanocapillaries to obtain current versus stage curves and uses them to differentiate proteins using conductivity drops [174].

Because the stochastic protein jumps are non-equilibrium events we utilise work analysis in order to extract equilibrium quantities used for protein discrimination. Our experiment starts in an equilibrium state at time t_A and at stage position z_A and ends in an equilibrium state at

time t_B and stage position z_B. The work done by a variation of the control parameter z is then

$$\tilde{W}_i = \int_{t_A}^{t_B} v \frac{\partial H}{\partial z} dt = \int_{z_A}^{z_B} F_{ot}(z) dz, \tag{3.7}$$

with $v = dz/dt \approx 500 \; nm/s$ the speed with which the stage is moving the capillary, and H the Hamiltonian of the system. This is connected to an integral of the measured optical tweezers force over the stage from the state at z_A to the state at z_B, where the protein event is wholly located in between these two stage positions. The work W_i done in an individual protein jump curve is computed as the area under the peak of the force-distance curve, from the point it starts to change from the base DNA level until the point it returns to this level. This work is corrected by subtracting the average force on the bare DNA $W_i = \tilde{W}_i - F_{DNA} \Delta z$ (the value before and after the jump event should be the same, see Fig. 3.22). The measured works W_i obtained from force curves can be inserted into the non-equilibrium work equation first shown by Jarzynski [148],

$$\langle \exp\left(-\frac{W_i}{k_B T}\right) \rangle = \exp\left(-\frac{\Delta G_{AB}}{k_B T}\right), \tag{3.8}$$
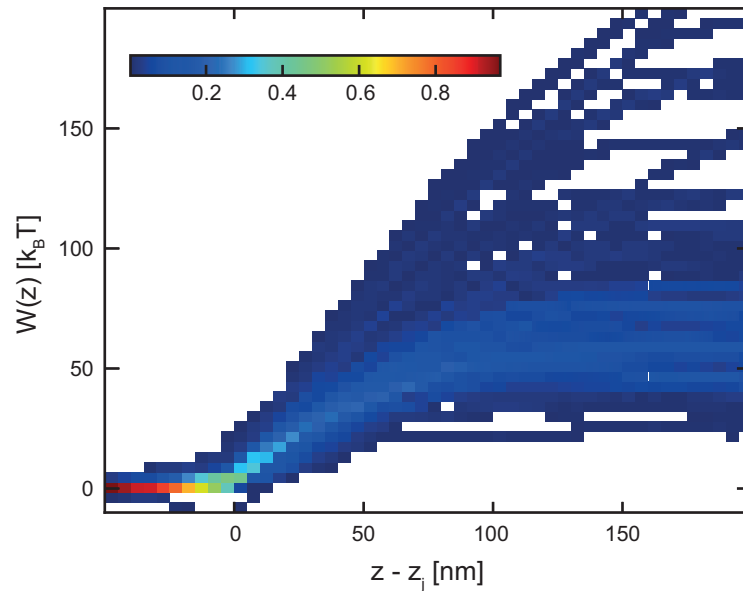
Figure 3.22 – **Density plot of calculated work versus stage W(z) trajectories during a jump event.** The plot was normalised to a probability of 1 for each z from 110 force versus stage curves for RNAP site at 750 nm. All force curves are shifted so that the jump location is at $z - z_j = 0$ before averaging.

and connected to the free energy difference between the state before and after the jump ΔG_{AB}. With knowledge of our setup geometry and parameters, we can connect free energy

differences to physical properties of the DNA-protein complexes. Assuming that the change of the worm like chain free energy before and after the jump is negligible, that the force profile returns to the same value after the jump, and that changes in stage and contour length are approximately equal $y_B - y_A \approx s_B - s_A$, the difference in free energies before and after the jump can be simplified to

$$\Delta G_{AB} = q^* \, V \cdot \frac{\Delta z}{\xi + \Delta z}, \tag{3.9}$$

where q^* is the effective charge of the complex, V the voltage at which the experiment was carried out, and Δz the width of the jump event (see section 2.6.4 for details).
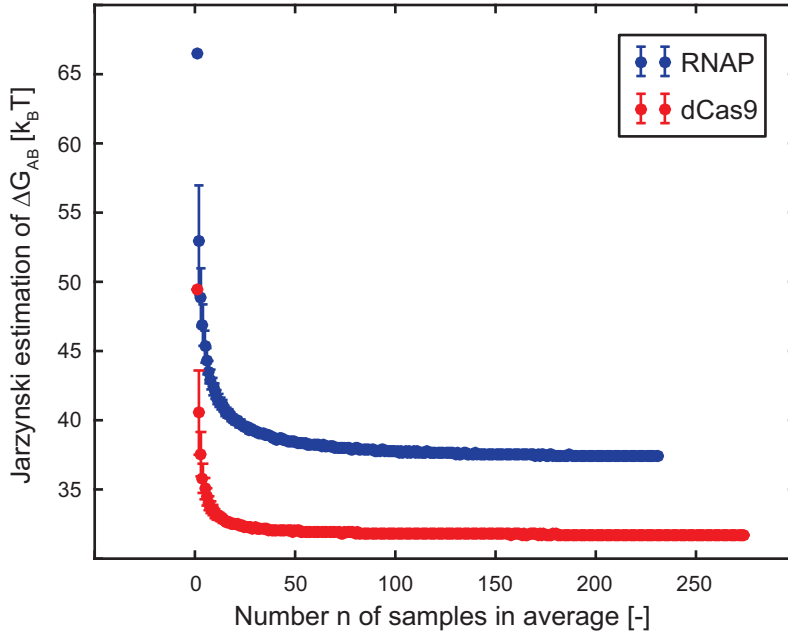
Figure 3.23 – **Convergence of Jarzynski estimator.** Value of ΔG_{AB} from the JE for all possible n combinations of works with $n = 1$ to N. A clear convergence is observed for a growing number of samples n. The curve being flat in the region of N number of measurements we consider that, in our case, the JE is a good estimator of ΔG_{AB}. The figure is taken from [146].

On the first step we checked if we can apply the JE equation to our experimental data. We computed the free energy of a total of N measured works using an average over $n < N$ possible combinations of works. While the number of included works n grows from 1 to N we should expect a convergence of the JE with n since the ensemble average should more precisely reflect the infinite average expressed in equation 2.46. On Fig. 3.23 we observed the expected convergence.

After having proved the applicability of the JE equation to our experimental data, we used it for discrimination of proteins based on their non-equilibrium works. Work analysis for both dCas9 and RNAP results in a wide clustering (Fig. 3.24 a and b) due to the non-equilibrium and
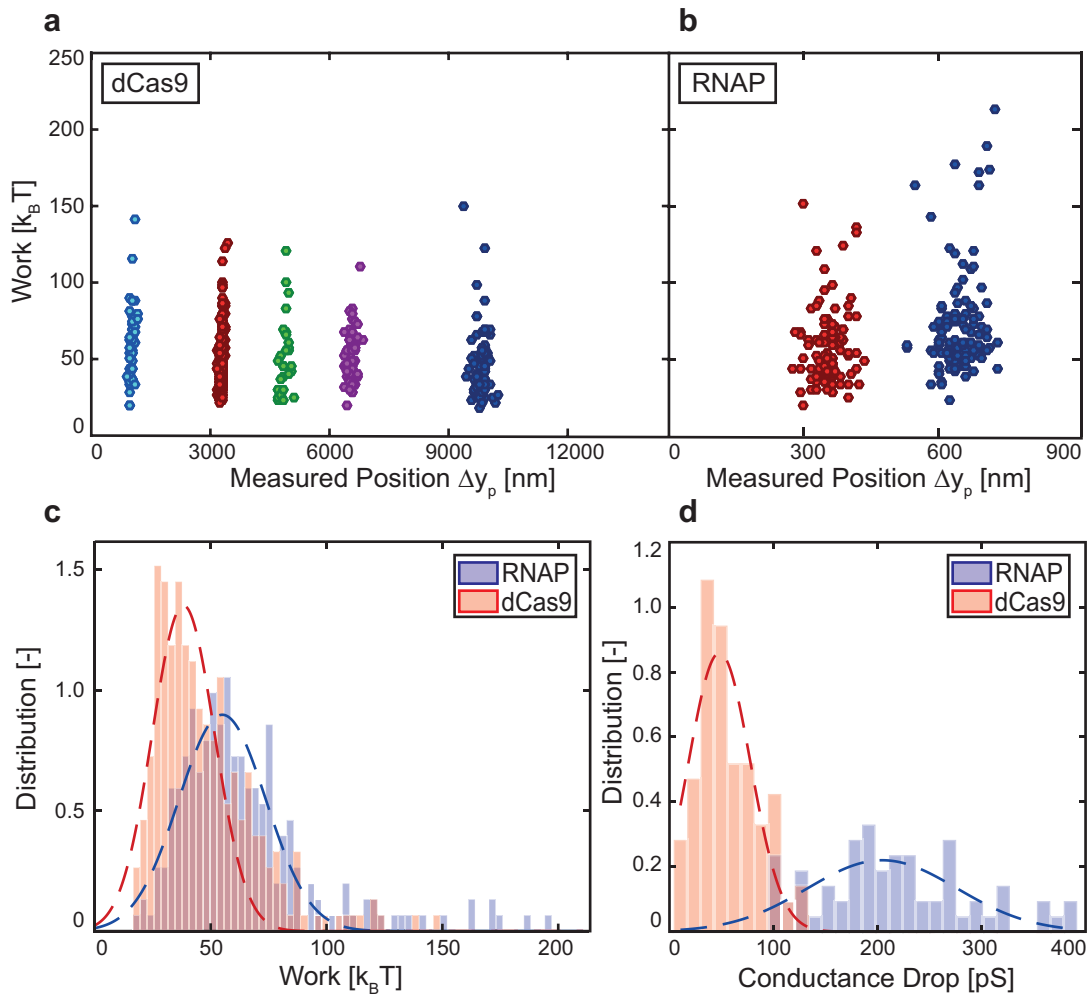
Figure 3.24 – **Analysis of works invested into protein jumps and conductance drops.** (a) Scatter plots of measured works W_i for five different dCas9 binding sites (as in Fig. 3.17 a). (b) Scatter plots of measured works W_i for two different RNAP binding sites (as in Fig. 3.17 b). Here the scale of the X-axis is ten times larger than in panel (a). (c) Comparison of jump event works obtained for dCas9 and RNAP. All binding site locations have been put together for all measurements done at $V = 200$ mV. Buffer conditions (100 mM KCl, 10 mM HEPES, 5% glycerol, pH 7.5) were the same for all dCas9 sites and with added 0.01% TWEEN 20 for RNAP. From these distributions ΔG_{AB} values were computed using the Jarzynski equality to be 31.7 and 37.9 k_BT for dCas9 and RNAP respectively (for convergence plot see Fig. 3.23). (d) Comparison of conductance changes for dCas9 and RNAP obtained from the maximal change of the conductance during a protein translocation relative to the DNA level. The figure is taken from [146].

stochastic nature of the translocation events as well as a wide distribution of electroosmotic flow induced drag. Assuming that there is no difference between binding sites, we can group all the work values obtained at the same voltage for both dCas9 and RNAP (Fig. 3.24 c). Although similar, it is possible to discern two different DNA-protein complex distributions.

In order to quantify the difference, we can apply the Jarzynski equality (3.8) to the obtained distributions. Using the free energy equation (3.9) with a determined average event width $\Delta z = 220$ and 170 nm, for dCas9 and RNAP respectively, and an electrostatic decay length $\xi = 75$ nm it is possible to obtain a value for the effective charge of the complex. For dCas9 we obtain $q^*_{dCas9} = 3.1e$ and for RNAP $q^*_{RNAP} = 3.4e$. We note that the charge value $\sim 3e$ obtained from the Jarzynski equality is much lower than the charge values obtained in the stochastic fit to the localisation shift ($\sim 10e$). As we have a wide distribution of drag forces, most likely due to different capillaries used, and thus different flow velocity distributions, we will have a distribution of effective charges q^* due to drag going into the work analysis. Because the Jarzynski equality is biased towards small works due to the factor $e^{-W_i/k_B T}$, we will preferentially obtain contributions from smaller charge values, i.e. works, and the distribution will be skewed to show the lower bound for the complex effective charge. Both RNAP and dCas9 (with GFP attached, section 2.4.1) having similar hydrodynamic radii (~ 5 nm [150, 175]) we expect them to experience a similar drag force which would explain the similarity of the determined effective charge. The determined effective charges will also have a contribution from the bare electrostatic charge, but we expect a minor contribution from it as drag overcomes electrostatic charge (section 3.2). In spite of the similarities of dCas9 and RNAP, the distributions of work values and effective charge from the Jarzynski equality support discrimination.

To complement the small difference in effective charges of RNAP and dCas9, we can additionally discriminate them by comparing the current drops obtained simultaneously with force peaks for both proteins (Fig. 3.24 d). In a buffer of same ionic strength, RNAP exhibits a larger current drop than dCas9 and enables a clearer discrimination between the proteins than the non-equilibrium work analysis. The origin of the conductance drop is known to depend strongly on salt conditions [162] and can be attributed to several different scenarios (current blockage [164], molecular friction [165], or a change in the advective current from current polarisation (section 3.2). A combination of conductance changes and non-equilibrium work analysis thus enables us to discriminate two proteins even if they have a similar charge or shape. In practice one could use either one, the other, or both methods to discriminate proteins while tailoring the sensitivity to either charge or size.

3.3.5   Conclusions

We have demonstrated the viability of single molecule force spectroscopy using optical tweezers and glass nanocapillaries as a sensing tool for discrimination and localisation of DNA-protein complexes on two proteins in physiological conditions: RNAP and dCas9. We detected the proteins shifted from their expected positions, but were able to explain and correct for it by using both analytical and numerical modelling and localise them to within an accuracy of 50 nm.

In the context of the wider applicability of this technique to other types of geometries, we note

the nanopore limit of eq. (3.9). For thin nanopores ($< 5nm$), like graphene [176, 177, 178, 179] and MoS$_2$ [77], the free energy difference for a jump simplifies, under the same assumptions, to $\Delta F = q\, V$, with q as the bare electrostatic charge, making the analysis of experiments much simpler as the dependence on geometry is negligible. However this comes at the cost of a worse signal-to-noise ratio for current measurements and harder experiments since combining optical tweezers with nanopores is significantly more complex than with nanocapillaries. In addition nanocapillaries sensitivity to the size of proteins could be tailored by reducing and controlling the electroosmotic flow induced drag with lipid or polymer surface coating [126, 91, 180]. Nanocapillaries can thus be tailored to be either sensitive to charge or size of proteins, enabling discrimination whilst simultaneously localising them.

4 Conclusions and perspectives

4.1 Conclusions

We constructed a setup combining nanocapillaries and optical tweezers and applied it for studying DNA-protein complexes. There were 3 milestones in this thesis:

1. **Combination of nanocapillaries and optical tweezers for measuring electrophoretic forces on DNA**

We built a rather simple and cheap system that includes glass nanocapillaries with tunable size and conventional optical tweezers. The combination of these two techniques was performed using a fluidic cell with two chambers made out of PDMS. In a well isolated system we were able to record force and current signals in single molecule experiments.

We trapped DNA molecules inside nanocapillaries and measured the electrophoretic forces acting on them. We showed that the forces are higher in nanocapillaries with smaller diameters due to the lower impact from the drag forces. We performed controlled pulling of DNA out of the capillaries and observed a decrease in the force when a smaller peace of DNA was left inside. We mapped the position-dependent force profiles for DNA in capillaries of different sizes and at different voltages. Smaller nanocapillaries showed decrease in the force only in their final parts close to the opening, whereas for the large ones it was pronounced along longer distances. We explained the obtained results based on the elongated geometry of nanocapillaries that leads to prolonged decrease of the potential drop inside it.

2. **Measuring electrophoretic forces on DNA-protein complexes**

We detected DNA-protein complexes and modelled the electrophoretic force acting on them inside nanocapillaries to explain the obtained results. We performed controlled translocations of three proteins (RNAP, RecA and EcoRI) that formed complexes with DNA. The complexes were visualised by additional peaks in the force and current signals comparing to the levels of bare DNA. The peaks were followed up by a decay in the signal after the stage moved the capillary further away. We made a stochastic model of the system that allowed us to explain

these profiles. In fact, the peak in the force/current signal was explained by the jump of the protein outside of the capillary to a new energy state. The decay of the signal corresponds to the restoration of the coiled DNA molecule after the jump to the extended state. From our model we extracted the effective charge of the proteins. Interestingly, it was positive even though the theoretical value of the charge is negative for all used proteins. We explained this phenomenon based on the impact of the drag force in nanocapillaries that has an additional effect on bulky proteins. Inside nanocapillaries the drag force dominates the electrostatic force and therefore changes the effective charge of the protein.

3. **Localization and discrimination of DNA-protein complexes**

We applied the setup to localise and discriminate different DNA-protein complexes. We designed a bimolecular construct to have protein binding sites at the certain locations of DNA handles for two proteins dCas9 and RNAP. During controlled translocation of DNA we measured the locations of the proteins close to designed sites yet slightly shifted. The shift demonstrated that we underestimated the positions of DNA-binding sites in our experiments. The further the site of the protein from a free end of DNA, the higher the shift we observed. The shift in the measured location was explained based on two factors 1. DNA is never extended to the condition of a straight line and 2. molecular fluctuations of DNA lead to its early exit. We provided an analytical model that allows to make a conversion from the measured to theoretical location. In addition to localisation, we discriminated DNA-protein complexes using their force and current signatures. From the force profiles we extracted effective charges of the proteins using the Jarzynski equation. For RNAP and dCas9 the average effective charge did not differ more than 10%. However, the conductance drop was significantly different allowing us to differentiate these proteins.

In conclusion, the constructed technique provides a powerful platform for studying DNA-protein interactions with the following advantages:

- operation in physiological conditions;
- application of forces in pN range that leaves the majority of DNA-protein complexes intact;
- detection of two signals at the same time: force and current;
- ability to probe one complex multiple times by translocating it back and forth;
- ability to tune the size of the nanocapillary to the protein size.

4.2 Future directions

On the example of protein discrimination and localisation we demonstrated how optical tweezers combined with nanocapillaries can be used for studying DNA-protein interactions. We envision that this technique can shed light on numerous phenomenon in the field of DNA-protein interactions.

As a follow up of the developed application, the setup can be used to precisely measure binding sites of previously uncharacterised proteins, which make up a large part of proteins known to bind to DNA. Not only does our method recognise specific or high affinity sites whilst characterising their size and charge, but with enough statistics could be used to infer about low affinity or non-specific binding sites. Based on the detected charge and hydrodynamic radius the method could allow to study differences between different binding conformations, for example, binding of RNAP in the initiation stage versus the elongation stage, or Cas9 versus dCas9. The use of the technique to detect multiple proteins bound to a single DNA (multiplexed detection) could also be applied for detecting the presence of tandem repeats, such as the expansion of a CGG repeat occurring in Fragile X syndrome [181].

Nanocapillaries combined with optical tweezers can also be used for studying stability of DNA-protein complexes by finding the force at which the complex is disrupted. There are at least two ways how a DNA-protein complex can be disrupted in the system: 1. due to electrostatic forces or 2. mechanically applied forces. In the first case an effectively positively charged complex can be trapped close to the entrance of the nanocapillary, where the electrostatic force is highest and where the protein can be visualised. Ramping of voltage and keeping the fixed position of the complex would increase the electrostatic force on the protein resulting in its disruption at a certain force value. In the second case such an experiment can be performed by having an opening size of the capillary smaller than the size of the complex. In this case an event of binding should take place in a trans chamber and afterwards the capillary should be moved until the complex reaches the opening. Since the opening is smaller than the complex, the further displacement of the stage will result in disruption of the complex.

We believe that one potential application of the setup is studying movement of proteins on DNA. For example RNAP stalled on DNA can be reactivated by addition of the missing NTP to the experimental buffer. Changes in force and current signals would reveal a displacement of the complex from the opening. It is worth nothing, even non motor proteins move along a DNA molecule before binding to its specific binding site [182]. Nanocapillaries combined with optical tweezers can be also applied for getting further insights on how a search of a specific binding site by proteins takes place.

All the applications mentioned above were related to studying DNA-protein interactions. However, this technique can be used in another areas like biophysics of nucleic acids or physics of nanoflows providing a vast scope of future applications.

A Appendix

Sequence of the plasmid pRL574

```
   1 CGCGCGTTTC GGTGATGACG GTGAAAACCT CTGACACATG CAGCTCCCGG AGACGGTCAC
  61 AGCTTGTCTG TAAGCGGATG CCGGGAGCAG ACAAGCCCGT CAGGGCGCGT CAGCGGGTGT
 121 TGGCGGGTGT CGGGGCTGGC TTAACTATGC GGCATCAGAG CAGATTGTAC TGAGAGTGCA
 181 CCATAAAATT GTAAACGTTA ATATTTTGTT AAAATTCGCG TTAAATTTTT GTTAAATCAG
 241 CTCATTTTTT AACCAATAGG CCGAAATCGG CAAAATCCCT TATAAATCAA AAGAATAGCC
 301 CGAGATAGGG TTGAGTGTTG TTCCAGTTTG GAACAAGAGT CCACTATTAA AGAACGTGGA
 361 CTCCAACGTC AAAGGGCGAA AAACCGTCTA TCAGGGCGAT GGCCCACTAC GTGAACCATC
 421 ACCCAAATCA AGTTTTTTGG GGTCGAGGTG CCGTAAAGCA CTAAATCGGA ACCCTAAAGG
 481 GAGCCCCCGA TTTAGAGCTT GACGGGGAAA GCCGGCGAAC GTGGCGAGAA AGGAAGGGAA
 541 GAAAGCGAAA GGAGCGGGCG CTAGGGCGCT GGCAAGTGTA GCGGTCACGC TGCGCGTAAC
 601 CACCACACCC GCCGCGCTTA ATGCGCCGCT ACAGGGCGCG TACTATGGTT GCTTTGACGT
 661 ATGCGGTGTG AAATACCGCA CAGATGCGTA AGGAGAAAAT ACCGCATCAG GCGCCATTCG
 721 CCATTCAGGC TGCGCAACTG TTGGGAAGGG CGATCGGTGC GGGCCTCTTC GCTATTACGC
 781 CAGCTGGCGA AAGGGGGATG TGCTGCAAGG CGATTAAGTT GGGTAACGCC AGGGTTTTCC
 841 CAGTCACGAC GTTGTAAAAC GACGGCCAGT GAATTCGAGC TCGGTACCCG ATCCAGATCC
 901 CGAACGCCTA TCTTAAAGTT TAAACATAAA GACCAGACCT AAAGACCAGA CCTAAAGACA
 961 CTACATAAAG ACCAGACCTA AAGACGCCTT GTTGTTAGCC ATAAAGTGAT AACCTTTAAT
1021 CATTGTCTTT ATTAATACAA CTCACTATAA GGAGAGACAA CTTAAAGAGA CTTAAAAGAT
1081 TAATTTAAAA TTTATCAAAA AGAGTATTGA CTTAAAGTCT AACCTATAGG ATACTTACAG
1141 CCATCGAGAG GGACACGGGG GATCCTCTAG AGTGCTTGGC GAACCGGTGT TTGACGTCCA
1201 GGAATGTCAA ATCCGTGGCG TGACCTATTC CGCACCGCTG CGCGTTAAAC TGCGTCTGGT
1261 GATCTATGAG CGCGAAGCGC CGGAAGGCAC CGTAAAAGAC ATTAAAGAAC AAGAAGTCTA
1321 CATGGGCGAA ATTCCGCTCA TGACAGACAA CGGTACCTTT GTTATCAACG GTACTGAGCG
1381 TGTTATCGTT TCCCAGCTGC ACCGTAGTCC GGGCGTCTTC TTTGACTCCG ACAAAGGTAA
1441 AACCCACTCT TCGGGTAAAG TGCTGTATAA CGCGCGTATC ATCCCTTACC GTGGTTCCTG
1501 GCTGGACTTC GAATTCGATC CGAAGGACAA CCTGTTCGTA CGTATCGACC GTCGCCGTAA
1561 ACTGCCTGCG ACCATCATTC TGCGCGCCCT GAACTACACC ACAGAGCAGA TCCTCGACCT
```

```
1621 GTTCTTTGAA AAAGTTATCT TTGAAATCCG TGATAACAAG CTGCAGATGG AACTGGTGCC
1681 GGAACGCCTG CGTGGTGAAA CCGCATCTTT TGACATCGAA GCTAACGGTA AAGTGTACGT
1741 AGAAAAAGGC CGCCGTATCA CTGCGCGCCA CATTCGCCAG CTGGAAAAAG ACGACGTCAA
1801 ACTGATCGAA GTCCCGGTTG AGTACATCGC AGGTAAAGTG GTTGCTAAAG ACTATATTGA
1861 TGAGTCTACC GGCGAGCTGA TCTGCGCAGC GAACATGGAG CTGAGCCTGG ATCTGCTGGC
1921 TAAGCTGAGC CAGTCTGGTC ACAAGCGTAT CGAAACGCTG TTCACCAACG ATCTGGATCA
1981 CGGCCCATAT ATCTCTGAAA CCTTACGTGT CGACCCAACT AACGACCGTC TGAGCGCACT
2041 GGTAGAAATC TACCGCATGA TGCGCCCTGG CGAGCCGCCG ACTCGTGAAG CAGCTGAAAG
2101 CCTGTTCGAG AACCTGTTCT TCTCCGAAGA CCGTTATGAC TTGTCTGCGG TTGGTCGTAT
2161 GAAGTTCAAC CGTTCTCTGC TGCGCGAAGA AATCGAAGGT TCCGGTATCC TGAGCAAAGA
2221 CGACATCATT GATGTTATGA AAAAGCTCAT CGATATCCGT AACGGTAAAG CGAAGTCGA
2281 TGATATCGAC CACCTCGGCA ACCGTCGTAT CCGTTCCGTT GGCGAAATGG CGGAAAACCA
2341 GTTCCGCGTT GGCCTGGTAC GTGTAGAGCG TGCGGTGAAA GAGCGTCTGT CTCTGGGCGA
2401 TCTGGATACC CTGATGCCAC AGGATATGAT CAACGCCAAG CCGATTTCCG CAGCAGTGAA
2461 AGAGTTCTTC GGTTCCAGCC AGCTGTCTCA GTTTATGGAC CAGAACAACC CGCTGTCTGA
2521 GATTACGCAC AAACGTCGTA TCTCCGCACT CGGCCCAGGC GGTCTGACCC GTGAACGTGC
2581 AGGCTTCGAA GTTCGAGACG TACACCCGAC TCACTACGGT CGCGTATGTC CAATCGAAAC
2641 CCCTGAAGGT CCGAACATCG GTCTGATCAA CTCTCTGTCC GTGTACGCAC AGACTAACGA
2701 ATACGGCTTC CTTGAGACTC CGTATCGTAA AGTGACCGAC GGTGTTGTAA CTGACGAAAT
2761 TCACTACCTG TCTGCTATCG AAGAAGGCAA CTACGTTATC GCCCAGGCGA ACTCCAACTT
2821 GGATGAAGAA GGCCACTTCG TAGAAGACCT GGTAACTTGC CGTAGCAAAG GCGAATCCAG
2881 CTTGTTCAGC CGCGACCAGG TTGACTACAT GGACGTATCC ACCCAGCAGG TGGTATCCGT
2941 CGGTGCGTCC CTGATCCCGT TCCTGGAACA CGATGACGCC AACCGTGCAT TGATGGGTGC
3001 GAACATGCAA CGTCAGGCCG TTCCGACTCT GCGCGCTGAT AAGCCGCTGG TTGGTACTGG
3061 TATGGAACGT GCTGTTGCCG TTGACTCCGG TGTAACTGCG GTAGCTAAAC GTGGTGGTGT
3121 CGTTCAGTAC GTGGATGCTT CCCGTATCGT TATCAAAGTT AACGAAGACG AGATGTATCC
3181 GGGTGAAGCA GGTATCGACA TCTACAACCT GACCAAATAC ACCCGTTCTA ACCAGAACAC
3241 CTGTATCAAC CAGATGCCGT GTGTGTCTCT GGGTGAACCG GTTGAACGTG GCGACGTGCT
3301 GGCAGACGGT CCGTCCACCG ACCTCGGTGA ACTGGCGCTT GGTCAGAACA TGCGCGTAGC
3361 GTTCATGCCG TGGAATGGTT ACAACTTCGA AGACTCCATC CTCGTATCCG AGCGTGTTGT
3421 TCAGGAAGAC CGTTTCACCA CCATCCACAT TCAGGAACTG GCGTGTGTGT CCCGTGACAC
3481 CAAGCTGGGT CCGGAAGAGA TCACCGCTGA CATCCCGAAC GTGGGTGAAG CTGCGCTCTC
3541 CAAACTGGAT GAATCCGGTA TCGTTTACAT TGGTGCGGAA GTGACCGGTG GCGACATTCT
3601 GGTTGGTAAG GTAACGCCGA AAGGTGAAAC TCAGCTGACC CCAGAAGAAA AACTGCTGCG
3661 TGCGATCTTC GGTGAGAAAG CCTCTGACGT TAAAGACTCT TCTCTGCGCG TACCAAACGG
3721 TGTATCCGGT ACGGTTATCG ACGTTCAGGT CTTTACTCGC GATGGCGTAG AAAAAGACAA
3781 ACGTGCGCTG GAAATCGAAG AAATGCAGCT CAAACAGGCG AAGAAAGACC TGTCTGAAGA
3841 ACTGCAGATC CTCGAAGCGG GTCTGTTCAG CCGTATCCGT GCTGTGCTGG TAGCCGGTGG
3901 CGTTGAAGCT GAGAAGCTCG ACAAACTGCC GCGCGATCGC TGGCTGGAGC TGGGCCTGAC
3961 AGACGAAGAG AAACAAAATC AGCTGGAACA GCTGGCTGAG CAGTATGACG AACTGAAACA
4021 CGAGTTCGAG AAGAAACTCG AAGCGAAACG CCGCAAAATC ACCCAGGGCG ACGATCTGGC
4081 ACCGGGCGTG CTGAAGATTG TTAAGGTATA TCTGGCGGTT AAACGCCGTA TCCAGCCTGG
```

```
4141 TGACAAGATG GCAGGTCGTC ACGGTAACAA GGGTGTAATT TCTAAGATCA ACCCGATCGA
4201 AGATATGCCT TACGATGAAA ACGGTACGCC GGTAGACATC GTACTGAACC CGCTGGGCGT
4261 ACCGTCTCGT ATGAACATCG GTCAGATCCT CGAAACCCAC CTGGGTATGG CTGCGAAAGG
4321 TATCGGCGAC AAGATCAACG CCATGCTGAA ACAGCAGCAA GAAGTCGCGA AACTGCGCGA
4381 ATTCATCCAG CGTGCGTACG ATCTGGGCGC TGACGTTCGT CAGAAAGTTG ACCTGAGTAC
4441 CTTCAGCGAT GAAGAAGTTA TGCGTCTGGC TGAAAACCTG CGCAAAGGTA TGCCAATCGC
4501 AACGCCGGTG TTCGACGGTG CGAAAGAAGC AGAAATTAAA GAGCTGCTGA AACTTGGCGA
4561 CCTGCCGACT TCCGGTCAGA TCCGCCTGTA CGATGGTCGC ACTGGTGAAC AGTTCGAGCG
4621 TCCGGTAACC GTTGGTTACA TGTACATGCT GAAACTGAAC CACCTGGTCG ACGACAAGAT
4681 GCACGCGCGT TCCACCGGTT CTTACAGCCT GGTTACTCAG CAGCCGCTGG GTGGTAAGGC
4741 ACAGTTCGGT GGTCAGCGTT TCGGGGAGAT GGAAGTGTGG GCGCTGGAAG CATACGGCGC
4801 AGCATACACC CTGCAGGAAA TGCTCACCGT TAAGTCTGAT GACGTGAACG GTCGTACCAA
4861 GATGTATAAA AACATCGTGG ACGGCAACCA TCAGATGGAG CCGGGCATGC GAGAGTAGGG
4921 AACTGCCAGG CATCAAAGAA AACGAAAGGC ACAGTCGAAA GACTGGGCCT TTCGTTTTAT
4981 CTGTTGTTTG TCGGTGAACG CTCTCCTGAG TAGGACAAAT CCGCCGGGAG CGGATTTGAA
5041 CGTTGCGAAG CAACGGCCCG GAGGGTGGCG GGCAGGACGC CCGCCATAAA CTGCCAGGCA
5101 TCAAATTAAG CAGAAGGCCA TCCTGACGGA TGGCCTTTTT GCGTTTCTAC AAACTCTTCC
5161 TGTCGTCATA TCTACAAGCC ATCCCCCCAC AGATACGGTA AACTAGCCTC GTTTTTGCAT
5221 CAGGAAAGCA GAAGCTTGGC GTAATCATGG TCATAGCTGT TTCCTGTGTG AAATTGTTAT
5281 CCGCTCACAA TTCCACACAA CATACGAGCC GGAAGCATAA AGTGTAAAGC CTGGGGTGCC
5341 TAATGAGTGA GCTAACTCAC ATTAATTGCG TTGCGCTCAC TGCCCGCTTT CCAGTCGGGA
5401 AACCTGTCGT GCCAGCTGCA TTAATGAATC GGCCAACGCG CGGGGAGAGG CGGTTTGCGT
5461 ATTGGGCGCT CTTCCGCTTC CTCGCTCACT GACTCGCTGC GCTCGGTCGT TCGGCTGCGG
5521 CGAGCGGTAT CAGCTCACTC AAAGGCGGTA ATACGGTTAT CCACAGAATC AGGGGATAAC
5581 GCAGGAAAGA ACATGTGAGC AAAAGGCCAG CAAAAGGCCA GGAACCGTAA AAAGGCCGCG
5641 TTGCTGGCGT TTTTCCATAG GCTCCGCCCC CCTGACGAGC ATCACAAAAA TCGACGCTCA
5701 AGTCAGAGGT GGCGAAACCC GACAGGACTA TAAAGATACC AGGCGTTTCC CCCTGGAAGC
5761 TCCCTCGTGC GCTCTCCTGT TCCGACCCTG CCGCTTACCG GATACCTGTC CGCCTTTCTC
5821 CCTTCGGGAA GCGTGGCGCT TTCTCATAGC TCACGCTGTA GGTATCTCAG TTCGGTGTAG
5881 GTCGTTCGCT CCAAGCTGGG CTGTGTGCAC GAACCCCCCG TTCAGCCCGA CCGCTGCGCC
5941 TTATCCGGTA ACTATCGTCT TGAGTCCAAC CCGGTAAGAC ACGACTTATC GCCACTGGCA
6001 GCAGCCACTG GTAACAGGAT TAGCAGAGCG AGGTATGTAG GCGGTGCTAC AGAGTTCTTG
6061 AAGTGGTGGC CTAACTACGG CTACACTAGA AGGACAGTAT TTGGTATCTG CGCTCTGCTG
6121 AAGCCAGTTA CCTTCGGAAA AAGAGTTGGT AGCTCTTGAT CCGGCAAACA AACCACCGCT
6181 GGTAGCGGTG GTTTTTTTGT TTGCAAGCAG CAGATTACGC GCAGAAAAAA AGGATCTCAA
6241 GAAGATCCTT TGATCTTTTC TACGGGGTCT GACGCTCAGT GGAACGAAAA CTCACGTTAA
6301 GGGATTTTGG TCATGAGATT ATCAAAAAGG ATCTTCACCT AGATCCTTTT AAATTAAAAA
6361 TGAAGTTTTA AATCAATCTA AAGTATATAT GAGTAAACTT GGTCTGACAG TTACCAATGC
6421 TTAATCAGTG AGGCACCTAT CTCAGCGATC TGTCTATTTC GTTCATCCAT AGTTGCCTGA
6481 CTCCCCGTCG TGTAGATAAC TACGATACGG GAGGGCTTAC CATCTGGCCC CAGTGCTGCA
6541 ATGATACCGC GAGACCCACG CTCACCGGCT CCAGATTTAT CAGCAATAAA CCAGCCAGCC
6601 GGAAGGGCCG AGCGCAGAAG TGGTCCTGCA ACTTTATCCG CCTCCATCCA GTCTATTAAT
```

```
6661 TGTTGCCGGG AAGCTAGAGT AAGTAGTTCG CCAGTTAATA GTTTGCGCAA CGTTGTTGCC
6721 ATTGCTACAG GCATCGTGGT GTCACGCTCG TCGTTTGGTA TGGCTTCATT CAGCTCCGGT
6781 TCCCAACGAT CAAGGCGAGT TACATGATCC CCCATGTTGT GCAAAAAAGC GGTTAGCTCC
6841 TTCGGTCCTC CGATCGTTGT CAGAAGTAAG TTGGCCGCAG TGTTATCACT CATGGTTATG
6901 GCAGCACTGC ATAATTCTCT TACTGTCATG CCATCCGTAA GATGCTTTTC TGTGACTGGT
6961 GAGTACTCAA CCAAGTCATT CTGAGAATAG TGTATGCGGC GACCGAGTTG CTCTTGCCCG
7021 GCGTCAATAC GGGATAATAC CGCGCCACAT AGCAGAACTT TAAAAGTGCT CATCATTGGA
7081 AAACGTTCTT CGGGGCGAAA ACTCTCAAGG ATCTTACCGC TGTTGAGATC CAGTTCGATG
7141 TAACCCACTC GTGCACCCAA CTGATCTTCA GCATCTTTTA CTTTCACCAG CGTTTCTGGG
7201 TGAGCAAAAA CAGGAAGGCA AAATGCCGCA AAAAAGGGAA TAAGGGCGAC ACGGAAATGT
7261 TGAATACTCA TACTCTTCCT TTTTCAATAT TATTGAAGCA TTTATCAGGG TTATTGTCTC
7321 ATGAGCGGAT ACATATTTGA ATGTATTTAG AAAAATAAAC AAATAGGGGT TCCGCGCACA
7381 TTTCCCCGAA AAGTGCCACC TGACGTCTAA GAAACCATTA TTATCATGAC ATTAACCTAT
7441 AAAAATAGGC GTATCACGAG GCCCTTTCGT CT
```

Link for the sequence of genomic DNA of phage T7:

https://www.ncbi.nlm.nih.gov/nuccore/9627425?report=fasta

Acknowledgements

If I could see this thesis in August 2012 when I just came to the lab I would never believe it would be my work. In that time I have never heard about optical tweezers, nanocapillaries, clean room and have never experienced any modeling or engineering. This means that my PhD was a steep learning curve! However, "No one lives long enough to learn everything they need to learn starting from scratch. To be successful, we absolutely, positively have to find people who have already paid the price to learn the things that we need to learn to achieve our goals (Brian Tracy)". Having said that I would like to come to acknowledgments of those people which were around during these 4 years and guided me throughout my project either professionally or personally.

First of all I would like to thank Prof. Aleksandra Radenovic for giving me the opportunity to work in her lab. I guess it was a little bit of a gamble from her side to hire a person that had a background in molecular biology for such an interdisciplinary project including a lot of physics and engineering. I hope Aleksandra does not regret her decision:) Here I will rather focus on her personality that deeply impressed me. Well, Aleksandra is probably the nicest boss I will ever have a chance to work with. Always optimistic and full of positive energy...Trusting people, taking their side and providing them freedom in their performance...Being always engaged in science and worrying about results sometimes even more than her students:) Thank you for understanding my interests and giving me the green light in my personal career development. I deeply appreciate what you have done for me.

Thanks to Prof. Philippe Renaud, Prof. Roderick Lim, Prof. Ulrich Keyser and Prof. Sebastian Maerkl that accepted to dedicate their time and be on my thesis jury. Especially I would like to acknowledge Ulrich Keyser. One of the things that impressed me in Ulrich is his openness. Working in our field, he was always open for collaboration and discussion of his future plans. When giving us advices, I got an impression that he sincerely wants us to succeed.

My collaborators... I used to collaborate with 5 different labs during my thesis (Prof. Keyser, Prof. Fierz, Prof. Maerkl, Prof. Nollman and Prof. Blokesch). It was always fun to work in collaboration using the principle "give and take". Not all projects were successful and led to a result, however I would still like to thank all students and their supervisors, especially Prof. Maerkl and Ekaterina Petrova that invested a lot of time in my work.

Acknowledgements

My colleagues... Quite many colleagues have changed during this time and at this point I feel like the oldest member of the lab. All these people were unique individuals that taught me something. Especial thanks to Fabrizia Dutto, Lorenz Steinbock and Flavio Mor that helped to figure the technical aspects of the project. Lely Feletti for incredible amount of time she invested in my project as well as her patience to stand my questions and jokes. Sanjin Marion that provided theoretical basis for my whole project and was a great host during my business trip to Zagreb. Sebastian Davis that finalized the third manuscript with help of Sanjin. I will say a couple of more words about Sebastian aka "the dude". I spent a year with him in the same office and I was always impressed by his sense of humor, positive attitude and openness. I also found him a good teacher that explained me physical parts of the projects and a friend beyond the lab. I would like to acknowledge the "beer time" team led by Prof. Chang and supported by Michael Graf, Ke Liu, Hendrik Deschout, Martina Lihter and Jiandong Feng. Moreover, thanks to all people on the 2nd floor of the BM building form LBEN, LANES and LBNC that kept me entrained and alive during my PhD.

I would like to acknowledge two student organization - the BioScience Network Lausanne (BSNL) and ShARE. Being their member I got to see a different side than Academia working in a team with brilliant students from all over the world. Eventually this experienced helped me to make my career choice, boosted my soft skills and also helped to make new friends.

My football and basketball teams, gym buddies and The Russian Society in Lausanne. These activities helped me to spend my spare time and truly enjoy staying in Switzerland.

Last but not least, I would like to thank my parents. I spent my childhood in a Siberian city in a family of scientists. I learned two things on their example 1. you need to work hard to get a valuable result and 2. you need to enjoy what you are doing. My parents made me passionate about science and guided towards EPFL. I do not think I will ever find means to thank them for what they have done for me and how they influenced my development.

Lausanne, 2017   Roman

Bibliography

[1] J. D. McGhee and P. H. von Hippel, "Theoretical aspects of DNA-protein interactions: co-operative and non-co-operative binding of large ligands to a one-dimensional homogeneous lattice," *Journal of Molecular Biology*, vol. 86, no. 2, pp. 469 – 489, 1974.

[2] B. Alberts, A. Johnson, L. Julian, D. Morgan, M. Raff, K. Roberts, and P. Walter, *Molecular Biology of the Cell*. 6th ed., 2014.

[3] M. Geertz and S. J. Maerkl, "Experimental strategies for studying transcription factor-DNA binding specificities," *Briefings in Functional Genomics*, vol. 9, no. 5-6, pp. 362–373, 2010.

[4] M. M. Garner and A. Revzin, "A gel electrophoresis method for quantifying the binding of proteins to specific DNA regions: application to components of the Escherichia coli lactose operon regulatory system," *Nucleic Acids Research*, vol. 9, no. 13, pp. 3047–3060, 1981.

[5] D. J. Galas and A. Schmitz, "DNAase footprinting a simple method for the detection of protein-DNA binding specificity," vol. 5, no. 9, pp. 3157–3170, 1978.

[6] E. Roulet, S. Busso, A. A. Camargo, A. J. G. Simpson, N. Mermod, and P. Bucher, "High-throughput SELEX-SAGE method for quantitative modeling of transcription-factor binding sites," *Nature Biotechnology*, vol. 20, no. 8, pp. 831–835, 2002.

[7] M. L. Bulyk, X. Huang, Y. Choo, and G. M. Church, "Exploring the DNA-binding specificities of zinc fingers with DNA microarrays," *Proceedings of the National Academy of Sciences*, vol. 98, no. 13, pp. 7158–7163, 2001.

[8] S. J. Maerkl and S. R. Quake, "A systems approach to measuring the binding energy landscapes of transcription factors," *Science*, vol. 315, no. 5809, pp. 233–237, 2007.

[9] D. S. Johnson, A. Mortazavi, R. M. Myers, and B. Wold, "Genome-wide mapping of in vivo protein-DNA interactions," *Science*, vol. 316, no. 5830, pp. 1497–1502, 2007.

[10] A. Barski, S. Cuddapah, K. Cui, T.-Y. Roh, D. E. Schones, Z. Wang, G. Wei, I. Chepelev, and K. Zhao, "High-resolution profiling of histone methylations in the human genome," *Cell*, vol. 129, no. 4, pp. 823 – 837, 2007.

[11] R. Nutiu, R. C. Friedman, S. Luo, I. Khrebtukova, D. Silva, R. Li, L. Zhang, G. P. Schroth, and C. B. Burge, "Direct measurement of DNA affinity landscapes on a high-throughput sequencing instrument," *Nature Biotechnology*, vol. 29, no. 7, pp. 659–664, 2011.

[12] L. G. Fägerstam, Åsa Frostell-Karlsson, R. Karlsson, B. Persson, and I. Rönnberg, "Biospecific interaction analysis using surface plasmon resonance detection applied to kinetic, binding site and concentration analysis," *Journal of Chromatography A*, vol. 597, no. 1, pp. 397 – 410, 1992.

[13] M. Geertz, D. Shore, and S. J. Maerkl, "Massively parallel measurements of molecular interaction kinetics on a microfluidic platform," *Proceedings of the National Academy of Sciences*, vol. 109, no. 41, pp. 16540–16545, 2012.

[14] A. A. Deniz, S. Mukhopadhyay, and E. A. Lemke, "Single-molecule biophysics: at the interface of biology, physics and chemistry," *Journal of The Royal Society Interface*, vol. 5, no. 18, pp. 15–45, 2008.

[15] L. Bai, T. J. Santangelo, and M. D. Wang, "Sinlge-molecule analysis of RNA Polymerase transcription," *Annual Review of Biophysics and Biomolecular Structure*, vol. 35, no. 1, pp. 343–360, 2006.

[16] S. Kasas, N. H. Thomson, B. L. Smith, H. G. Hansma, X. Zhu, M. Guthold, C. Bustamante, E. T. Kool, M. Kashlev, and P. K. Hansma, "Escherichia coli RNA Polymerase activity observed using Atomic Force Microscopy," *Biochemistry*, vol. 36, no. 3, pp. 461–468, 1997.

[17] A. Hillisch, M. Lorenz, and S. Diekmann, "Recent advances in FRET: distance determination in protein–DNA complexes," *Current Opinion in Structural Biology*, vol. 11, no. 2, pp. 201 – 207, 2001.

[18] A. Asanov, A. Zepeda, and L. Vaca, "A platform for combined DNA and protein microarrays based on Total Internal Reflection Fluorescence," *Sensors*, vol. 12, no. 2, p. 1800, 2012.

[19] J. C. M. Gebhardt, D. M. Suter, R. Roy, Z. W. Zhao, A. R. Chapman, S. Basu, T. Maniatis, and X. S. Xie, "Single-molecule imaging of transcription factor binding to DNA in live mammalian cells," *Nature Methods*, vol. 10, no. 5, pp. 421–426, 2013.

[20] J. Fan, M. Leroux-Coyau, N. J. Savery, and T. R. Strick, "Reconstruction of bacterial transcription-coupled repair at single-molecule resolution," *Nature*, vol. 536, no. 7615, pp. 234–237, 2016.

[21] A. Ashkin, J. M. Dziedzic, J. E. Bjorkholm, and S. Chu, "Observation of a single-beam gradient force optical trap for dielectric particles," *Optics Letters*, vol. 11, no. 5, pp. 288–290, 1986.

[22] F. Dutto, C. Raillon, K. Schenk, and A. Radenovic, "Nonlinear optical response in single alkaline niobate nanowires," *Nano Letters*, vol. 11, no. 6, pp. 2517–2521, 2011.

[23] K. C. Neuman, E. H. Chadd, G. F. Liou, K. Bergman, and S. M. Block, "Characterization of photodamage to Escherichia coli in optical traps," *Biophysical Journal*, vol. 77, no. 5, pp. 2856–2863, 1999.

[24] H. Zhang and K.-K. Liu, "Optical tweezers for single cells," *Journal of the Royal Society, Interface*, vol. 5, no. 24, pp. 671–690, 2008.

[25] P. Barak, A. Rai, P. Rai, and R. Mallik, "Quantitative optical trapping on single organelles in cell extract," *Nature Methods*, vol. 10, no. 1, pp. 68–70, 2013.

[26] V. V. Thacker, K. Bromek, B. Meijer, J. Kotar, B. Sclavi, M. C. Lagomarsino, U. F. Keyser, and P. Cicuta, "Bacterial nucleoid structure probed by active drag and resistive pulse sensing," *Integrative biology: quantitative biosciences from nano to macro*, vol. 6, no. 2, pp. 184–191, 2014.

[27] A. M. Kaufman, B. J. Lester, and C. A. Regal, "Cooling a single atom in an optical tweezer to its quantum ground state," *Physical Review X*, vol. 2, pp. 041014–1–7, 2012.

[28] I. Heller, T. P. Hoekstra, G. A. King, E. J. G. Peterman, and G. J. L. Wuite, "Optical tweezers analysis of DNA–protein complexes," *Chemical Reviews*, vol. 114, no. 6, pp. 3087–3119, 2014.

[29] J. Liphardt, B. Onoa, S. B. Smith, I. Tinoco, and C. Bustamante, "Reversible unfolding of single RNA molecules by mechanical force," *Science*, vol. 292, no. 5517, pp. 733–737, 2001.

[30] M. S. Z. Kellermayer, S. B. Smith, H. L. Granzier, and C. Bustamante, "Folding-unfolding transitions in single titin molecules characterized with laser tweezers," *Science*, vol. 276, no. 5315, pp. 1112–1116, 1997.

[31] J. W. Shaevitz, "A practical guide to optical trapping," *Berkeley handout*, pp. 1–19, 2006.

[32] K. C. Neuman and S. M. Block, "Optical trapping," *The Review of Scientific Instruments*, vol. 75, no. 9, pp. 2787–2809, 2004.

[33] S. B. Smith, Y. Cui, and C. Bustamante, "Overstretching B-DNA: the elastic response of individual double-stranded and single-stranded DNA molecules," *Science*, vol. 271, no. 5250, pp. 795–799, 1996.

[34] B. D. Brower-Toland, C. L. Smith, R. C. Yeh, J. T. Lis, C. L. Peterson, and M. D. Wang, "Mechanical disruption of individual nucleosomes reveals a reversible multistage release of DNA," *Proceedings of the National Academy of Sciences*, vol. 99, no. 4, pp. 1960–1965, 2002.

Bibliography

[35] S. J. Koch, A. Shundrovsky, B. C. Jantzen, and M. D. Wang, "Probing protein-DNA interactions by unzipping a single DNA double helix," *Biophysical Journal*, vol. 83, no. 2, pp. 1098 – 1105, 2002.

[36] M. D. Wang, M. J. Schnitzer, H. Yin, R. Landick, J. Gelles, and S. M. Block, "Force and velocity measured for single molecules of RNA polymerase," *Science*, vol. 282, no. 5390, pp. 902–907, 1998.

[37] K. C. Neuman, E. A. Abbondanzieri, R. Landick, J. Gelles, and S. M. Block, "Ubiquitous transcriptional pausing is independent of RNA polymerase backtracking," *Cell*, vol. 115, pp. 437–447, 2003.

[38] J. W. Shaevitz, E. A. Abbondanzieri, R. Landick, and S. M. Block, "Backtracking by single RNA polymerase molecules observed at near-base-pair resolution," *Nature*, vol. 426, no. 6967, pp. 684–687, 2003.

[39] E. A. Abbondanzieri, W. J. Greenleaf, J. W. Shaevitz, R. Landick, and S. M. Block, "Direct observation of base-pair stepping by RNA polymerase," *Nature*, vol. 438, pp. 460–465, 2005.

[40] J. Ma, L. Bai, and M. D. Wang, "Transcription under torsion," *Science*, vol. 340, no. 6140, pp. 1580–1583, 2013.

[41] B. Ibarra, Y. R. Chemla, S. Plyasunov, S. B. Smith, J. M. Lazaro, M. Salas, and C. Bustamante, "Proofreading dynamics of a processive DNA polymerase," *Embo Journal*, vol. 28, no. 18, pp. 2794–2802, 2009.

[42] M. Spies, P. R. Bianco, M. S. Dillingham, N. Handa, R. J. Baskin, and S. C. Kowalczykowski, "A molecular throttle: the recombination hotspot chi controls DNA translocation by the RecBCD helicase," *Cell*, vol. 114, no. 5, pp. 647–654, 2003.

[43] B. Sun, D. S. Johnson, G. Patel, B. Y. Smith, M. Pandey, S. S. Patel, and M. D. Wang, "ATP-induced helicase slippage reveals highly coordinated subunits," *Nature*, vol. 478, no. 7367, pp. 132–135, 2011.

[44] I. Heller, G. Sitters, O. D. Broekmans, G. Farge, C. Menges, W. Wende, S. W. Hell, E. J. G. Peterman, and G. J. L. Wuite, "STED nanoscopy combined with optical tweezers reveals protein dynamics on densely covered DNA," *Nature Methods*, vol. 10, no. 9, pp. 910–916, 2013.

[45] J. V. Mameren, M. Modesti, R. Kanaar, C. Wyman, E. J. G. Peterman, and G. J. L. Wuite, "Counting RAD51 proteins disassembling from nucleoprotein filaments under tension," *Nature*, vol. 457, no. 7230, pp. 745–748, 2008.

[46] R. Galletto, I. Amitani, R. J. Baskin, and S. C. Kowalczykowski, "Direct observation of individual RecA filaments assembling on single DNA molecules," *Nature*, vol. 443, no. 7113, pp. 875–878, 2006.

[47] J. Feng, M. Graf, K. Liu, D. Ovchinnikov, D. Dumcenco, M. Heiranian, V. Nandigana, N. R. Aluru, A. Kis, and A. Radenovic, "Single-layer MoS2 nanopores as nanopower generators," *Nature*, vol. 536, no. 7615, pp. 197–200, 2016.

[48] W. Shui, J. Fan, P. Yang, C. Liu, J. Zhai, J. Lei, Yan, D. Zhao, and X. Chen, "Nanopore-based proteolytic reactor for sensitive and comprehensive proteomic analyses," *Analytical Chemistry*, vol. 78, no. 14, pp. 4811–4819, 2006.

[49] M. Heiranian, A. B. Farimani, and N. R. Aluru, "Water desalination with a single-layer MoS2 nanopore," *Nature Communications*, vol. 6, p. 8616, 2015.

[50] S. P. Surwade, S. N. Smirnov, I. V. Vlassiouk, R. R. Unocic, G. M. Veith, S. Dai, and S. M. Mahurin, "Water desalination using nanoporous single-layer graphene," *Nature Nanotechnology*, vol. 10, no. 5, pp. 459–464, 2015.

[51] S. W. Kowalczyk, L. Kapinos, T. R. Blosser, T. Magalhaes, P. van Nies, L. Y. H., and C. Dekker, "Single-molecule transport across an individual biomimetic nuclear pore complex," *Nature Nanotechnology*, vol. 6, no. 7, pp. 433–438, 2011.

[52] N. Laohakunakorn, B. Gollnick, F. Moreno-Herrero, D. G. A. L. Aarts, R. P. A. Dullens, S. Ghosal, and U. F. Keyser, "A Landau-Squire nanojet," *Nano Letters*, vol. 13, no. 11, pp. 5141–5146, 2013.

[53] N. Laohakunakorn, S. Ghosal, O. Otto, K. Misiunas, and U. F. Keyser, "DNA interactions in crowded nanopores.," *Nano Letters*, vol. 13, no. 6, pp. 2798–2802, 2013.

[54] J. Feng, K. Liu, R. D. Bulushev, S. Khlybov, D. Dumcenco, A. Kis, and A. Radenovic, "Identification of single nucleotides in MoS2 nanopores," *Nature Nanotechnology*, vol. 10, no. 12, pp. 1070–1076, 2015.

[55] A. J. Storm, C. Storm, J. Chen, H. Zandbergen, J. F. Joanny, and C. Dekker, "Fast DNA translocation through a solid-state nanopore," *Nano Letters*, vol. 5, pp. 1193–1197, 2005.

[56] C. Shasha, R. Y. Henley, D. H. Stoloff, K. D. Rynearson, T. Hermann, and M. Wanunu, "Nanopore-based conformational analysis of a viral RNA drug target," *ACS Nano*, vol. 8, no. 6, pp. 6425–6430, 2014.

[57] E. C. Yusko, J. M. Johnson, S. Majd, P. Prangkio, R. C. Rollings, J. Li, J. Yang, and M. Mayer, "Controlling protein translocation through nanopores with bio-inspired fluid walls," *Nature Nanotechnology*, vol. 6, no. 4, pp. 253–260, 2011.

[58] C. Raillon, P. Cousin, F. Traversi, E. Garcia-Cordero, N. Hernandez, and A. Radenovic, "Nanopore detection of single molecule RNAP–DNA transcription complex," *Nano Letters*, vol. 12, no. 3, pp. 1157–1164, 2012.

[59] A. McMullen, H. W. de Haan, J. X. Tang, and D. Stein, "Stiff filamentous virus translocations through solid-state nanopores," *Nature Communications*, vol. 5, p. 4171, 2014.

[60] G. S. Roberts, D. Kozak, W. Anderson, M. F. Broom, R. Vogel, and M. Trau, "Tunable nano/micropores for particle detection and discrimination: Scanning ion occlusion spectroscopy," *Small*, vol. 6, no. 23, pp. 2653–2658, 2010.

[61] A. R. Hall, J. M. Keegstra, M. C. Duch, M. C. Hersam, and C. Dekker, "Translocation of single-wall carbon nanotubes through solid-state nanopores," *Nano Letters*, vol. 11, no. 6, pp. 2446–2450, 2011.

[62] M. Wanunu, "Nanopores: A journey towards DNA sequencing," *Physics of Life Reviews*, vol. 9, no. 2, pp. 125 – 158, 2012.

[63] B. N. Miles, A. P. Ivanov, K. A. Wilson, F. Dogan, D. Japrung, and J. B. Edel, "Single molecule sensing with solid-state nanopores: novel materials, methods, and applications," *Chemical Society Reviews*, vol. 42, pp. 15–28, 2013.

[64] F. Haque, J. Li, H.-C. Wu, X.-J. Liang, and P. Guo, "Solid-state and biological nanopore for real-time sensing of single chemical and sequencing of DNA," *Nano Today*, vol. 8, no. 1, pp. 56 – 74, 2013.

[65] K. Göpfrich, C. V. Kulkarni, O. J. Pambos, and U. F. Keyser, "Lipid nanobilayers to host biological nanopores for DNA translocations," *Langmuir*, vol. 29, no. 1, pp. 355–364, 2013.

[66] J. J. Kasianowicz, "Characterization of individual polynucleotide molecules using a membrane channel," *Proceedings of the National Academy of Sciences*, vol. 93, pp. 13770–13773, 1996.

[67] E. A. Manrao, I. M. Derrington, A. H. Laszlo, K. W. Langford, M. K. Hopper, N. Gillgren, M. Pavlenok, M. Niederweis, and J. H. Gundlach, "Reading DNA at single-nucleotide resolution with a mutant MspA nanopore and phi29 DNA polymerase," *Nature Biotechnology*, vol. 30, no. 4, pp. 349–353, 2012.

[68] J. Quick, N. J. Loman, S. Duraffour, J. T. Simpson, E. Severi, L. Cowley, J. A. Bore, R. Koundouno, G. Dudas, A. Mikhail, N. Ouédraogo, B. Afrough, A. Bah, J. H. J. Baum, B. Becker-Ziaja, J. P. Boettcher, M. Cabeza-Cabrerizo, Á. Camino-Sánchez, L. L. Carter, J. Doerrbecker, T. Enkirch, I. G. Dorival, N. Hetzelt, J. Hinzmann, T. Holm, L. E. Kafetzopoulou, M. Koropogui, A. Kosgey, E. Kuisma, C. H. Logue, A. Mazzarelli, S. Meisel, M. Mertens, J. Michel, D. Ngabo, K. Nitzsche, E. Pallasch, L. V. Patrono, J. Portmann, J. G. Repits, N. Y. Rickett, A. Sachse, K. Singethan, I. Vitoriano, R. L. Yemanaberhan, E. G. Zekeng, T. Racine, A. Bello, A. A. Sall, O. Faye, O. Faye, N. Magassouba, C. V. Williams, V. Amburgey, L. Winona, E. Davis, J. Gerlach, F. Washington, V. Monteil, M. Jourdain, M. Bererd, A. Camara, H. Somlare, A. Camara, M. Gerard, G. Bado, B. Baillet, D. Delaune, K. Y. Nebie, A. Diarra, Y. Savane, R. B. Pallawo, G. J. Gutierrez, N. Milhano, I. Roger, C. J. Williams, F. Yattara, K. Lewandowski, J. Taylor, P. Rachwal, D. J. Turner, G. Pollakis, J. A. Hiscox, D. A. Matthews, M. K. O. Shea, A. M. Johnston, D. Wilson, E. Hutley, E. Smit, A. Di Caro, R. Wölfel, K. Stoecker, E. Fleischmann, M. Gabriel, S. A. Weller, L. Koivogui,

B. Diallo, S. Keïta, A. Rambaut, P. Formenty, S. Günther, and M. W. Carroll, "Real-time, portable genome sequencing for Ebola surveillance," *Nature*, vol. 530, no. 7589, pp. 228–232, 2016.

[69] M. Wanunu, T. Dadosh, V. Ray, J. Jin, L. McReynolds, and M. Drndić, "Rapid electronic detection of probe-specific microRNAs using thin nanopore sensors," *Nature Nanotechnology*, vol. 5, no. 11, pp. 807–814, 2010.

[70] S. Garaj, W. Hubbard, A. Reina, J. Kong, D. Branton, and J. A. Golovchenko, "Graphene as a subnanometre trans-electrode membrane," *Nature*, vol. 467, no. 7312, pp. 190–193, 2010.

[71] L. J. Steinbock, O. Otto, C. Chimerel, J. Gornall, and U. F. Keyser, "Detecting DNA folding with nanocapillaries," *Nano Letters*, vol. 10, no. 7, pp. 2493–2497, 2010.

[72] T. Z. Butler, M. Pavlenok, I. M. Derrington, M. Niederweis, and J. H. Gundlach, "Single-molecule DNA detection with an engineered MspA protein nanopore," *Proceedings of the National Academy of Sciences*, vol. 105, no. 52, pp. 20647–20652, 2008.

[73] N. A. W. Bell, C. R. Engst, M. Ablay, G. Divitini, C. Ducati, T. Liedl, and U. F. Keyser, "DNA origami nanopores," *Nano Letters*, vol. 12, no. 1, pp. 512–517, 2012.

[74] J. Li, M. Gershow, D. Stein, E. Brandin, and J. A. Golovchenko, "DNA molecules and configurations in a solid-state nanopore microscope," *Nature Materials*, vol. 2, no. 9, pp. 611–615, 2003.

[75] J. Li, D. Stein, C. McMullan, D. Branton, M. Aziz, and J. Golovchenko, "Ion-beam sculpting at nanometre length scales.," *Nature*, vol. 412, pp. 166–169, 2001.

[76] A. J. Storm, J. H. Chen, X. S. Ling, H. W. Zandbergen, and C. Dekker, "Fabrication of solid-state nanopores with single-nanometre precision," *Nature Materials*, vol. 2, no. 8, pp. 537–540, 2003.

[77] K. Liu, J. Feng, A. Kis, and A. Radenovic, "Atomically thin molybdenum disulfide nanopores with high sensitivity for DNA translocation," *ACS Nano*, vol. 8, no. 3, pp. 2504–2511, 2014.

[78] H. Kwok, K. Briggs, and V. Tabard-Cossa, "Nanopore fabrication by controlled dielectric breakdown," *PLoS ONE*, vol. 9, no. 3, 2014.

[79] J. Feng, K. Liu, M. Graf, M. Lihter, R. D. Bulushev, D. Dumcenco, D. T. L. Alexander, D. Krasnozhon, T. Vuletic, A. Kis, and A. Radenovic, "Electrochemical reaction in single layer MoS$_2$: Nanopores opened atom by atom," *Nano Letters*, vol. 15, no. 5, pp. 3431–3438, 2015.

[80] S. Cabello-Aguilar, S. Balme, A. A. Chaaya, M. Bechelany, E. Balanzat, J.-M. Janot, C. Pochat-Bohatier, P. Miele, and P. Dejardin, "Slow translocation of polynucleotides

and their discrimination by small α-hemolysin inside a single track-etched nanopore designed by atomic layer deposition," *Nanoscale*, vol. 5, pp. 9582–9586, 2013.

[81] R. W. Clarke, S. S. White, D. Zhou, L. Ying, and D. Klenerman, "Trapping of proteins under physiological conditions in a nanopipette," *Angewandte Chemie*, vol. 44, no. 24, pp. 3747–3750, 2005.

[82] Y. Youn, C. Lee, J. H. Kim, Y. W. Chang, D. Y. Kim, and K.-H. Yoo, "Selective detection of single-stranded DNA molecules using a glass nanocapillary functionalized with DNA," *Analytical Chemistry*, vol. 88, no. 1, pp. 688–694, 2016.

[83] P. Terejánszky, I. Makra, P. Fürjes, and R. E. Gyurcsányi, "Calibration-less sizing and quantitation of polymeric nanoparticles and viruses with quartz nanopipets," *Analytical Chemistry*, vol. 86, no. 10, pp. 4688–4697, 2014.

[84] J. A. Bafna and G. V. Soni, "Fabrication of low noise borosilicate glass nanopores for single molecule sensing," *PLoS ONE*, vol. 11, no. 6, pp. 1–15, 2016.

[85] E. Neher and B. Sakmann, "Single-channel currents recorded from membrane of denervated frog muscle fibres," *Nature*, vol. 260, no. 5554, pp. 799–802, 1976.

[86] N. A. W. Bell and U. F. Keyser, "Specific protein detection using designed DNA carriers and nanopores," *Journal of the American Chemical Society*, vol. 137, no. 5, pp. 2035–2041, 2015.

[87] L. J. Steinbock, R. D. Bulushev, S. Krishnan, C. Raillon, and A. Radenovic, "DNA translocation through low-noise glass nanopores," *ACS Nano*, vol. 7, no. 12, pp. 11255–11262, 2013.

[88] L. P. Zweifel, I. Shorubalko, and R. Y. Lim, "Helium scanning transmission ion microscopy and electrical characterization of glass nanocapillaries with reproducible tip geometries," *ACS Nano*, vol. 10, no. 2, pp. 1918–1925, 2016.

[89] L. J. Steinbock, J. F. Steinbock, and A. Radenovic, "Controllable shrinking and shaping of glass nanocapillaries under electron irradiation," *Nano Letters*, vol. 13, no. 4, pp. 1717–1723, 2013.

[90] J. Y. Y. Sze, S. Kumar, A. P. Ivanov, S.-H. Oh, and J. B. Edel, "Fine tuning of nanopipettes using atomic layer deposition for single molecule sensing," *Analyst*, vol. 140, pp. 4828–4834, 2015.

[91] S. Hernández-Ainsa, C. Muus, N. A. W. Bell, L. J. Steinbock, V. V. Thacker, and U. F. Keyser, "Lipid-coated nanocapillaries for DNA sensing.," *The Analyst*, vol. 138, no. 1, pp. 104–106, 2013.

[92] M. Langecker, V. Arnaut, T. G. Martin, J. List, S. Renner, M. Mayer, H. Dietz, and F. C. Simmel, "Synthetic lipid membrane channels formed by designed DNA nanostructures," *Science*, vol. 338, no. 6109, pp. 932–936, 2012.

[93] S. Hernandez-Ainsa, N. A. W. Bell, V. V. Thacker, K. Göpfrich, K. Misiunas, M. E. Fuentes-Perez, F. Moreno-Herrero, and U. F. Keyser, "DNA origami nanopores for controlling DNA translocation," *ACS Nano*, vol. 7, no. 7, pp. 6024–6030, 2013.

[94] A. Seifert, K. Göpfrich, J. R. Burns, N. Fertig, U. F. Keyser, and S. Howorka, "Bilayer-spanning DNA nanopores with voltage-switching between open and closed state," *ACS Nano*, vol. 9, no. 2, pp. 1117–1126, 2015.

[95] J. R. Burns, A. Seifert, N. Fertig, and S. Howorka, "A biomimetic DNA-based channel for the ligand-controlled transport of charged molecular cargo across a biological membrane," *Nature Nanotechnology*, vol. 11, no. 2, pp. 152–156, 2016.

[96] S. W. Kowalczyk, A. R. Hall, and C. Dekker, "Detection of local protein structures along DNA using solid-state nanopores," *Nano Letters*, vol. 10, no. 1, pp. 324–328, 2010.

[97] J.-S. Yu, M.-C. Lim, D. Thi, N. Huynh, H.-J. Kim, H.-M. Kim, and Y.-R. Kim, "Identifying the location of a single protein along the DNA strand," *ACS Nano*, vol. 9, no. 5, pp. 5289–5298, 2015.

[98] R. M. M. Smeets, S. W. Kowalczyk, A. R. Hall, N. H. Dekker, and C. Dekker, "Translocation of RecA-coated double-stranded DNA through solid-state nanopores," *Nano Letters*, vol. 9, no. 9, pp. 3089–3095, 2009.

[99] G. V. Soni and C. Dekker, "Detection of nucleosomal substructures using solid-state nanopores," *Nano Letters*, vol. 12, no. 6, pp. 3180–3186, 2012.

[100] C. Plesa, J. W. Ruitenberg, M. J. Witteveen, and C. Dekker, "Detection of single proteins bound along DNA with solid-state nanopores," *Nano Letters*, vol. 15, no. 5, pp. 3153–3158, 2015.

[101] A. Squires, E. Atas, and A. Meller, "Nanopore sensing of individual transcription factors bound to DNA," *Scientific Reports*, vol. 5, p. 11643, 2015.

[102] M. M. Marshall, J. Ruzicka, O. K. Zahid, V. C. Henrich, E. W. Taylor, and A. R. Hall, "Nanopore analysis of single-stranded binding protein interactions with DNA," *Langmuir*, vol. 31, no. 15, pp. 4582–4588, 2015.

[103] J. Shim, Y. Kim, G. I. Humphreys, A. M. Nardulli, F. Kosari, G. Vasmatzis, W. R. Taylor, D. A. Ahlquist, S. Myong, and R. Bashir, "Nanopore-based assay for detection of methylation in double-stranded DNA fragments," *ACS Nano*, vol. 9, no. 1, pp. 290–300, 2015.

[104] B. Hornblower, A. Coombs, R. D. Whitaker, A. Kolomeisky, S. J. Picone, A. Meller, and M. Akeson, "Single-molecule analysis of DNA-protein complexes using nanopores," *Nature Methods*, vol. 4, no. 4, pp. 2006–2008, 2007.

[105] M. Langecker, A. Ivankin, S. Carson, S. R. M. Kinney, F. C. Simmel, and M. Wanunu, "Nanopores suggest a negligible influence of CpG methylation on nucleosome packaging and stability," *Nano Letters*, vol. 15, no. 1, pp. 783–790, 2015.

[106] B. Dorvel, G. Sigalov, Q. Zhao, J. Comer, V. Dimitrov, U. Mirsaidov, A. Aksimentiev, and G. Timp, "Analyzing the forces binding a restriction endonuclease to DNA using a synthetic nanopore," *Nucleic Acids Research*, vol. 37, no. 12, pp. 4170–4179, 2009.

[107] U. F. Keyser, B. N. Koeleman, S. van Dorp, D. Krapf, R. M. M. Smeets, S. G. Lemay, N. H. Dekker, and C. Dekker, "Direct force measurements on DNA in a solid-state nanopore," *Nature Physics*, vol. 2, no. 7, pp. 473–477, 2006.

[108] E. H. Trepagnier, A. Radenovic, D. Sivak, P. Geissler, and J. Liphardt, "Controlling DNA capture and propagation through artificial nanopores," *Nano Letters*, vol. 7, no. 9, pp. 2824–2830, 2007.

[109] A. Sischka, C. Kleimann, W. Hachmann, M. M. Schäfer, I. Seuffert, K. Tönsing, and D. Anselmetti, "Single beam optical tweezers setup with backscattered light detection for three-dimensional measurements on DNA and nanopores," *The Review of Scientific Instruments*, vol. 79, no. 6, p. 063702, 2008.

[110] M. van den Hout, I. D. Vilfan, S. Hage, and N. H. Dekker, "Direct force measurements on double-stranded RNA in solid-state nanopores," *Nano Letters*, vol. 10, no. 2, pp. 701–707, 2010.

[111] U. F. Keyser, D. Krapf, B. N. Koeleman, R. M. M. Smeets, N. H. Dekker, and C. Dekker, "Nanopore tomography of a laser focus," *Nano Letters*, vol. 5, no. 11, pp. 2253–2256, 2005.

[112] U. F. Keyser, J. van der Does, C. Dekker, and N. H. Dekker, "Optical tweezers for force measurements on DNA in nanopores," *Review of Scientific Instruments*, vol. 77, no. 10, 2006.

[113] S. van Dorp, U. F. Keyser, N. H. Dekker, C. Dekker, and S. G. Lemay, "Origin of the electrophoretic force on DNA in solid-state nanopores," *Nature Physics*, vol. 5, no. 5, pp. 347–351, 2009.

[114] L. Galla, A. J. Meyer, A. Spiering, A. Sischka, M. Mayer, A. R. Hall, P. Reimann, and D. Anselmetti, "Hydrodynamic slip on DNA observed by optical tweezers-controlled translocation experiments with solid-state and lipid-coated nanopores," *Nano Letters*, vol. 14, pp. 4176–4182, 2014.

[115] A. R. Hall, S. van Dorp, S. G. Lemay, and C. Dekker, "Electrophoretic force on a protein-coated DNA molecule in a solid-state nanopore," *Nano Letters*, vol. 9, no. 12, pp. 4441–4445, 2009.

[116] S. Knust, A. Spiering, H. Vieker, A. Beyer, A. Gölzhäuser, K. Tönsing, A. Sischka, and D. Anselmetti, "Video-based and interference-free axial force detection and analysis for optical tweezers," *The Review of Scientific Instruments*, vol. 83, p. 103704, 2012.

[117] A. Sischka, A. Spiering, M. Khaksar, M. Laxa, J. König, K.-J. Dietz, and D. Anselmetti, "Dynamic translocation of ligand-complexed DNA through solid-state nanopores with optical tweezers," *Journal of Physics: Condensed Matter*, vol. 22, no. 45, p. 454121, 2010.

[118] A. Spiering, S. Getfert, A. Sischka, P. Reimann, and D. Anselmetti, "Nanopore transloca-tion dynamics of a single DNA-bound protein," *Nano Letters*, vol. 11, no. 7, pp. 2978–2982, 2011.

[119] L. J. Steinbock, O. Otto, D. R. Skarstam, S. Jahn, C. Chimerel, J. L. Gornall, and U. F. Keyser, "Probing DNA with micro- and nanocapillaries and optical tweezers," *Journal of physics. Condensed matter : an Institute of Physics journal*, vol. 22, no. 45, p. 454113, 2010.

[120] O. Otto, L. J. Steinbock, D. W. Wong, J. L. Gornall, and U. F. Keyser, "Note: Direct force and ionic-current measurements on DNA in a nanocapillary," *Review of Scientific In-struments*, vol. 82, no. 8, 2011.

[121] V. V. Thacker, S. Ghosal, S. Hernández-Ainsa, N. A. W. Bell, and U. F. Keyser, "Studying DNA translocation in nanocapillaries using single molecule fluorescence," *Applied Physics Letters*, vol. 101, no. 22, 2012.

[122] N. Laohakunakorn, V. V. Thacker, M. Muthukumar, and U. F. Keyser, "Electroosmotic flow reversal outside glass nanopores," *Nano Letters*, vol. 15, no. 1, pp. 695–702, 2015.

[123] O. Otto, S. Sturm, N. Laohakunakorn, U. F. Keyser, and K. Kroy, "Rapid internal contrac-tion boosts DNA friction," *Nature Communications*, vol. 4, p. 1780, 2013.

[124] G. Romanowski, M. G. Lorenz, and W. Wackernagel, "Adsorption of plasmid DNA to min-eral surfaces and protection against DNase I," *Applied and Environmental Microbiology*, vol. 57, no. 4, pp. 1057–1061, 1991.

[125] E. M. Abad-Villar, J. Tanyanyiwa, M. T. Fernández-Abedul, A. Costa-García, and P. C. Hauser, "Detection of human immunoglobulin in microchip and conventional capillary electrophoresis with contactless conductivity measurements," *Analytical Chemistry*, vol. 76, no. 5, pp. 1282–1288, 2004.

[126] L. Sola and M. Chiari, "Modulation of electroosmotic flow in capillary electrophoresis using functional polymer coatings," *Journal of Chromatography A*, vol. 1270, pp. 324 – 329, 2012.

[127] R. D. Bulushev, L. J. Steinbock, S. Khlybov, J. F. Steinbock, U. F. Keyser, and A. Raden-ovic, "Measurement of the position-dependent electrophoretic force on DNA in a glass nanocapillary," *Nano Letters*, vol. 14, no. 11, pp. 6606–6613, 2014.

[128] U. F. Keyser, "Nanopore-Based Technology," *Methods in Molecular Biology*, vol. 870, pp. 115–134, 2012.

[129] C. Raillon, P. Granjon, M. Graf, L. J. Steinbock, and A. Radenovic, "Fast and automatic processing of multi-level events in nanopore translocation experiments," *Nanoscale*, vol. 4, pp. 4916–4924, 2012.

[130] R. D. Bulushev, S. Marion, and A. Radenovic, "Relevance of the drag force during controlled translocation of a DNA-protein complex through a glass nanocapillary," *Nano Letters*, vol. 15, no. 10, pp. 7118–7125, 2015.

[131] U. F. Keyser, S. van Dorp, and S. G. Lemay, "Tether forces in DNA electrophoresis," *Chemical Society Reviews*, vol. 39, no. 3, pp. 939–947, 2010.

[132] D. E. Smith, T. T. Perkins, and S. Chu, "Dynamical scaling of DNA diffusion coefficients," *Macromolecules*, vol. 29, pp. 1372–1373, 1995.

[133] J. R. Levin, B. Krummel, and M. J. Chamberlin, "Isolation and properties of transcribing ternary complexes of Escherichia coli RNA polymerase positioned at a single template base," *Journal of Molecular Biology*, vol. 196, no. 1, pp. 85–100, 1987.

[134] B. Krummel and M. J. Chamberlin, "RNA chain initiation by Escherichia coli RNA polymerase. Structural transitions of the enzyme in early ternary complexes," *Biochemistry*, vol. 28, no. 19, pp. 7829–7842, 1989.

[135] M. J. Allen, X. F. Dong, T. E. O'Neill, P. Yau, S. C. Kowalczykowski, J. Gatewood, R. Balhorn, and E. M. Bradbury, "Atomic force microscope measurements of nucleosome cores assembled along defined DNA sequences," *Biochemistry*, vol. 32, no. 33, pp. 8390–8396, 1993.

[136] G. H. Seong, T. Niimi, Y. Yanagida, E. Kobatake, and M. Aizawa, "Single-molecular AFM probing of specific DNA sequencing using RecA-promoted homologous pairing and strand exchange," *Analytical Chemistry*, vol. 72, no. 6, pp. 1288–1293, 2000.

[137] D. P. Allison, P. S. Kerper, M. J. Doktycz, J. A. Spain, P. Modrich, F. W. Larimer, T. Thundat, and R. J. Warmack, "Direct atomic force microscope imaging of EcoRI endonuclease site specifically bound to plasmid DNA molecules," *Proceedings of the National Academy of Sciences*, vol. 93, pp. 8826–8829, 1996.

[138] D. Lohr, R. Bash, H. Wang, J. Yodh, and S. Lindsay, "Using atomic force microscopy to study chromatin structure and nucleosome remodeling," *Methods (San Diego, Calif.)*, vol. 41, no. 3, pp. 333–341, 2007.

[139] P. Seitz, H. Pezeshgi Modarres, S. Borgeaud, R. D. Bulushev, L. J. Steinbock, A. Radenovic, M. Dal Peraro, and M. Blokesch, "ComEA is essential for the transfer of external DNA into the periplasm in naturally transformable Vibrio cholerae cells," *PLoS Genetics*, vol. 10, no. 1, p. e1004066, 2014.

[140] L. M. Hellman and M. G. Fried, "Electrophoretic mobility shift assay (EMSA) for detecting protein-nucleic acid interactions," *Nature Protocols*, vol. 2, no. 8, pp. 1849–1861, 2007.

[141] S. Ghosal, "Electrophoresis of a polyelectrolyte through a nanopore," *Physical Review E*, vol. 74, no. 4, p. 041901, 2006.

[142] G. Hummer and A. Szabo, "Kinetics from nonequilibrium single-molecule pulling experiments," *Biophysical Journal*, vol. 85, no. 1, pp. 5–15, 2003.

[143] J. F. Marko and E. D. Siggia, "Stretching DNA," *Macromolecules*, vol. 28, no. 26, pp. 8759–8770, 1995.

[144] S. Ghosal, "Electrokinetic-flow-induced viscous drag on a tethered DNA inside a nanopore," *Physical Review E*, vol. 76, no. 6, p. 061916, 2007.

[145] B. Lu, D. P. Hoogerheide, Q. Zhao, and D. Yu, "Effective driving force applied on DNA inside a solid-state nanopore," *Physical Review E*, vol. 86, no. 1, p. 011921, 2012.

[146] R. D. Bulushev, S. Marion, E. Petrova, S. J. Davis, S. J. Maerkl, and A. Radenovic, "Single molecule localization and discrimination of DNA–protein complexes by controlled translocation through nanocapillaries," *Nano Letters*, vol. 16, no. 12, pp. 7882–7890, 2016.

[147] A. P. A. Bérut and S. Ciliberto, "Detailed Jarzynski equality applied to a logically irreversible procedure," *Europhysics Letters*, vol. 103, no. 6, p. 60002, 2013.

[148] C. Jarzynski, "Nonequilibrium equality for free energy differences," *Physical Review Letters*, vol. 78, pp. 2690–2693, 1997.

[149] C. Aiken and R. I. Gumport, "Restriction endonuclease RsrI from Rhodobacter sphaeroides, an isoschizomer of EcoRI: purification and properties," *Nucleic Acids Research*, vol. 16, no. 16, pp. 7901–7916, 1988.

[150] C. Rivetti, M. Guthold, and C. Bustamante, "Wrapping of DNA around the E. coli RNA polymerase open promoter complex," *EMBO Journal*, vol. 18, no. 16, pp. 4464–4475, 1999.

[151] N. Loizos and S. A. Darst, "Mapping interactions of Escherichia coli GreB with RNA polymerase and ternary elongation complexes," *Journal of Biological Chemistry*, vol. 274, no. 33, pp. 23378–23386, 1999.

[152] S. E. Halford, N. P. Johnson, and J. Grinsted, "The EcoRI restriction endonuclease with bacteriophage lambda DNA. Kinetic studies," *The Biochemical Journal*, vol. 191, pp. 581–592, 1980.

[153] S. E. Halford and N. P. Johnson, "The EcoRI restriction endonuclease with bacteriophage lambda DNA. Equilibrium binding studies," *The Biochemical journal*, vol. 191, pp. 593–604, 1980.

[154] N. Y. Sidorova and D. C. Rau, "Differences in water release for the binding of EcoRI to specific and nonspecific DNA sequences.," *Proceedings of the National Academy of Sciences*, vol. 93, no. 22, pp. 12272–12277, 1996.

Bibliography

[155] C. R. Robinson and S. G. Sligar, "Changes in solvation during DNA binding and cleavage are critical to altered specificity of the EcoRI endonuclease," *Proceedings of the National Academy of Sciences*, vol. 95, no. 5, pp. 2186–2191, 1998.

[156] G. C. Walker, "Inducible DNA repair systems.," *Annual Review of Biochemistry*, vol. 54, pp. 425–457, 1985.

[157] K. P. Rice, A. L. Eggler, P. Sung, and M. M. Cox, "DNA pairing and strand exchange by the Escherichia coli RecA and yeast Rad51 proteins without ATP hydrolysis. On the importance of not getting stuck," *Journal of Biological Chemistry*, vol. 276, no. 42, pp. 38570–38581, 2001.

[158] M. Takahashi and B. Nordén, "Strucutre of RecA-DNA complex and mechanism of DNA strand exchange reaction in homologous recombination," *Advances in Biophysics*, vol. 30, pp. 1–35, 1994.

[159] K. Severinov and A. Goldfarb, "Topology of the product binding site in RNA polymerase revealed by transcript slippage at the phage lambda PL promoter.," *The Journal of Biological Chemistry*, vol. 269, no. 50, pp. 31701–31705, 1994.

[160] N. Laohakunakorn and U. F. Keyser, "Electroosmotic flow rectification in conical nanopores," *Nanotechnology*, vol. 26, no. 27, p. 275202, 2015.

[161] A. Sischka, L. Galla, A. J. Meyer, A. Spiering, S. Knust, M. Mayer, A. R. Hall, A. Beyer, P. Reimann, A. Golzhauser, and D. Anselmetti, "Controlled translocation of DNA through nanopores in carbon nano-, silicon-nitride- and lipid-coated membranes," *Analyst*, vol. 140, pp. 4843–4847, 2015.

[162] R. M. M. Smeets, U. F. Keyser, D. Krapf, M.-Y. Wu, N. H. Dekker, and C. Dekker, "Salt dependence of ion transport and DNA translocation through solid-state nanopores," *Nano Letters*, vol. 6, no. 1, pp. 89–95, 2006.

[163] G. R. Willmott and B. E. T. Parry, "Resistive pulse asymmetry for nanospheres passing through tunable submicron pores," *Journal of Applied Physics*, vol. 109, no. 9, 2011.

[164] S. C. Kim, S. K. Kannam, S. Harrer, M. T. Downton, S. Moore, and J. M. Wagner, "Geometric dependence of the conductance drop in a nanopore due to a particle," *Physical Review E - Statistical, Nonlinear, and Soft Matter Physics*, vol. 89, no. 4, pp. 1–9, 2014.

[165] S. Kesselheim, W. Müller, and C. Holm, "Origin of current blockades in nanopore translocation experiments," *Physical Review Letters*, vol. 112, no. 1, pp. 1–5, 2014.

[166] M. Firnkes, D. Pedone, J. Knezevic, M. Döblinger, and U. Rant, "Electrically facilitated translocations of proteins through silicon nitride nanopores: conjoint and competitive action of diffusion, electrophoresis, and electroosmosis," *Nano Letters*, vol. 10, no. 6, pp. 2162–2167, 2010.

112

[167] B. Iglewicz and D. C. Hoaglin, "How to detect and handle outliers, ASQC basic references in quality control," *ASQC Quality Press*, 1993.

[168] X. Wu, D. A. Scott, A. J. Kriz, A. C. Chiu, P. D. Hsu, D. B. Dadon, A. W. Cheng, A. E. Trevino, S. Konermann, S. Chen, R. Jaenisch, F. Zhang, and P. A. Sharp, "Genome-wide binding of the CRISPR endonuclease Cas9 in mammalian cells," *Nature Biotechnology*, vol. 32, no. 7, pp. 670–676, 2014.

[169] C. Kuscu, S. Arslan, R. Singh, J. Thorpe, and M. Adli, "Genome-wide analysis reveals characteristics of off-target sites bound by the Cas9 endonuclease," *Nature Biotechnology*, vol. 32, no. 7, pp. 677–683, 2014.

[170] R. Cencic, H. Miura, A. Malina, F. Robert, S. Ethier, T. M. Schmeing, J. Dostie, and J. Pelletier, "Protospacer adjacent motif (PAM)-distal sequences engage CRISPR Cas9 DNA target cleavage," *PLOS ONE*, vol. 9, no. 10, pp. 1–13, 2014.

[171] H. O'Geen, I. M. Henry, M. S. Bhakta, J. F. Meckler, and D. J. Segal, "A genome-wide analysis of Cas9 binding specificity using ChIP-seq and targeted sequence capture," *Nucleic Acids Research*, vol. 43, no. 6, pp. 3389–3404, 2015.

[172] S. H. Sternberg, S. Redding, M. Jinek, E. C. Greene, and J. A. Doudna, "DNA interrogation by the CRISPR RNA-guided endonuclease Cas9," *Nature*, vol. 507, no. 7490, pp. 62–67, 2014.

[173] M. Wang, H. Yin, R. Landick, J. Gelles, and S. Block, "Stretching DNA with optical tweezers," *Biophysical Journal*, vol. 72, no. 3, pp. 1335 – 1346, 1997.

[174] L. J. Steinbock, S. Krishnan, R. D. Bulushev, S. Borgeaud, M. Blokesch, L. Feletti, and A. Radenovic, "Probing the size of proteins with glass nanopores," *Nanoscale*, vol. 6, pp. 14380–14387, 2014.

[175] M. Jinek, F. Jiang, D. W. Taylor, S. H. Sternberg, E. Kaya, E. Ma, C. Anders, M. Hauer, K. Zhou, S. Lin, M. Kaplan, A. T. Iavarone, E. Charpentier, E. Nogales, and J. A. Doudna, "Structures of Cas9 endonucleases reveal RNA-mediated conformational activation," *Science*, vol. 343, no. 6176, 2014.

[176] A. Aksimentiev, "Deciphering ionic current signatures of DNA transport through a nanopore," *Nanoscale*, vol. 2, pp. 468–483, 2010.

[177] V. Dimitrov, U. Mirsaidov, D. Wang, T. Sorsch, W. Mansfield, J. Miner, F. Klemens, R. Cirelli, S. Yemenicioglu, and G. Timp, "Nanopores in solid-state membranes engineered for single molecule detection," *Nanotechnology*, vol. 21, no. 6, p. 065502, 2010.

[178] M. Wanunu, T. Dadosh, V. Ray, J. Jin, L. McReynolds, and M. Drndic, "Rapid electronic detection of probe-specific microRNAs using thin nanopore sensors," *Nature Nanotechnology*, vol. 5, no. 11, pp. 807–814, 2010.

Bibliography

[179] B. M. Venkatesan, D. Estrada, S. Banerjee, X. Jin, V. E. Dorgan, M.-H. Bae, N. R. Aluru, E. Pop, and R. Bashir, "Stacked graphene-Al2O3 nanopore sensors for sensitive detection of DNA and DNA–protein complexes," *ACS Nano*, vol. 6, no. 1, pp. 441–450, 2012.

[180] H. He, X. Xu, and Y. Jin, "Wet-chemical enzymatic preparation and characterization of ultrathin gold-decorated single glass nanopore," *Analytical Chemistry*, vol. 86, no. 10, pp. 4815–4821, 2014.

[181] Y.-H. Fu, D. P. A. Kuhl, A. Pizzuti, M. Pieretti, J. S. Sutcliffe, S. Richards, A. J. M. H. Verkert, J. J. A. Holden, R. G. Fenwick Jr., S. T. Warren, B. A. Oostra, D. L. Nelson, and C. Caskey, "Variation of the CGG repeat at the fragile X site results in genetic instability: resolution of the Sherman paradox," *Cell*, vol. 67, no. 6, pp. 1047–1058, 2016.

[182] S. E. Halford and J. F. Marko, "How do site-specific DNA-binding proteins find their targets?," *Nucleic Acids Research*, vol. 32, no. 10, pp. 3040–3052, 2004.

Roman Bulushev

Avenue de l´Eglise Anglaise 10,
1006 Lausanne, Switzerland
rbulushev@gmail.com
+(41)787688496

Education

École Polytechnique Fédérale de Lausanne (EPFL) – PhD in bioengineering/biotechnology
08.2012 – present (02.2017 expected), Lausanne, Switzerland
- Developed a technique for studying biophysical properties of DNA-protein interactions on a single molecule level using glass nanocapillaries and optical tweezers.
- Contributed to development of electric sensors of DNA and proteins using glass nanocapillaries.
- Contributed to development of a nanopore-based next generation DNA sequencing method.
- Supervised 2 MSc and one PhD student.

Novosibirsk State University (NSU) – Degree equal to MSc in biology
09.2007 – 06.2012, Novosibirsk, Russia
- Diploma with honors (GPA 4.94/5.0, among top 1 % students).
- 3 awards for academic excellence.

Work Experience

Merck – Intern in strategic marketing (Global fertility franchise)
05.2016 – 11.2016, Darmstadt, Germany
- Performed competitor and market analysis for fertility technologies.
- Contributed to development of an e-commerce platform.

Merck Serono – Home pharma consultant
07.2014 – 11.2014, Lausanne, Switzerland
- Developed a business plan for launching novel drug formulations for tumor targeting.

Technical skills

- **Instrumentation for nanometric measurements**: AFM, SEM, optical tweezers, DLS, nanopores.

- **Clean room nano- and microfabrication**: e-beam, wet and dry etching, photolithography, PDMS microfluidics.
- **Molecular biology**: PCR, electrophoresis (DNA, proteins, DNA/proteins), protein purification, cloning.

- **Stem cell culturing**.

- **Software**: Microsoft Office (Word, Excel, PowerPoint), LaTeX, Adobe Illustrator, IgorPRO, COMSOL, Solidworks, Fiji.

Conferences

- Presented work on 6 international conferences in the USA, Switzerland, Spain and Russia (2 oral presentations, 4 posters).

Publications

- **Bulushev R.D.,** Marion S., Petrova E, Davis S.J., Maerkel S.J., Radenovic A. *Nano Letters*. Single molecule localization and discrimination of DNA-protein complexes by controlled translocation through nanocapillaries. 16 (12), 7882-90, 2016.
- **Bulushev R.D.**, Marion S., Radenovic A. *Nano Letters*. Relevance of the drag force during controlled translocation of a DNA-protein complex through a glass nanocapillary. 15, pp 7118-25, 2015.
- Feng J., Liu K., **Bulushev R.D.**, Khlybov S., Dumcenco D., Kis. A., Radenovic A. *Nature Nanotechnology.* Identification of single nucleotides in MoS2 nanopores. 10, pp 1070-76, 2015.
- Feng J., Liu K., Graf M., Lihter M., **Bulushev R.D.**, Dumcenco D., Alexander D.T.L., Krasnozhon D.,Vuletic T., Kis A., Radenovic A. *Nano Letters*. Electrochemical reaction in single layer MoS2: nanopores opened atom by atom. 15(5), pp 3431-38, 2015.
- **Bulushev R.D.**, Steinbock L., Khlybov S., Steinbock J., Keyser U., Radenovic, A. *Nano Letters.* Measurment the position-dependent electrophoretic force on DNA in a glass nanocapillary. 14(11), pp 6606-13, 2014.
- Steinbock L.J., Krishnan, S., **Bulushev R.D.**, Borgeuad S., Blokesch M., Feletti L., Radenovic A. *Nanoscale*. Probing the size of proteins with glass nanopores. 6(23), pp 14380-87, 2014.
- Seitz P., Modarres H., Borgeaud S., **Bulushev R.D.**, Steinbock, L.J., Radenovic A., Dal Peraro M., Blokesch M. *PLoS Genet.* ComEA Is Essential for the Transfer of External DNA into the Periplasm in Naturally Transformable *Vibrio cholerae* Cells. 10(1), 2014.
- Steinbock L.J., **Bulushev R.D.**, Krishnan S., Raillon C., Radenovic A. *ACS Nano*. DNA translocation through low-noise glass nanopores. 7(12), pp 11255–62, 2013.
- Dmitrienko E., **Bulushev, R.D.**, Haupt K., Kosolobov S., Latyshev A., Pyshnaya I., Pyshnyi D. A simple approach to prepare molecularly imprinted polymers from nylon-6. *J. Mol. Recognition,* 26(8), pp 368-75, 2013.

Extracurricular activities, leadership and volunteering

Participant in the Novartis Biotechnology Leadership Camp 2014
- Learned to work on case studies under strict deadlines.
- Learned current trends in the biotech industry.

Member of the international student consulting organization ShARE
- Performed market analysis of Middle East countries for a Swiss digital security company.
- Developed a market entry strategy for a biotech start up at EPFL.

Event manager at the student association BioScience Network Lausanne (BSNL)
- Managed organization and organized +10 events for career development of students, including:
  - 6 informational meetings (≈100 students, 12 industrial experts).
  - A workshop with McKinsey for students in life sciences at EPFL.
  - An international science communication competition FameLab.

Languages

- **English**: fluent (verbally and written).
- **French**: upper-intermediate (B2).
- **Russian**: native.

Interests

- Dancing (bachata, west-coast swing), snowboarding, soccer (champion at the university competition), underwater swimming (Russian champion among teenagers).